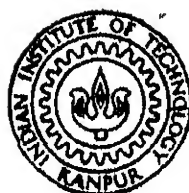


ROLE OF ELECTRON DENSITY AND ELECTRON TEMPERATURE
IN DISSOCIATION OF NITROGEN IN DIFFUSE GLOW PLASMAS

by

C. S. SREEKANTH



DEPARTMENT OF CHEMISTRY

INDIAN INSTITUTE OF TECHNOLOGY KANPUR

AUGUST, 1985

CHM
1985
D
SRE
ROL
TH
CHM/1985/D
Sx 18 x

✓
**ROLE OF ELECTRON DENSITY AND ELECTRON TEMPERATURE
IN DISSOCIATION OF NITROGEN IN DIFFUSE GLOW PLASMAS**

A Thesis Submitted
In Partial Fulfilment of the Requirements
for the Degree of

DOCTOR OF PHILOSOPHY

by
C. S. SREEKANTH

to the
**DEPARTMENT OF CHEMISTRY
INDIAN INSTITUTE OF TECHNOLOGY KANPUR
AUGUST, 1985**

11/11/87

21 DEC 1987

CENTRAL LIBRARY

199203

Act. No. A 99203

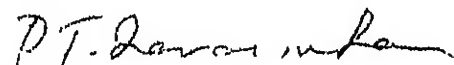
DEPARTMENT OF CHEMISTRY
INDIAN INSTITUTE OF TECHNOLOGY KANPUR

CERTIFICATE I

This is to certify that Mr. C.S. Sreekanth has satisfactorily completed all the courses required for the Ph.D. degree programme. These courses include:

Chm 521 Chemical Binding
Chm 523 Chemical Thermodynamics
Chm 524 Modern Physical Methods in Chemistry
Chm 543 Introduction to Nuclear Chemistry
Chm 800 General Seminars
Chm 801 Graduate Seminar
Chm 900 Graduate Research

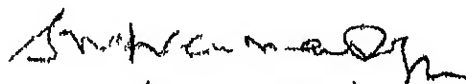
Mr. C.S. Sreekanth has successfully completed his Ph.D. Qualifying Examination in March 1980.



(P.T. Narasimhan)

Head,

Department of Chemistry,
IIT - KANPUR



(S.K. Dogra)

Convener,

Departmental Post-Graduate
Committee, Department of
Chemistry, I.I.T., Kanpur

CERTIFICATE II

Certified that the work 'ROLE OF ELECTRON DENSITY AND ELECTRON TEMPERATURE IN DISSOCIATION OF NITROGEN IN DIFFUSE GLOW PLASMAS' has been carried out by Mr. C.S. Sreekanth under my supervision and the same has not been submitted elsewhere for a degree.



(P. K. Ghosh)
Thesis Supervisor

ACKNOWLEDGEMENTS

It is with pleasure that I express my deep sense of indebtedness to Professor P. K. Ghosh, who suggested the problem and guided me at all stages of the work.

I thank

Mr. Milind K.J., Mr. Santhosh Kumar and Mr. Anand Hariharan for constantly being with me during the entire period of the present work,

Dr. Ashraf Ali and Dr. H.C. Srivastava, my seniors, for the helpful discussions I had in the initial stages of this work,

Mr. K.M.S. Prasad and Mr. M. Muralikrishna for lending various instruments needed in this work,

Mr. K. Raghavan, Mr. S.C. Sivasubramanian, Mr. Y. Kamalakara Rao, Mr. N. Subba Rao and Mr. P.K. Chowdhury, fellow graduate students of this department, for the help I received from them during the various stages of the work,

Mr. Gauri Singh for his valuable assistance,

Mr. J.N. Sharma, Mr. M.J. Bhaskaran and Mr. B. Sairam of the Glass Blowing Workshop, and Mr. V.L. Rajani and Mr. S.L. Yadav of the Central Workshop for their cooperation,

Mr. R.D. Singh for very carefully typing this thesis and Mr. Dilip Kumar for making photocopies of the Figures.

C.S. SREEKANTH

CONTENTS

	Page
LIST OF TABLES	vii
LIST OF FIGURES	viii
ABSTRACT	xi
CHAPTER	
1. INTRODUCTION	1
2. EXPERIMENTAL METHODS	13
2.1 Discharge Tube	13
2.2 Electrodes	15
2.3 Vacuum System	18
2.4 Pressure Measurements	18
2.5 Afterglow Intensity Measurements	19
2.6 Wall Temperature Measurements	19
2.7 Gas Handling	23
2.8 Double Probe	23
2.9 Principle of Double Probe Operation	24
2.10 Procedure of Experiments	27
3. RESULTS	28
3.1 Paschen Breakdown Curve of Nitrogen	28
3.2 Voltage-Current Characteristics of Glows and Arcs	28
3.3 Evaluation of Electron Temperature and Density	35
3.4 Wall Temperature Data	44
3.5 Total Intensity Measurements of the Afterglow	48
3.6 Effect of Variations in the Flow Rate	48
3.7 NO Titration Data	48

...contd.

Contents (contd.)

		Page
CHAPTER		
4. DISCUSSION	57
4.1 Present Knowledge About Electron Impact Dissociation	58
4.2 A Model of the Dissociation and Recombination Processes	60
4.3 The Volume and the Surface Recombination Processes	64
4.4 Power Dissipated in the Plasma and n_e, kT_e Variation	67
4.5 N Atom Concentration from the Model	68
4.6 Estimates of N Atom Density from Photomultiplier Data	72
4.7 N Atom Density in the Plasma and at the position of the Afterglow Measurements	84
4.8 Comparison of N Atom Densities from Afterglow Intensities and those from Calculations	89
4.9 Conclusion and Critique	94
REFERENCES	97
APPENDIX	101

...

LIST OF TABLES

- 3.1 Diagnostic Data Using Double Probe (interelectrode distance 5 cm)
- 3.2 Diagnostic Data Using Double Probe (interelectrode distance 10 cm)
- 3.3 Diagnostic Data Using Double Probe (interelectrode distance 15 cm)
- 3.4 Visual Appearance of the Glow
- 3.5 Temperature Measurements Using Chromel Aluminium Thermocouple
- 3.6 Total Intensity Measurements of the Afterglow (photo-multiplier data)
- 4.1 Total Cross Section for the Dissociation of N_2 of Electron Energy
- 4.2 Nitrogen Atom Recombination Data
- 4.3 Nitrogen Atom Concentration from Model Using Electron Impact Dissociation and Surface Recombination (inter-electrode spacing 5 cm)
- 4.4 Nitrogen Atom Concentration from Model Using Electron Impact Dissociation and Surface Recombination (inter-electrode spacing 10 cm)
- 4.5 Nitrogen Atom Concentration from Model Using Electron Impact Dissociation and Surface Recombination (inter-electrode Spacing 15 cm)

LIST OF FIGURES

- 1.1 Schematic Characteristic for a Gaseous Discharge
- 2.1 Schematic Diagram of the Discharge Tube and the Afterglow Region
- 2.2 Discharge Tube Showing: (1) Electrodes, (2) High Voltage Power Supply, (3) Double Probe, (4) Differential Voltage Supply
- 2.3 Arc Power Supply Showing the Ignition Circuit and Sustaining Power Supply
- 2.4 The Digital Voltmeter Interface used to Enhance the Precision of the Pressure Transducer BHL 4400-10-02MO Readout
- 2.5 Circuitry Associated with 1P28 (PMT) for Intensity Measurements
- 2.6 Transmittance Characteristics of the Orange Filter Used with 1P28 (PMT)
- 2.7 Double Probe Characteristic and Explanation of Terminology Used in n_e , kT_e Evaluation by the Intercept Method
- 3.1 Paschen Breakdown Curve of Nitrogen
- 3.2 (a) V-I Data of Glow Discharge
(b) V-I Data of Arc Discharge
- 3.3 I-V Data of Glows (interelectrode distance 5 cm)
- 3.4 I-V Data of Glows (interelectrode distance 10 cm)
- 3.5 I-V Data of Glows (interelectrode distance 15 cm)

List of Figures (contd.)

- 3.6 Double Probe Characteristics at 1 Torr Pressure, 90 mA Discharge Current, and 15 cm Interelectrode Distance
- 3.7 Double Probe Characteristics at 1 Torr Pressure, 220 mA Discharge Current, and 15 cm Interelectrode Distance
- 3.8 VI vs Afterglow Intensity (interelectrode distance 5 cm)
- 3.9 VI vs Afterglow Intensity (interelectrode distance 10 cm)
- 3.10 VI vs Afterglow Intensity (interelectrode distance 15 cm)
- 3.11 VI vs Afterglow Intensity Measurements at Different Pressures Realized by Partially Closing the Butterfly Valve (interelectrode distance 5 cm)
- 3.12 VI vs Afterglow Intensity Measurements at Different Pressures Realized by Partially Closing the Butterfly Valve (interelectrode distance 10 cm)
- 3.13 Nitric Oxide Flow Needed to Titrate the N Atoms to the end point (abscissa scale represents the needle valve opening)
- 4.1 (a) Plot of Total Dissociation Cross Section vs Electron Energy
(b) Plot of the Rate Coefficient vs Electron Temperature (kT_e)
- 4.2 Plot of the Product of Electron Temperature and Density ($n_e kT_e$) vs VI (power in Watts) (interelectrode distance 5 cm)
- 4.3 Plot of the Product of Electron Temperature and Density ($n_e kT_e$) vs VI (power in Watts) (interelectrode distance 10 cm)

List of Figures (contd.)

- 4.4 Plot of the Product of Electron Temperature and Density ($n_e kT_e$) vs VI (power in Watts) (interelectrode distance 15 cm)
- 4.5 Plot of VI (Watts) vs Nitrogen Atom Density (cm^{-3})
Calculated from Experimental Values of n_e and kT_e (inter-electrode distance 5 cm)
- 4.6 Plot of VI (Watts) vs Nitrogen Atom Density (cm^{-3})
Calculated from Experimental Values of n_e and kT_e (inter-electrode distance 10 cm)
- 4.7 Plot of VI (Watts) vs Nitrogen Atom Density (cm^{-3})
Calculated from Experimental Values of n_e and kT_e (inter-electrode distance 15 cm)
- 4.8 VI (Watts) vs Afterglow Intensity for all the Discharge Tubes (interelectrode distance 5, 10 and 15 cm) and for Pressure Range 1 Torr - 3 Torr
- 4.9 VI (Watts) vs Nitrogen Atom Density (from PMT data)
- 4.10 VI (Watts) vs Nitrogen Atom Density (calculated from experimental Values of n_e and kT_e , obtained for inter-electrode distances 5, 10, and 15 cm; and surface recombination rate coefficient at 300°K)
- 4.11 VI (Watts) vs Nitrogen Atom Density (calculated from experimental values of n_e and kT_e obtained for inter-electrode distances 5, 10, and 15 cm; and surface recombination coefficient at 350°K)

Abstract

Nitrogen plasmas in dc glows have been studied to examine the role of the plasma parameters, electron density and electron temperature, in controlling the extent of dissociation of the gas into nitrogen atoms.

Experiments are conducted in a flow system with a linear flow rate of 27.5 m/sec and a volume flow rate of 945 lit/min and in the pressure range of 1-6 torr. Three sets of interelectrode distance of 5, 10 and 15 cm are used. Plasma diagnostics are carried out using double probes. Atom concentrations are estimated from afterglow emission intensities.

The electron density n_e varied in the range $1.9 \times 10^{10} \text{ cm}^{-3}$ to $10.90 \times 10^{10} \text{ cm}^{-3}$ and the electron temperature kT_e varied in the range 2.4 eV - 4.8 eV. This correspond to 75 - 325 Watts of CW (IV) power dissipated in the discharge. The $n_e kT_e$ product increased with power. In the isobaric $n_e kT_e$ - IV plots, the isobars shift to higher values of IV at higher pressures.

A model based on electron impact dissociation for generating nitrogen atoms (rate coefficient k_1), volume recombination (rate coefficient k_2) and surface recombination (rate coefficient k_3) gives $[N] = \{k_1(T_e)[N_2]n_e / (k_2(T_g)[N_2] + k_3(T_w, T_g))\}^{1/2}$. The model is broadly in agreement with the experimental results.

CHAPTER 1

INTRODUCTION

Gaseous plasmas provide a unique medium for study of chemical reactions of atoms, molecules, and ions both in their ground states and a wide variety of excited states. The richness in the nature of species present in plasmas arises primarily from the large variety of electron impact processes that can occur with the ground state stable neutrals followed by collisions involving the excited species. Many chemical processes which proceed with negligible rate under ordinary reaction conditions, including even fairly high gas temperatures, proceed rapidly in presence of significant concentration of excited states generated by collisions of heavy particles with high energy electrons.

The potential richness of such a reaction medium, however, is accompanied by an almost impenetrable barrier of difficulty that one faces when one attempts a quantitative physico-

chemical analysis of a plasma system, the latter constituting the single most important factor in putting plasma chemistry on a solid scientific basis. Thus far the chemist's approach towards plasma chemistry has mostly been, with varying degree of sophistication, to define the operational parameters of the plasma system used and studying the chemical products formed either from directly feeding stable molecules in the plasma, or, by using a second reactant to the effluents of the plasma through which the primary reactant is passed. Devices to generate gaseous plasmas in the laboratory have been of many types, and the efforts in chemical applications have mostly been in empirical studies on the nature of product formation as a function of operational parameters. In contrast, the physicist's involvement with low temperature plasmas, the type of plasma with which most chemical experiments have been done, have been mostly in characterization of such plasmas in terms of diagnostic parameters such as electron densities and electron energy distribution, and associated radiative properties. There also have been a number of collisional-radiative models, but because of the enormous complexities involved, these mostly consider atomic systems; relatively very little has been done with molecular systems. It would seem that if plasma chemistry is to be provided a sound physical basis, it is essential that there are systematic and simultaneous studies of both the chemical and physical aspects and evolve quantitative correlations. The

present work is an effort in this direction that attempts to synthesize the physical and chemical approaches in plasma investigations. Specifically it considers dissociation of nitrogen molecules in glow plasmas. In this introductory chapter, we shall present some elementary but fundamental properties of gaseous plasmas, and outline the background as well as the objective of the present work.

Plasmas are ionized gases containing an ensemble of ions and electrons which satisfy certain conditions between the positive ion density n^+ , the electron density n_e , and the electron energy distribution, which, if the electron kinetic energy distribution is maxwellian, can be characterised by an electron temperature T_e . Since a gaseous plasma is on the whole electrically neutral, one can write

$$n^+ \simeq n_e \quad \dots(1.1)$$

This constitutes the first plasma criterion. The second criterion involves the Debye shielding length λ_D which is a measure of the distance at which a positive ion is effectively shielded by the surrounding electrons. Quantitatively λ_D represents the distance at which the potential with respect to a positive ion is of $(1/e)$ th value of that with no electrons present, which may be said to be a measure of the screened Coulomb potential. The distance over which a plasma can have an appreciable departure from the positive-negative charge equilibrium is

of the order of debye length λ_D , and one can derive the following expression for λ_D

$$\lambda_D = (\epsilon kT_e / 4\pi e^2 n_e) \quad \dots(1.2)$$

where ϵ is the dielectric constant of the medium, k the Boltzmann constant, and e is the electronic charge. In order to have the necessary electrostatic interaction between the plasma particles, the debye shielding length must be considerably less than the minimum dimension L of the plasma, i.e., $\lambda_D \ll L$. The ionized gas behaves like an ordinary collection of free charges if this criterion is not satisfied. While the chemical consequences of atom-atom or atom-electron collisions are not known to be any different depending on whether the plasma criteria are satisfied, most laboratory discharge conditions satisfy the plasma criteria. For example, at an electron temperature kT_e of 1 eV and n_e of 10^{10} cm^{-3} , which would commonly be the case of a dilute discharged gas, the λ_D calculated from (1.2) is only 10^{-2} cm , much smaller than usual container dimensions. At higher electron densities therefore such systems would easily be meeting the plasma criteria.

The plasma particles, i.e., positive ions, negative ions, and electrons can have a wide range of translational energy distribution, and the population densities of internal energy states of the heavy particles also depend on the nature of the

equilibrium condition present in the plasma, various equilibrium conditions being, complete thermodynamic equilibrium (CTE), local thermodynamic equilibrium (LTE), and non-local thermodynamic equilibrium (non-LTE). In CTE all the properties of the plasma particles are determined by one plasma temperature T . The translational energy distribution of the heavy particles as well as of the electrons is given by the Maxwell-Boltzmann law corresponding to the plasma temperature, and the population densities of the internal excited states of the heavy particles, which would include all rotational, vibrational, and electronic excited states of molecules, are given by the Boltzmann distribution at the same temperature. The degree of ionization is given by the Saha law for the plasma temperature. The spectral intensity of the radiation is governed by the Planck's law at the same temperature.

When only the Planck's radiation law is not obeyed in a Plasma, but the other laws valid in CTE mentioned above hold, the plasma is said to be in local thermodynamic equilibrium. In LTE the population densities of quantum states are as would in CTE for a system having the same density, temperature, and composition of the system under consideration. In dense laboratory plasmas where electron impact processes are dominant, the electron temperature determines the distribution function of the species. Dominance of electron impact processes arises because electron impact cross sections are

not lower than the corresponding cross sections of ions, but the electron velocities are high.

In LTE, both electrons and ions have approximately Maxwellian velocity distributions, but their kinetic temperatures may be very different; these two temperatures approach each other as the heavy particle density of the plasma increases.

In plasmas with Maxwellian electron energy distribution where electron impact processes are dominant, LTE may be expected to hold good. The internal population density distribution of heavy particles above a critical level characterised by a principal quantum number conform to LTE (Boltzmann distribution). This is because of the fact that the spontaneous radiative decay rates decrease and electron impact cross sections increase with increasing principal quantum number; at the critical level the electron impact excitation rate and radiative decay rates are comparable.

The present investigation has to do with plasma physico-chemical processes in dc discharges. While the fundamental atomic processes are of course independent of the macroscopic processes associated with generation of the plasma, we choose dc discharges for the relative convenience of ignitions of these plasmas and also relative simplicity of the equipment needed to sustain such discharges. The dc discharges are categorised into following several distinct regions in terms of voltage-current characteristics (Fig. 1.1). At low applied voltages,

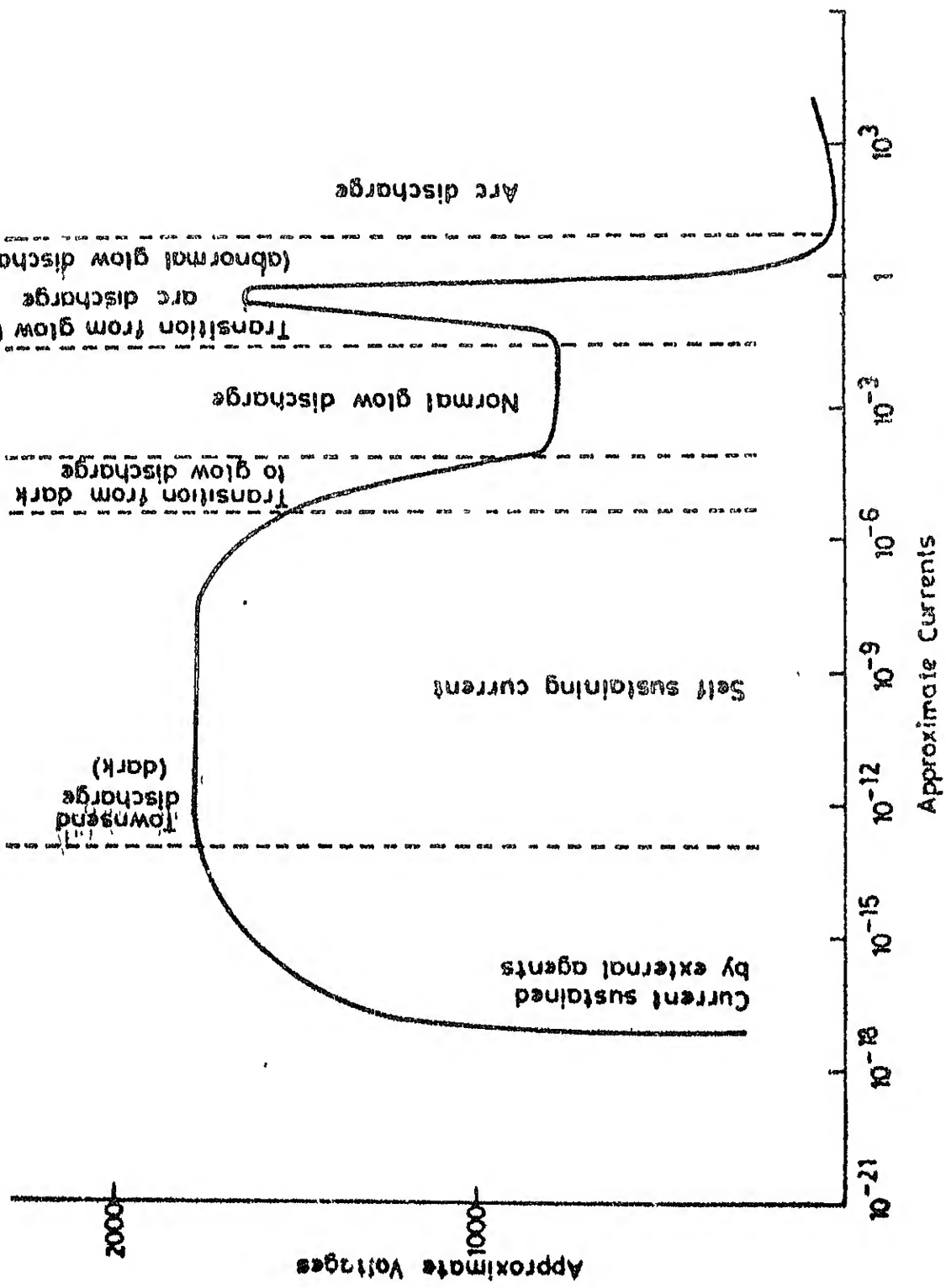


Fig. 1.1.1 SCHEMATIC CHARACTERISTIC FOR A GASEOUS DISCHARGE

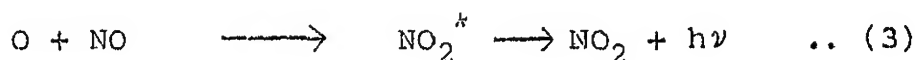
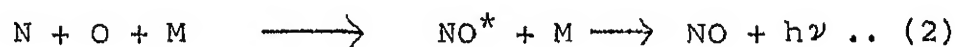
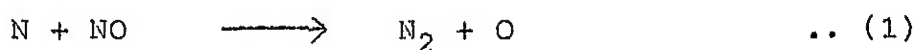
a very low current of 10^{-13} A is observed which is due to collection of charges produced by external sources. This is non-self sustaining region. Increase in voltage results in increasing the mobility of the charged particles which would by collision generate more ion pairs in the gas. When this multiplication factor is equal to 1 the discharge becomes self-sustaining. This region is the Townsend region. In this region, the space charges formed near the electrodes become predominant. This increase in field concentration increases the current and the discharge undergoes a transition into glow discharge. This region is characterised by a voltage drop across the electrodes which remains constant over 2-3 order of increment in the discharge current. The current density at the cathode, however, remains constant and the cathode surface is increasingly covered as the discharge current increases. When the entire cathode surface gets covered, an increase in the discharge current can be achieved only by increasing the current density at the cathode, which implies a large cathode emission, and this in turn, would increase the cathode fall. This corresponds to the abnormal glow discharge. In this region, ionisation increases resulting in the collection of larger number of increasingly more energetic positive ions. This process heats up the cathode till it attains a temperature sufficient for thermionic emission of electrons. Thermionic emission, increases exponentially with temperature. This results in a decreased voltage drop between the electrodes and increase in

current by many orders. This region is designated as arc discharge.

From the point of view of plasma chemistry, specially with interest of chemical synthesis, one would be most interested in systems where the electron densities are high, so that the concentration and flux of the excited species which act as initiators of chemical reactions could be high. Logically, therefore, these systems should be high current arcs. However, there are several severe problems associated with managing such high current arcs, the chief one being able to hold the container at reasonably low temperature. With huge amount of power dissipation the cooling problem becomes enormous and, the problems of generating high power dc sources for both igniting and sustenance of the system are no simpler. Due to this reason we constrain ourselves to relatively low current systems.

Specifically we investigate here the correlations that can be evolved, by considering the relevant atomic processes, between the plasma parameters in dc glow plasmas and the dissociation of nitrogen gas when it passes through the plasma. Plasma parameters are obtained by standard probe techniques, and nitrogen atom concentration estimates are made by following the afterglow intensities. There have been numerous phenomenological studies on nitrogen discharges and afterglows, and the observed phenomena and possible processes have been reviewed.²⁻⁴

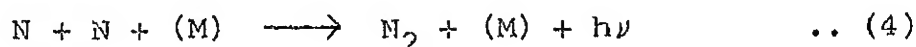
The reaction of N atoms with NO has been often used as a chemical 'titration' method of estimation of N atoms. Some early applications of the method are reported in.⁵⁻⁸ The method was first used in kinetic study by Harteck, Reeves and Mannella⁸ and involves flowing NO into the stream containing nitrogen atoms. It is believed that the reaction proceeds through the following mechanism



The reaction sequence is associated with a visual change of luminescence. When nitrogen atoms are present in a nitrogen afterglow, then the orange-yellow glow gradually decreases in intensity as nitrogen atoms are consumed in the reaction (1). This is accompanied by a blue-violet glow from the NO' formed in reaction (2) between oxygen atoms formed in reaction (1) and the nitrogen atoms. Beyond the end point, when there are no N atoms present the NO is in excess, the excess NO reacts with oxygen atoms to form excited NO_2^* which gives a greenish-yellow luminescence. At the end point the reaction (2) does not take place as nitrogen atoms are absent, and (3) does not take place as there is no excess NO. Thus there is practically no luminescence from the reaction region.

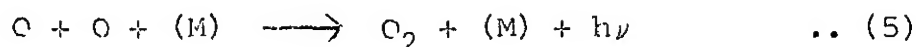
The results obtained in the titration method has received support from nitrogen atom concentration measurements by physical methods. For example, in the ESR method of directly following nitrogen atom concentration, Westenberg and de Haas⁹ found results in the pressure range 0.4 - 3.0 torr agreeing with the titration method. Weyssenhoff and Patapoff¹⁰ found that the method gives correct measurement of nitrogen atom concentration if the discharge region is sufficiently separated from the titration zone so that deactivation of excited species interfering with the titration process can take place. They found the agreement to be within $\pm 10\%$ ¹⁰ except at pressures above 3 torr and high flow rates ($\approx 10^3$ cm sec⁻¹) when the titration method gave higher concentrations, which was believed to be due to reaction of NO with the species responsible for the "pink" afterglow. The reaction scheme above has been used recently by Sutoh et al.¹¹ to measure the absolute rate constant for the chemiluminescent reaction of atomic oxygen with nitric oxide, the atomic oxygen being generated by reaction (1).

A detailed investigation of the radiation observed from the reaction zone was done by Young and Sharpless.¹² The spectral studies, (a) the first positive bands ($B^3\Pi_g - A^3\Sigma_u^+$) generated by the reaction:

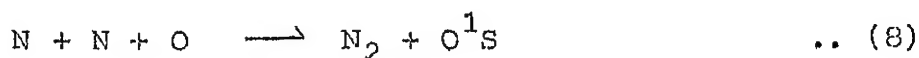
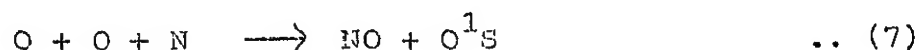
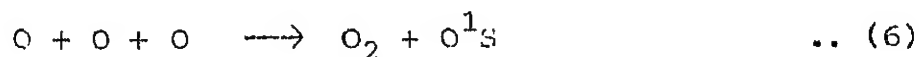


(b) the NO $\beta(B^2\Pi - X^2\Pi)$, $\gamma(A^2\Sigma^+ - X^2\Pi)$, and $\delta(C^2\Pi - X^2\Pi)$ bands generated by the reaction (2), and (c) the O₂ atmospheric

bands ($b^1\Sigma_g^+ - X^2\Pi$) and Herzberg bands ($A^3\Sigma_u^+ - X^3\Sigma_g^-$) generated by the reaction



and the $W O_2$ "continuum" generated by reaction (3). There are a number of alternative ways which can lead to the excitation of the 1S state of atomic oxygen spontaneous deexcitation of which leads to emission of the 5577\AA auroral green line



The major purpose of the work is to examine the role of plasma electron density and electron temperature in dissociation of nitrogen in low pressure dc glow plasmas.

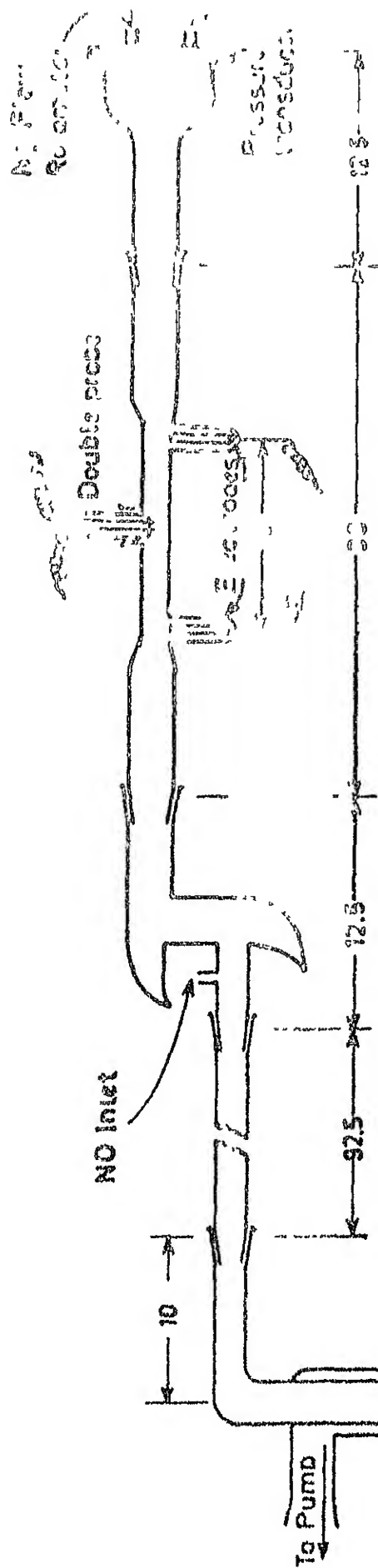
CHAPTER 2

EXPERIMENTAL METHODS

The various implements used in the experimental studies are (a) the discharge tube and associated gas handling system, (b) electric probes for n_e , kT_e measurements, (c) afterglow radiation intensity measurements using a photomultiplier.

2.1 Discharge Tube

Both the discharge tube and the vacuum system are constructed out of a glass tube of 2.5 cm internal diameter and 2.9 cm outer diameter. The length of the discharge section is 35 cm and the length of the afterglow section including a liquid nitrogen trap is 130 cm. A schematic diagram of the discharge tube and the afterglow region is given in Fig. 2.1. Three separate sets of interelectrode distances are used in the discharge tube: 5 cm, 10 cm and 15 cm. For the arcs interelectrode distances of 2.5 cm and 5 cm are used. Cooling of the discharge tube was by ambient air; neither forced air



$d = 3, 10 \text{ and } 15 \text{ cm}$
All dimensions are in cm

Fig. 2.1 SCHEMATIC DIAGRAM OF THE DISCHARGE TUBE AND THE AFTERGLOW REGION

nor any other coolant was used.

The glow discharge is ignited by a Perkin Elmer 5000 V, 250 mA stabilized power supply (Model 222-0450, originally for an ion pump) as shown in Fig. 2.2. The measurements are made within a 30 sec interval during which all parameters measured reached stable values except the wall temperature which, even at the end of the interval, continued to show an increasing trend. Near the end of the 30 sec period the cathode became red hot. Both orientations of the electrodes (cathode toward the pump and away from the pump) were used.

Ignition of the arc is done by the Illumination Industries Inc. (U.S.) high pressure Hg arc power supply model CA-200. After the arc ignited, the dc power to sustain the arc is supplied by a home-made dc power supply as shown in Fig. 2.3. Maximum arc current used was 6 amperes. The I-V measurements are made within 4 secs. Invariably the tube melted in another few seconds if the arc were kept on.

2.2 Electrodes

Hollow E & G electrodes (E & G Electricals, Newark) of size 0.9 cm outer diameter and 3.6 cm in length, were used that were procured from an importer. The analysis of the electrode material by the National Metallurgical Laboratory showed Fe as

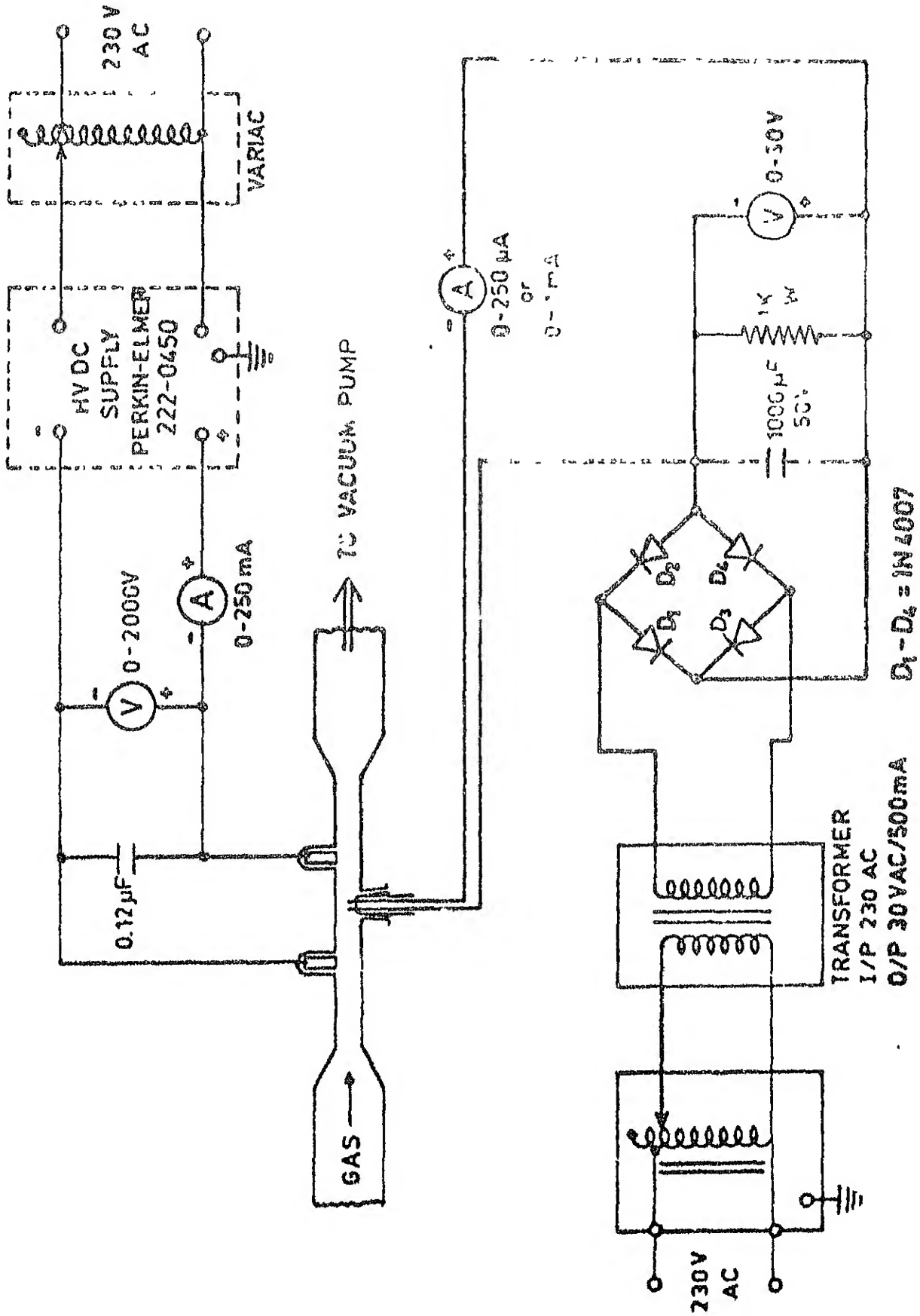


Fig. 2.2 DISCHARGE TUBE SHOWING (1) ELECTRODES, (2) HIGH VOLTAGE POWER SUPPLY, (3) DOUBLE PROBE, (4) DIFFERENTIAL VOLTAGE SUPPLY

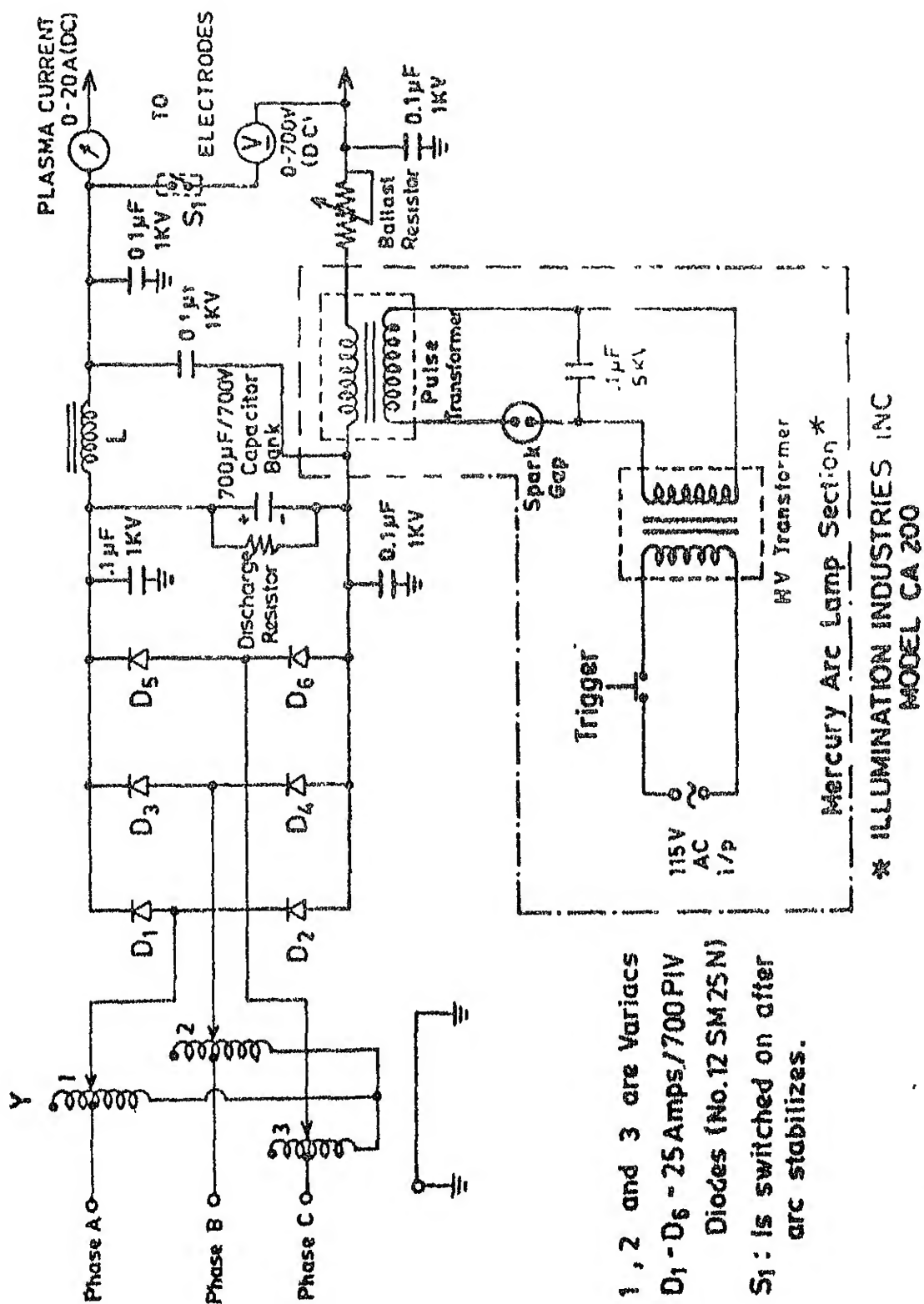


Fig. 2.3 ARC POWER SUPPLY SHOWING THE IGNITION CIRCUIT AND SUSTAINING POWER SUPPLY

the major constituent, the trace constituents being Cr, Al, Mg, Mn and Cu.

The chemical analysis of the electrode material was done spectroscopically (by NML) by exciting a small amount of the electrode material, in a dc arc of 6 amperes struck between a 10 mm diameter graphite rod and a 6 mm diameter carbon rod. A shallow crater made on the graphite rod served as the sample holder. The optical spectrum of the excited sample was recorded using a Hilger Quartz Spectrograph (Littrow type) in the range of 2700-4400 Å. The identification of the constituents of the sample was done by superposing this spectrum on a 'Master spectrogram' recorded on the same instrument, obtained by arcing ~~raies~~ Ultimes powder, which consists of small amount of about 50 elements incorporated in a base of Zn, Mg and Ca oxides.

2.3 Vacuum System

The gases are pumped by a Welch 1275 M Duoseal high vacuum pump with a pumping speed of 945 lit/min. For the tube diameter used, this implies a maximum linear flow rate of 27.5 m/sec. The discharge tube and the afterglow part of the system are separated from the Welch pump by a large butterfly valve, that could be partially closed to reduce flow velocity or increase the residence time of the gas in the system.

2.4 Pressure Measurements

The vacuum is monitored by Veeco thermocouple gauges (DV1M) and Control, and the gas pressure in the system during

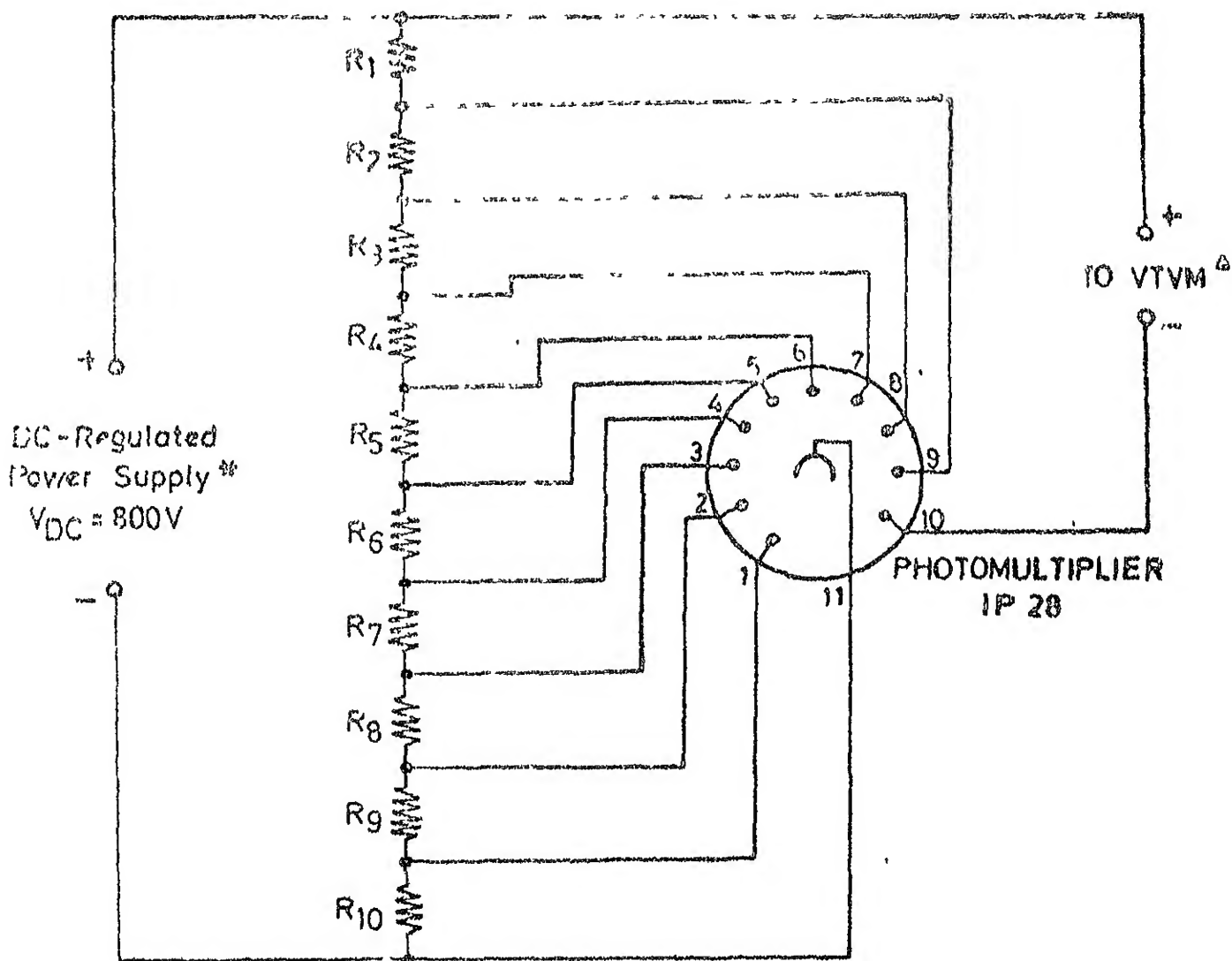
experiments are measured by a CEC (U.K.) Instrumentation pressure transducer BHL 4400-10-02 MO. The precision of this transducer as displayed in the built-in digital meter was inadequate. Therefore, the analog output provided in the external terminal of the pressure transducer was taken to a digital voltmeter interface, designed and fabricated in the laboratory, with the help of which final measurements were made (Fig. 2.4).

2.5 Afterglow Intensity Measurements

The afterglow radiation intensity is measured at 120 cm away from the electrode that is nearest to the pump by an RCA 1P28 photomultiplier tube (PMT) (spectral response S5). The circuits associated with the PMT are shown in Fig. 2.5. The PMT is enclosed in an aluminium box with a slit width of 0.025 cm. The distance of the PMT photocathode to the edge of the pyrex tube is approx. 5 mm. The PMT is powered by a Fluke 408B high voltage power supply. An orange filter is used whose filtering properties are shown in Fig. 2.6.

2.6 Wall Temperature Measurements

The temperature was measured on the outer side of wall in the discharge region using a Chromel-Alumel thermocouple for the pressures 1.0 torr, 2.0 torr and 3.0 torr. These temperatures were recorded 30 seconds after the discharge was on. Though all other parameters stabilised at the end of the 30 seconds, the wall temperature continued to rise. The electrodes became red hot and the discharge had to be switched off.


$$R_1 - R_{10} = 100 \text{ K}\Omega$$

* FLUKE HV POWER SUPPLY MODEL 408B

A SIMPSON VTVM MODEL 321-1

1-9 Dynodes, 10 Anode, 11 Photocathode

Fig. 2.5 CIRCUITRY ASSOCIATED WITH 1P28 (PMT) FOR INTENSITY MEASUREMENTS

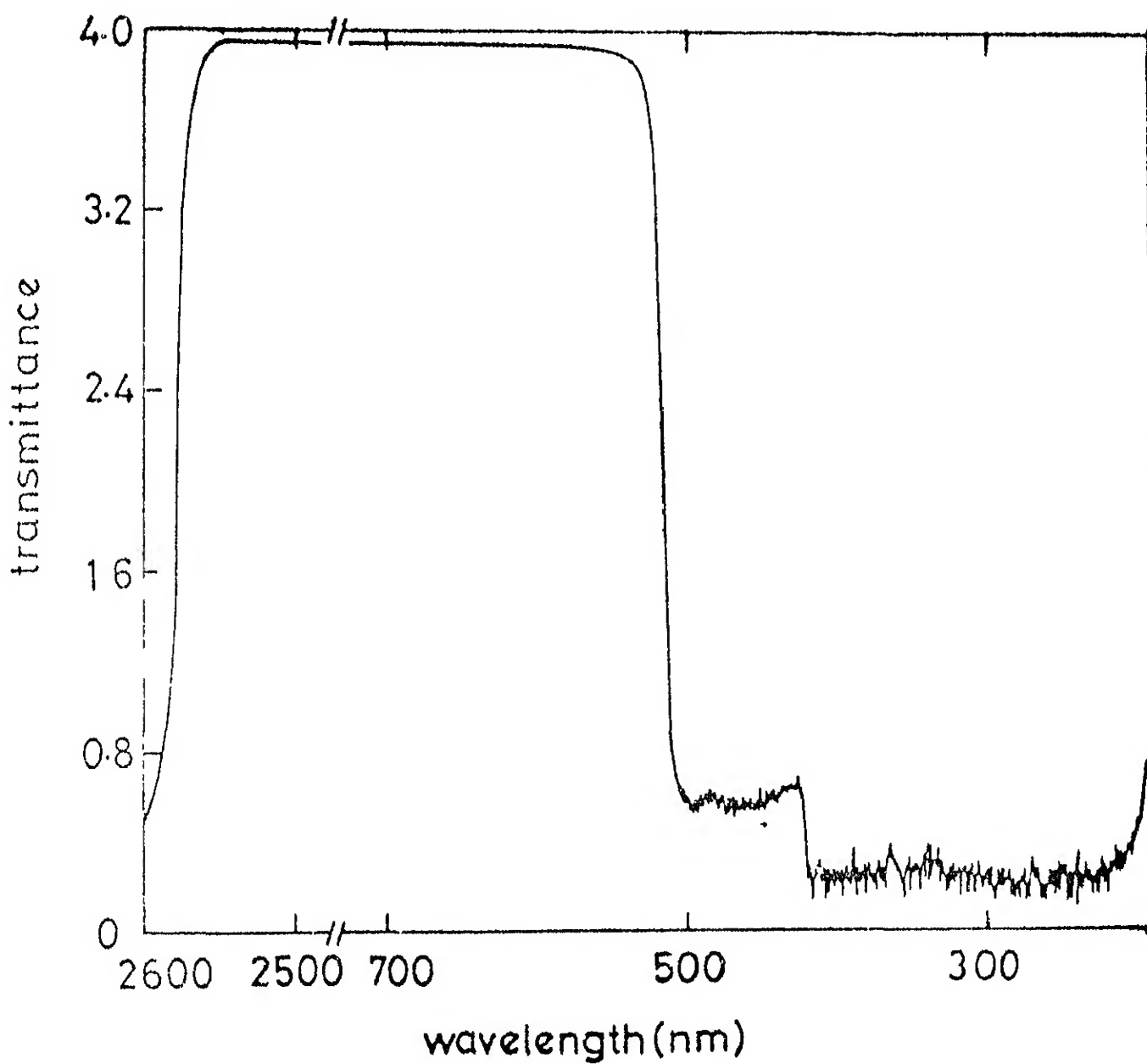


Fig. 2.6 TRANSMITTANCE CHARACTERISTICS OF THE ORANGE FILTER
USED WITH 1P28 (PMT)

2.7 Gas Handling

Matheson UHP nitrogen and IOL (Indian Oxygen) AR-2 nitrogen are used. Most of the trial experiments are carried with the latter, and are repeated with the former for final data. The gas was let in through a rotameter (Aluminium Float of 0.936 g weight) from which the flow rate is obtained.

In the titration experiment of N atoms by NO, Matheson UHP NO is used and a Hoke needle valve was used to control the flow. We could not manage to procure a mass flowmeter; so the flow parameter that will be referred to later pertains to the position of the needle valve plug. Since the flow rates involved are very small, despite much and prolonged efforts a rotameter similar to that used in the N₂ line could not be constructed.

2.8 Double Probe

The double probe consists of a pair of tungsten wires of 3 mm length and 1.5 mm diameter and fused into a glass tube with 4 mm separation between each other. The differential voltage to the double probe is applied by a floating dc supply as shown in Fig. 2.2. The conditions (i) the dimension of the probe < the mean free path for collisions of charged with neutral particles; and (ii) probe current \ll discharge current are satisfied. The

probe is introduced into the discharge column mostly midway between the electrodes, and the tip of the double probe is placed on the tube axis symmetrically between the electrodes in the discharge glow.

2.9 Principle of Operation of the Double Probe

The double probe was originally proposed by Johnson and Malter.¹³ A dc bias voltage isolated from the ground is applied between the probes; the entire system floats with the plasma and therefore follows plasma potential.

A voltage V is applied between the probes 1 and 2.

If an assumption is made that V_1 is positive relative to V_2 , that is

$$V = V_1 - V_2 > 0$$

a current I flows from 1 to 2 and is positive if V is positive. Since electron velocities are much higher than ion velocities, the probes in general will be negative with respect to space potential. For larger positive voltages the probe 2 will be very negative, drawing ion saturation current. The same would happen at probe 1 when the voltages are reversed. The advantage of a double probe over a single probe is that the total current is never more than the ion saturation current, thus causing least disturbance in the plasma. From the double probe

characteristics, the kT_e can be calculated by the intercept method as suggested by Johnson and Malter¹³:

$$kT_e \text{ (eV)} = (V_d'' - V_d') / \ln \left(\frac{F-1}{D-1} \right)$$

where V_d' and V_d'' are arbitrarily chosen different voltages on the double probe characteristic as indicated in Fig. 2.7 and

$$D = \frac{\sum i_p}{i_{e1}} \text{ at } V_d'$$

$$F = \frac{\sum i_p}{i_{e2}} \text{ at } V_d''$$

where $\sum i_p = i_{p1} + i_{p2}$, i_{p1} and i_{p2} being saturation current at each probe, and i_{e1} and i_{e2} are the probe currents at differential voltages V_d' and V_d'' .

Once kT_e is known, from the knowledge of the saturation current at either probe, and the probe area, the electron density can be calculated from the equation given by Bohm et al.¹⁴,

$$I_{+0} = 0.4 [N_2^+] e A_p \left[\frac{kT_e}{M^+} \right]^{1/2}$$

where

I_{+0} = ion saturation current in amperes

e = electronic charge in Coulombs

A_p = probe area in cm^2

kT_e = electron temperature in eV

M^+ = mass of the N_2^+ ion in gm

$[N_2^+]$ is the predominant ionic species with $n_e \simeq N_2^+$.

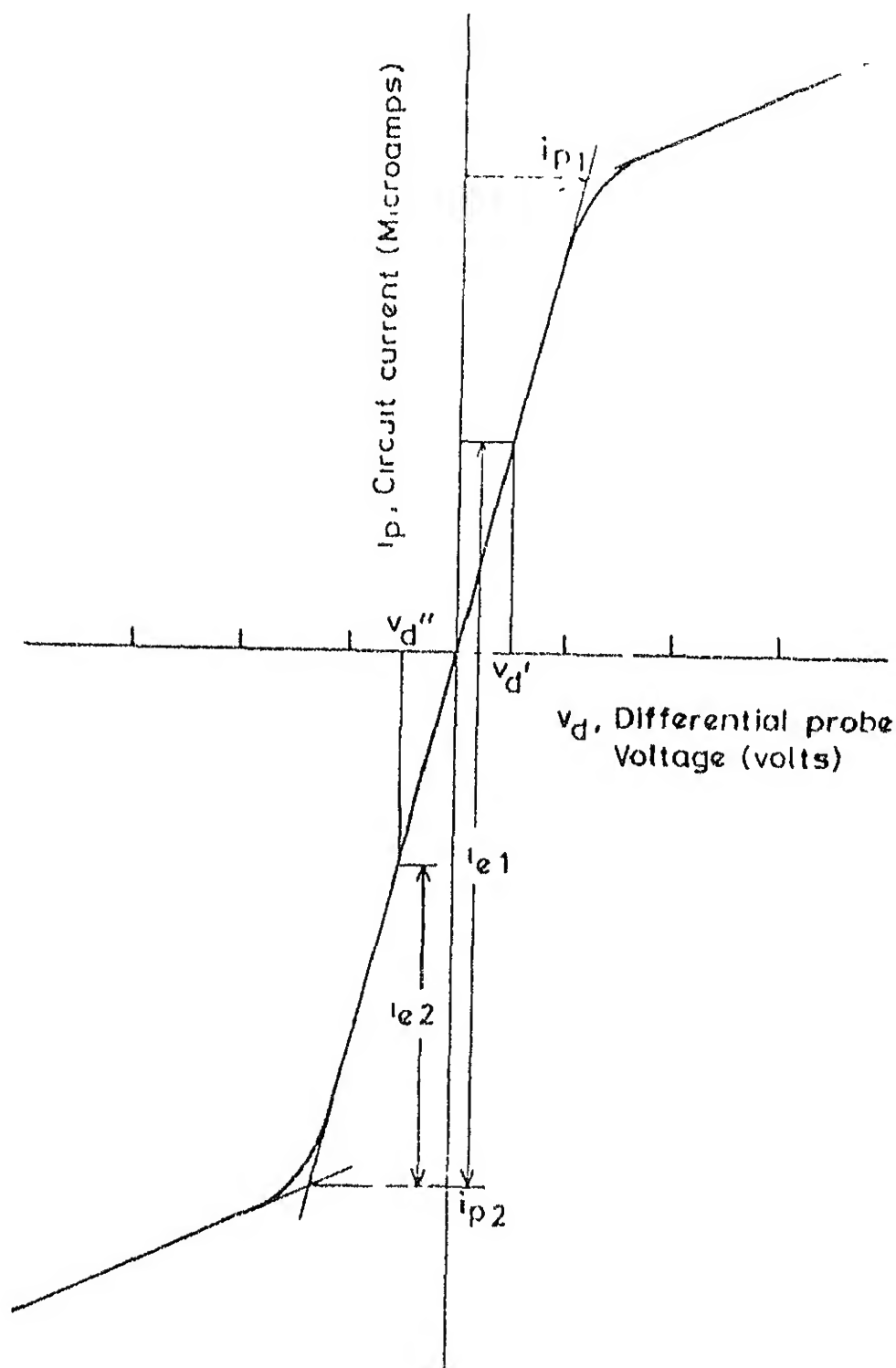


Fig. 2.7 DOUBLE PROBE CHARACTERISTIC AND EXPLANATION OF TERMINOLOGY USED IN n_e , kT_e EVALUATION BY THE INTERCEPT METHOD

2.10 Procedure of Experiments

The experiments were conducted using all the three discharge tubes which differed only in interelectrode distances. In most experiments, the double probe was placed in the centre of the glow discharge and at equal distance from either electrode. The differential voltage is varied in the range 0 - 30 V dc. From the double probe characteristic the n_e and kT_e were determined by the above mentioned method. The experiments were carried out for each discharge tube at pressures of 1.0, 1.5, 2.0, 2.5, 3.0 torr, and at each pressure for three discharge currents of 90 mA, 140 mA, 220 mA. Radiation intensity measurements using 1P28 were conducted simultaneously.

Experiments to examine the effects of flow rates/ pressures on afterglow emission were carried out by controlling the foreline butterfly valve for any given fixed position of the nitrogen flow control needle valve as follows.

With the foreline valve fully open, the pressure in the system was maintained at 1.0 torr. Then by partially closing the foreline valve, the pressure in the system was increased to 2 torr and then in another experiment to 3 torr. The same experiment was conducted by keeping the initial pressure at 2 torr and then increasing it to 3 torr and 4 torr by partially closing the foreline valve. In both these measurements, the afterglow intensities were recorded at 90 mA, 140 mA and 220 mA of discharge currents.

CHAPTER 3

RESULTS

3.1 Paschen Breakdown Curve of Nitrogen

These measurements were conducted using two discharge tubes with interelectrode distances of 2.5 cm and 5 cm. The Paschen breakdown curve is shown in Fig. 3.1. The curve shows a breakdown potential of 1850 V at pd value of 0.2 torr-cm, the lowest pd value used in the experiments, and passes through a minimum of $V_D = 250$ V at pd of 1 torr-cm. The curve increased to a value of 2770 V at a pd of 48.15 torr-cm the highest pd value used. The maximum error in the pressure measurement was ± 0.1 torr and in the voltage measurements ± 30 V.

3.2 Voltage-Current Characteristics of Glows and Arcs

Figure 3.2(a) shows the V-I characteristics of glows recorded at 0.8 torr, 1.45 torr, 2.4 torr and 3.3 torr. For

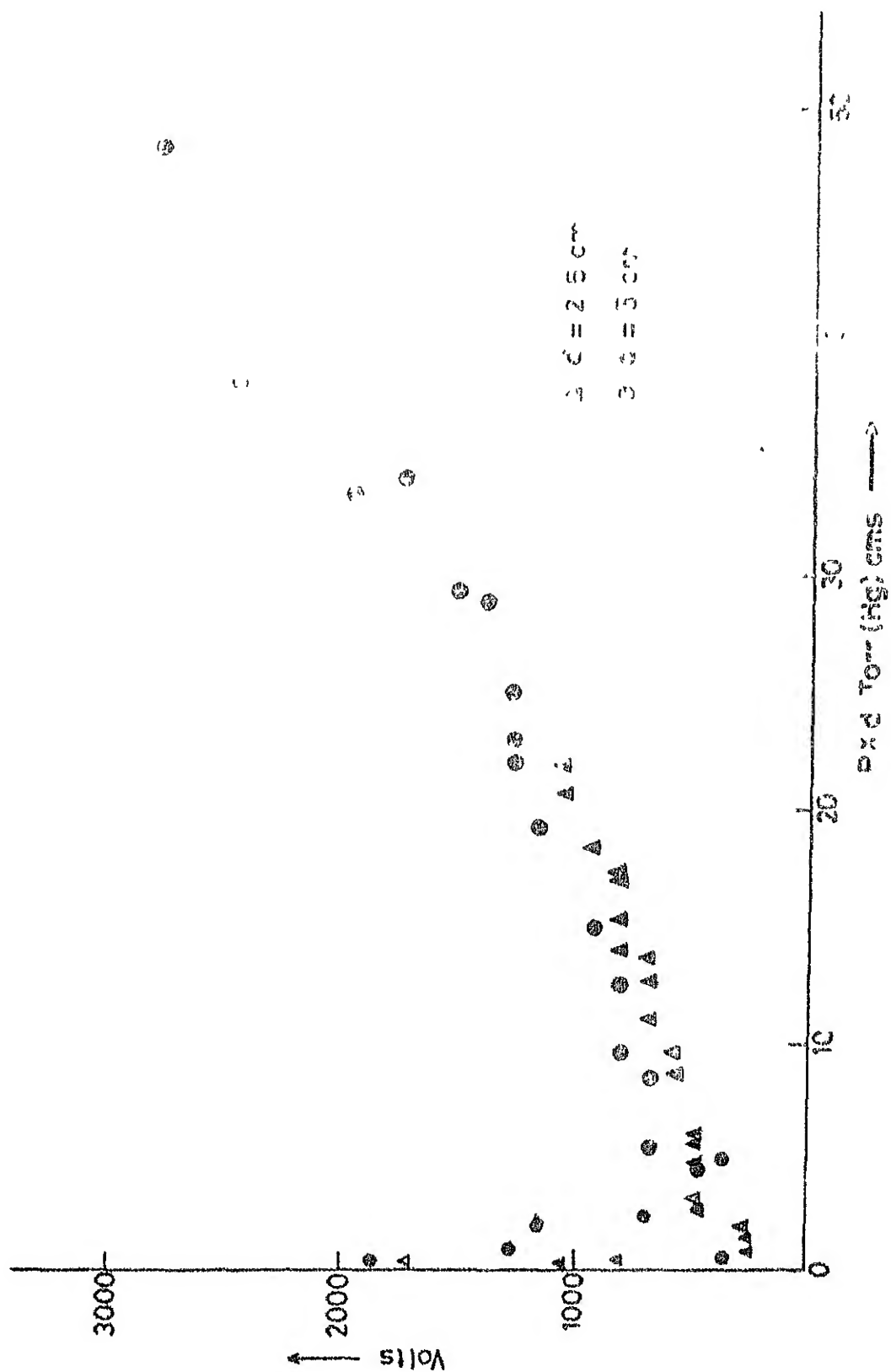


Fig. 3.1 PASCHEN BREAKDOWN CURVE OF NITROGEN

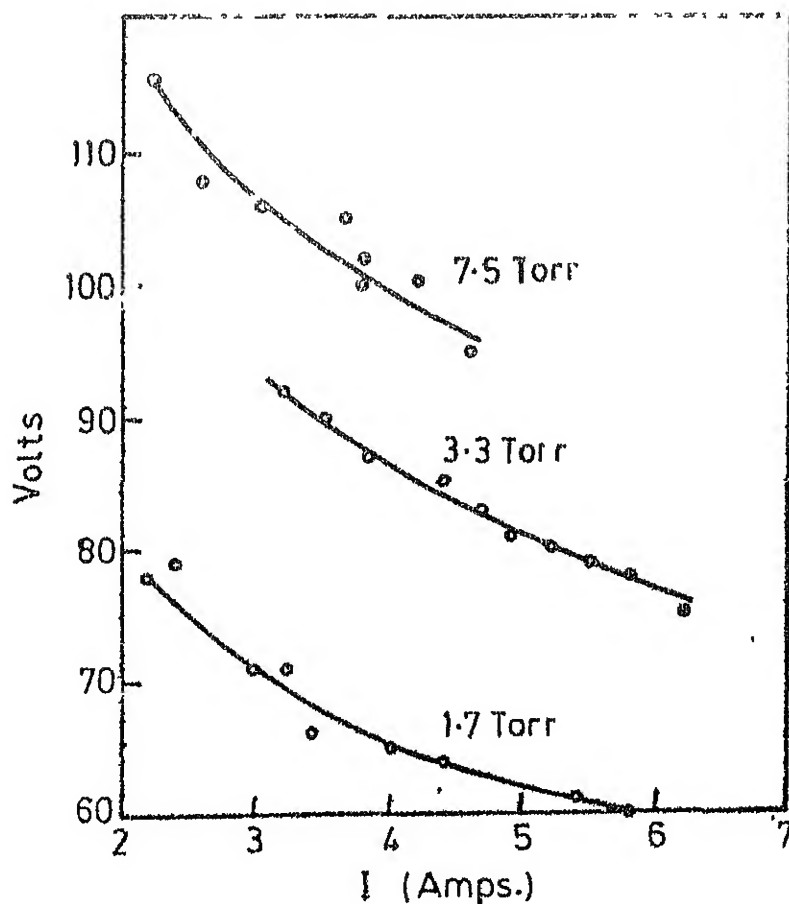
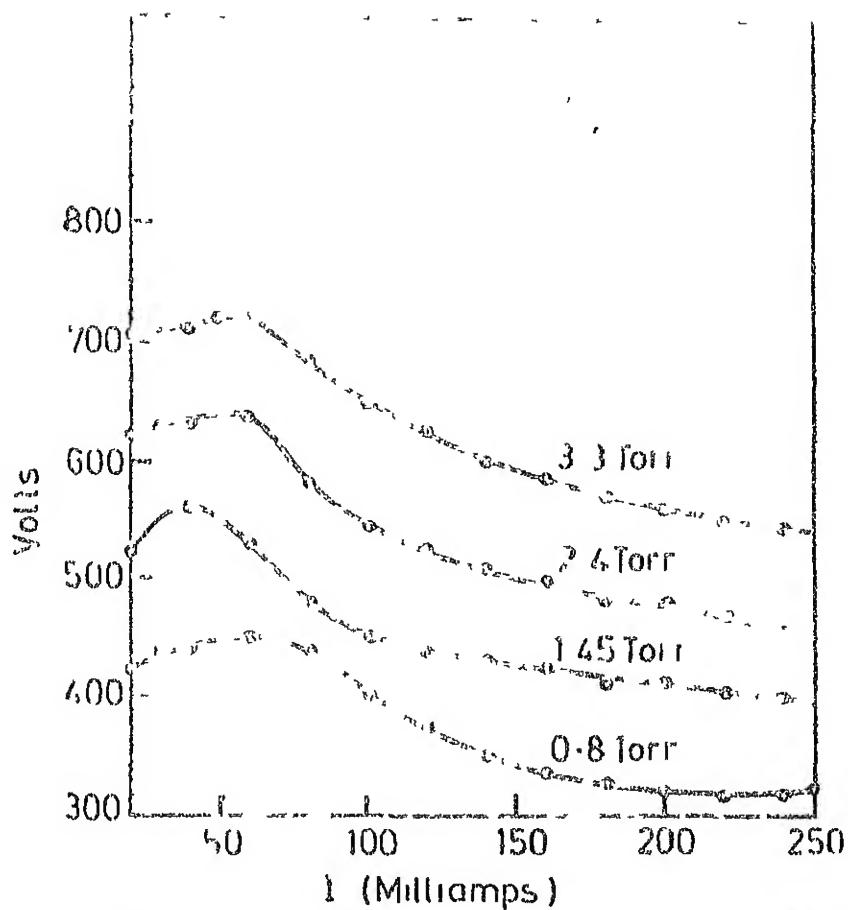


Fig. 3.2 (a) V-I DATA OF GLOW DISCHARGE
(b) V-I DATA OF ARC DISCHARGE

the range of pressures considered here the potential difference between the electrodes increase directly as pressure, and varies little with discharge current. These early experiments were done in a static system. The pressures were measured by a McLeod gauge where the maximum measurement error was ± 0.1 torr.

The V-I characteristics of the arc with a discharge tube of interelectrode distance 5 cm and pressures of 1.7 torr, 3.3 torr, and 7.5 torr are shown in Fig. 3.2(b). Higher the pressure higher was the potential difference between the electrodes. These experiments were done in a flow system and the pressures were measured by a McLeod gauge.

Figures 3.3 - 3.5 show the current-voltage characteristics of glows in three discharge tubes with interelectrode distances 5 cm, 10 cm and 15 cm, respectively. These measurements were made in a flow system at discharge currents of 90 mA, 140 mA, 220 mA, and at each current, for 1.0 torr, 1.5 torr, 2.0 torr, 2.5 torr and 3.0 torr pressures. The dependence of the current-voltage characteristics on the interelectrode spacing and pressure are as follows. At a given current and interelectrode distance, higher the pressure, higher is the potential difference between the electrodes. At a given current and pressure, the potential difference increases as the interelectrode distance increases. The power ($V \times I$) varies directly as the interelectrode distance and pressure.

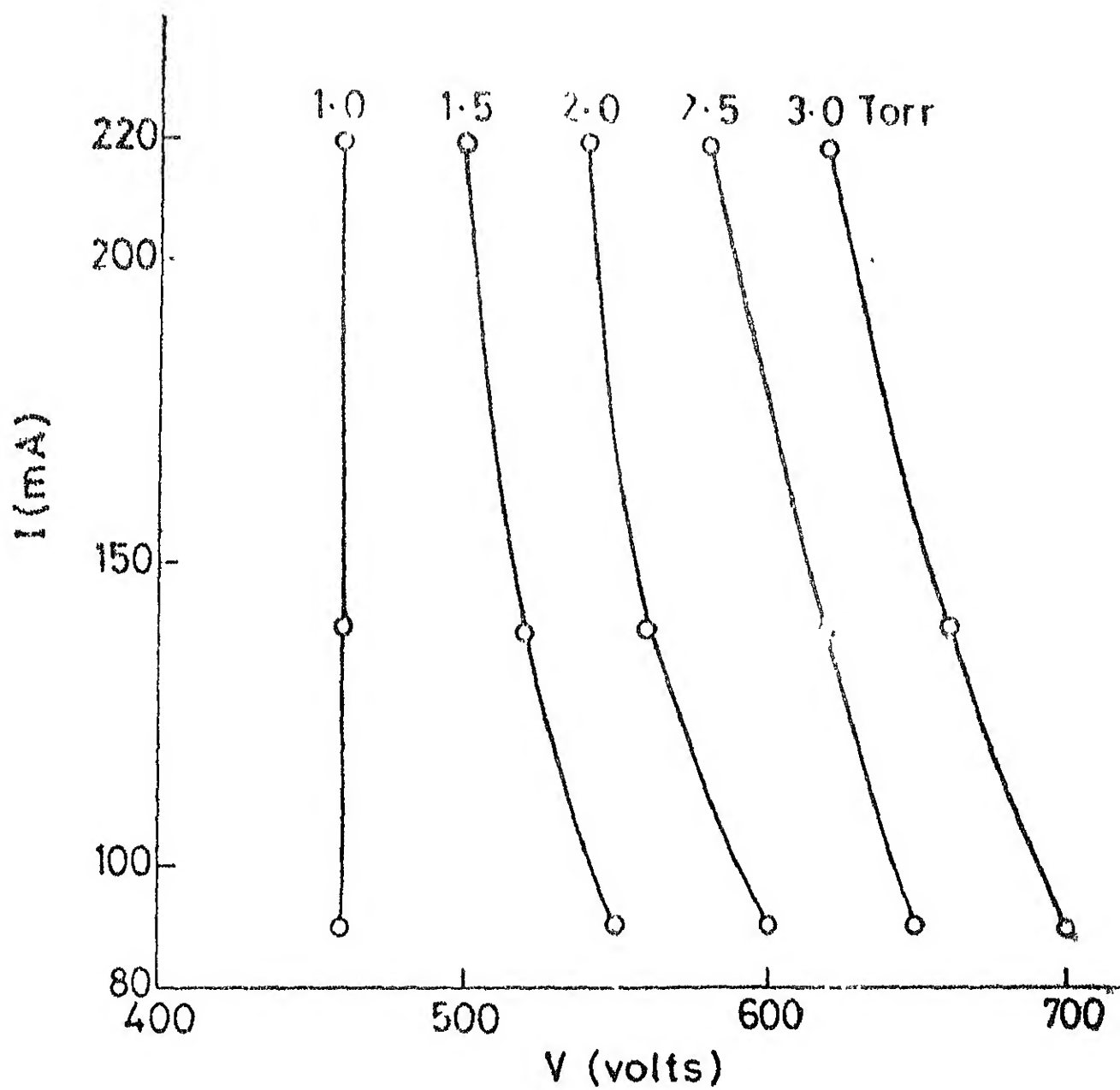


FIG. 3.3 I-V DATA OF GLOWS (INTERELECTRODE DISTANCE 5 cm)

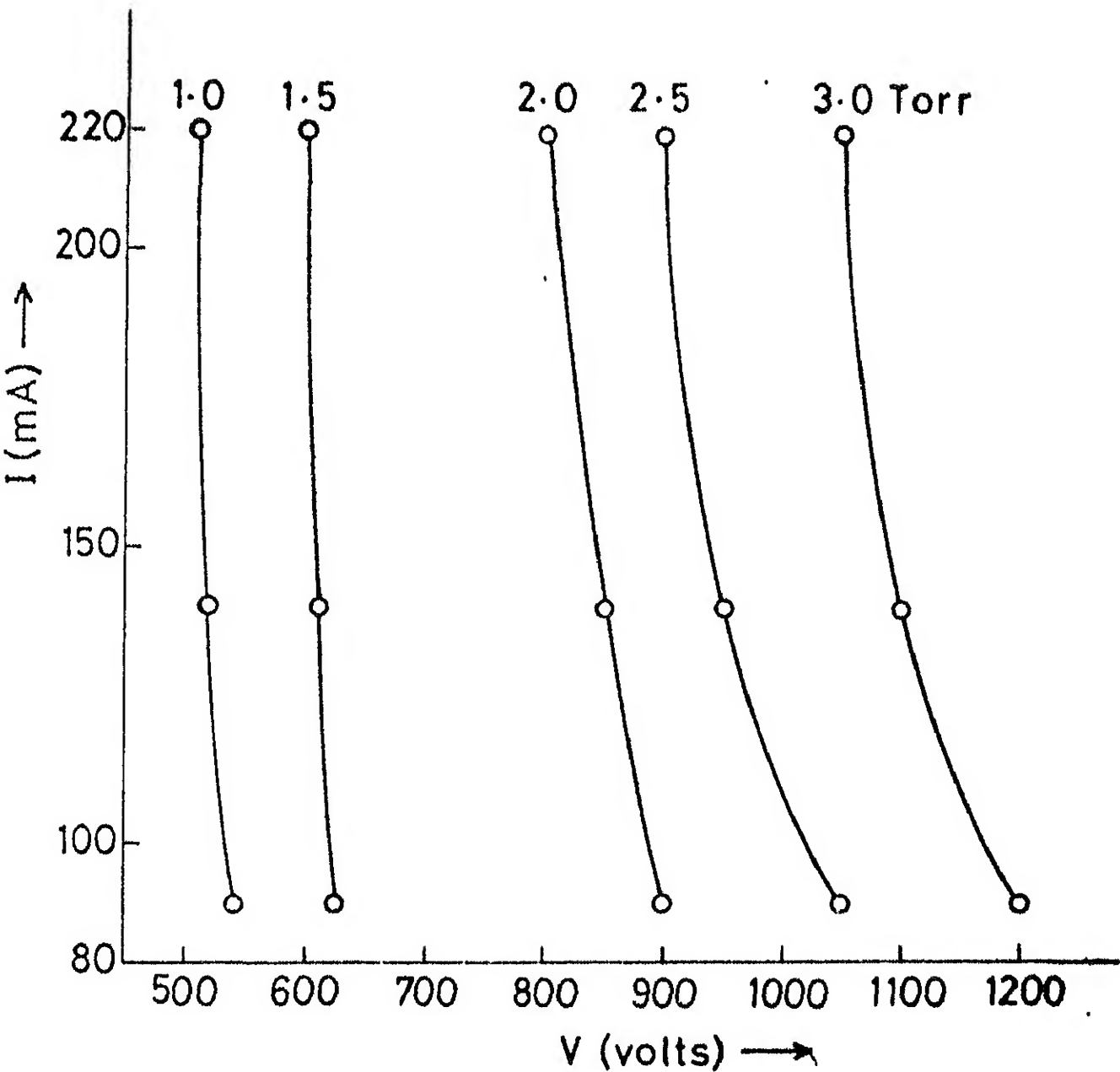


Fig. 3.4 I-V DATA OF GLOWS (INTERELECTRODE DISTANCE 10 cm)

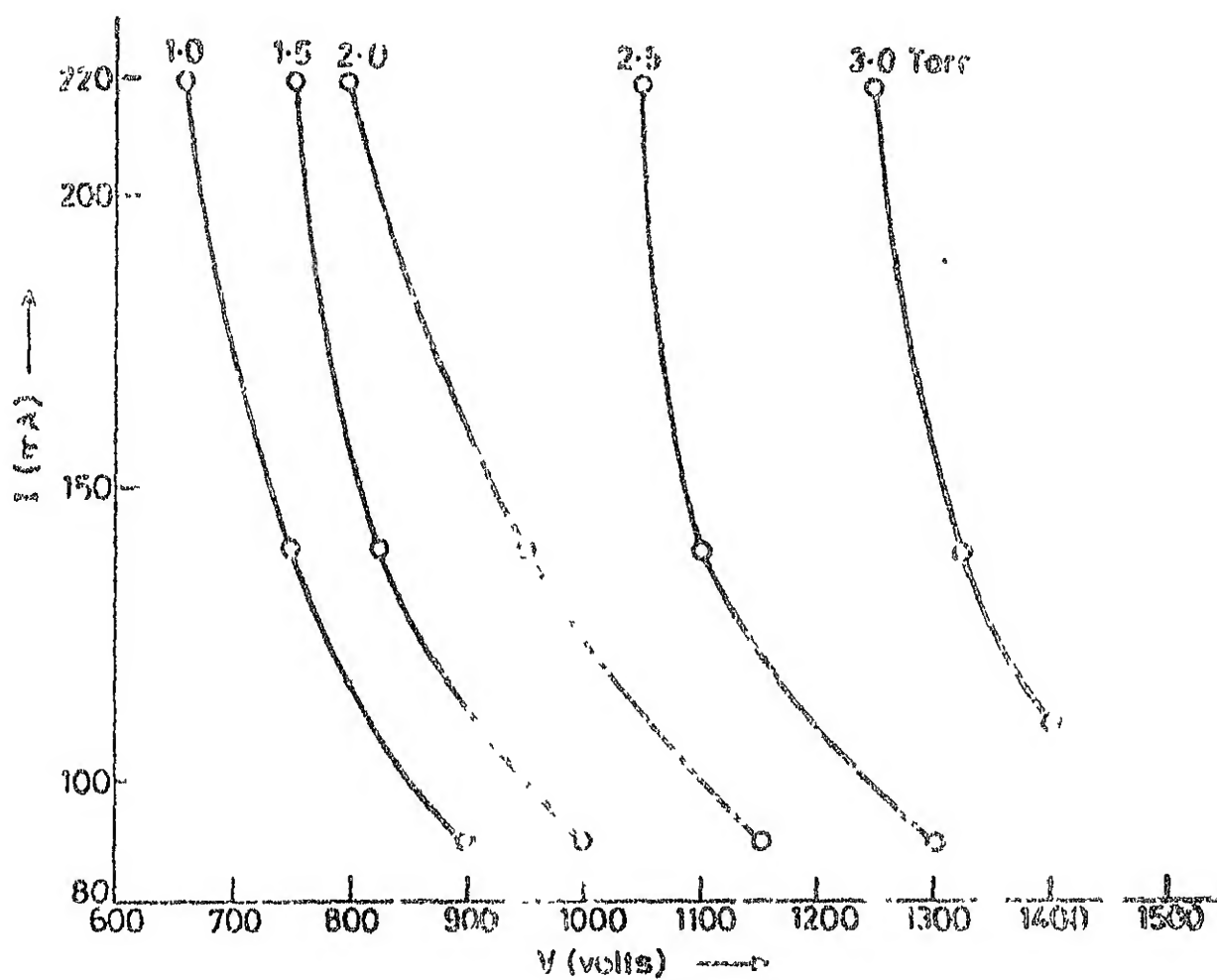


Fig. 3.5 I-V DATA OF GLOWS (INTERELECTRODE DISTANCE 15 cm)

3.3 Evaluation of Electron Temperature and Density

The electron temperature and density were measured using a double probe. The double probe characteristics were obtained using discharge tubes with interelectrode spacings of 5 cm, 10 cm, and 15 cm, and in each case at pressures of 1.0 torr, 1.5 torr, 2.0 torr, 2.5 torr, 3.0 torr and three discharge currents of 90 mA, 140 mA, and 220 mA.

A couple of sample double probe characteristics are shown in Figs. 3.6 and 3.7. In Fig. 3.6 the double probe characteristics are shown for discharge current of 90 mA at a pressure of 1.0 torr. In Fig. 3.7 it is shown for a discharge current of 220 mA at a pressure of 1.0 torr. Both these characteristics were recorded with a discharge tube having interelectrode distance of 15 cm.

The electron temperature was determined by the intercept method, as discussed by Johnson and Malter.¹³ The electron density was determined by using the expression by Bohm et al.¹⁴ The calculated values of electron densities and electron temperatures for the experiments with the three discharge tubes are presented in Tables 3.1, 3.2 and 3.3. Maximum experimental errors in n_e and KT_e measurements are estimated to be $0 \pm 0.71 \times 10^{10} \text{ cm}^{-3}$ and $\pm 0.11 \text{ eV}$, respectively.

The following general observations can be made from the KT_e , n_e data shown in Tables 3.1 - 3.3. (i) The electron

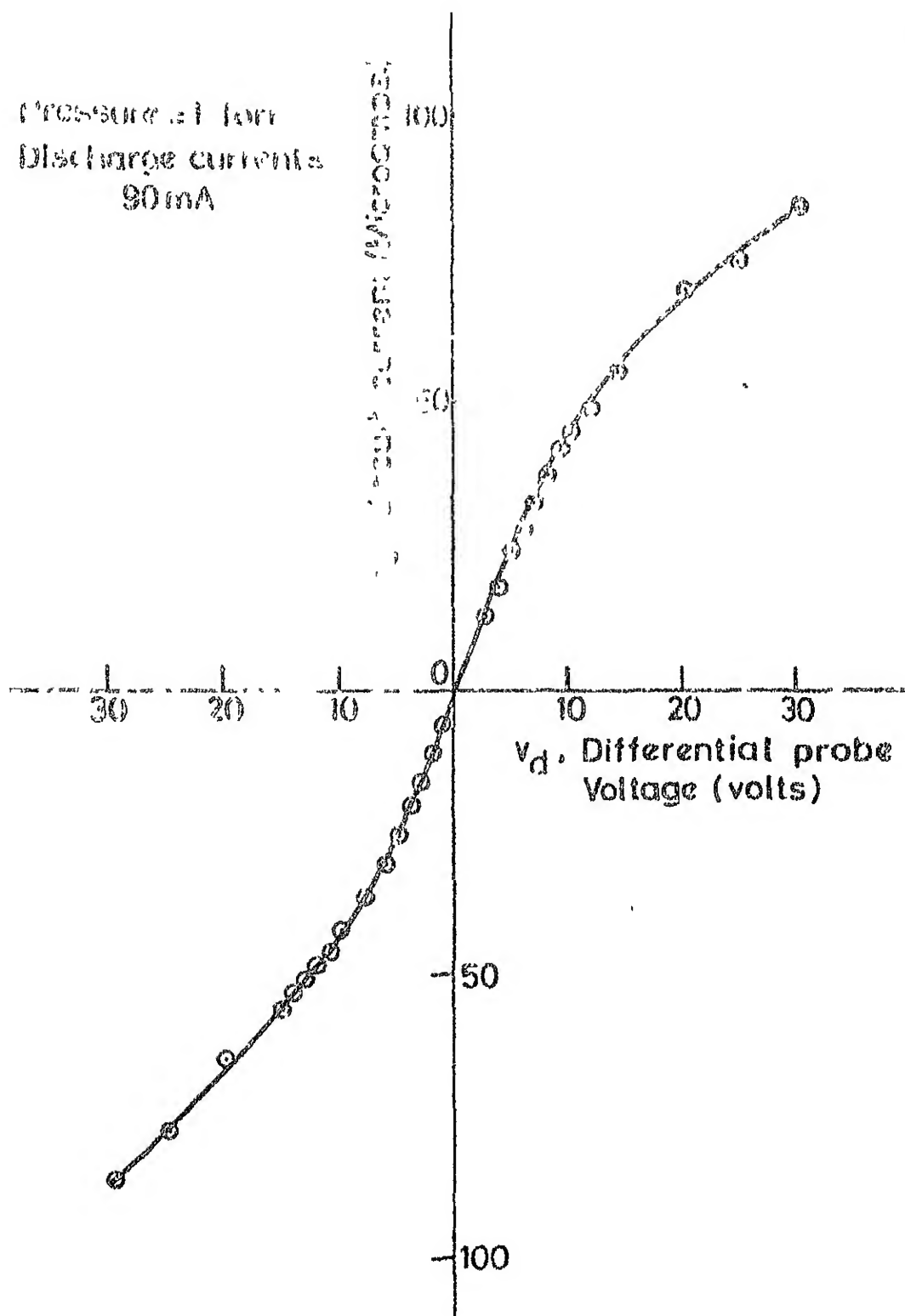


Fig. 3.6 DOUBLE PROBE CHARACTERISTICS AT 1 TORR PRESSURE, 90 mA DISCHARGE CURRENT, AND 15 cm INTERELECTRODE DISTANCE

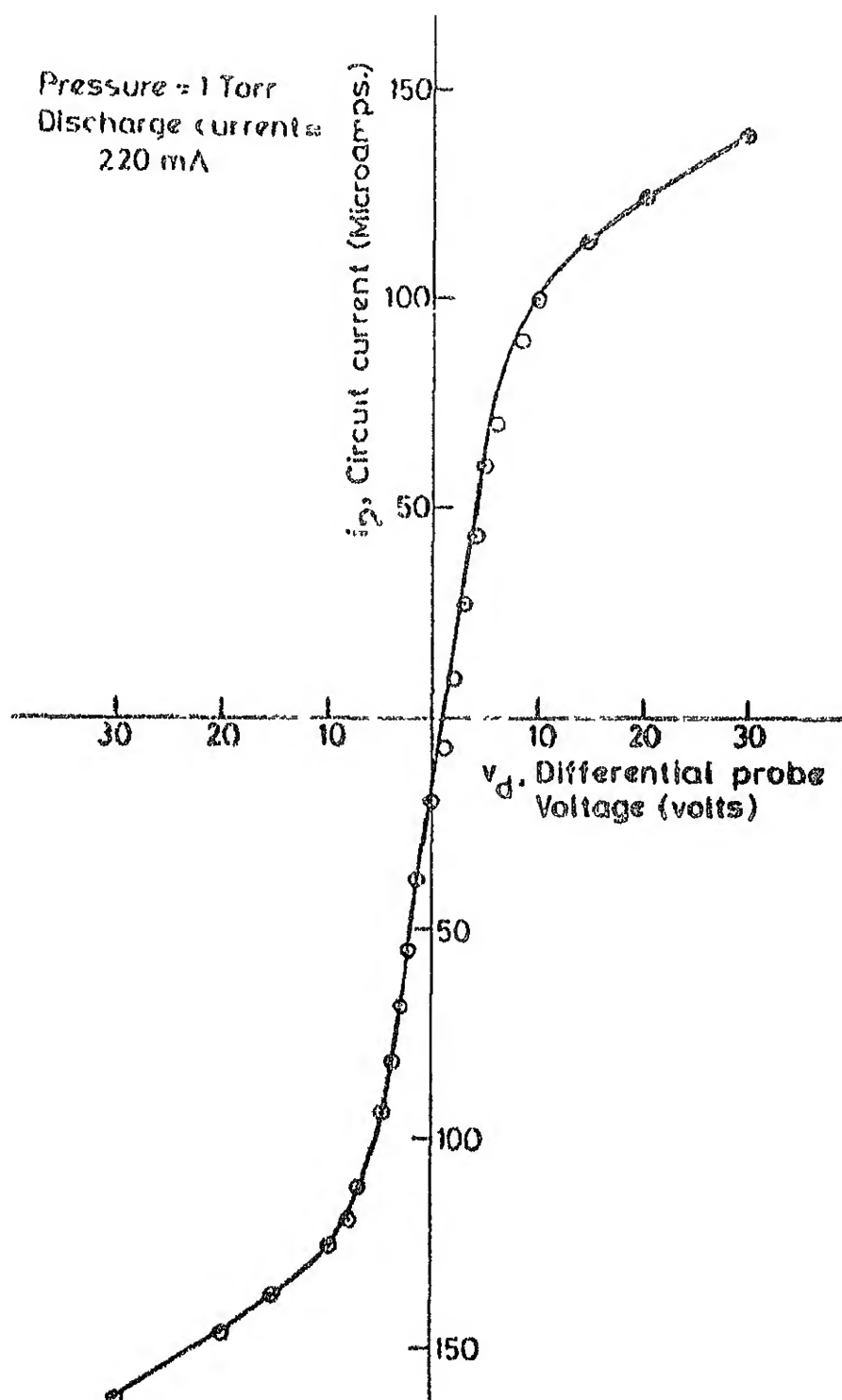


Fig. 3.7 DOUBLE PROBE CHARACTERISTICS AT 1 TORR PRESSURE, 220 mA DISCHARGE CURRENT, AND 15 cm INTERELECTRODE DISTANCE

Table 3.1 Diagnostic Data Using Double Probe

Distance between the electrode: 5 cm; Probe position: 2.5 cm from either electrode							
<u>Pressure (Torr)</u> <u>Flow (Arb. Unit)</u>	<u>I</u> mA	<u>V</u> Volts	<u>I x V</u> Watts	<u>kT_e</u> (eV)	<u>n_e</u> (10 ¹⁰ cm ⁻³)	<u>kT_e x n_e</u> (10 ¹⁰ eV cm ⁻³)	
	2	3	4	5	6	7	
<u>1.0</u> <u>1.8</u>	90±5	460±11	41.4±2	3.50±0.08	1.97±0.12	6.90±0.14	
	140±7	460±11	64.4±2	2.98±0.07	3.02±0.20	9.00±0.18	
	220±11	460±11	101.2±3	2.85±0.07	4.75±0.31	13.53±0.27	
<u>1.5</u> <u>2.1</u>	90±5	550±13	49.5±2	3.31±0.08	3.18±0.21	10.52±0.21	
	140±7	520±13	72.8±3	3.09±0.07	4.77±0.31	14.74±0.29	
	220±11	500±12	110.0±4	2.40±0.06	8.82±0.57	21.17±0.42	
<u>2.0</u> <u>2.2-2.3</u>	90±5	600±15	54.0±2	3.33±0.08	3.07±0.20	10.23±0.20	
	140±7	560±14	78.4±3	3.11±0.07	5.05±0.33	15.69±0.31	
	220±11	540±13	118.8±4	2.35±0.05	10.91±0.71	25.80±0.51	

...contd.

Table 3.1 (contd.)

1	2	3	4	5	6	7
$\frac{2.5}{2.4}$	90 \pm 5	650 \pm 16	58.5 \pm 2	3.16 \pm 0.08	3.05 \pm 0.20	9.64 \pm 0.19
	140 \pm 7	620 \pm 15	86.8 \pm 3	2.81 \pm 0.07	5.69 \pm 0.30	15.74 \pm 0.31
	220 \pm 11	580 \pm 14	127.6 \pm 4	2.58 \pm 0.06	9.22 \pm 0.60	23.77 \pm 0.47
<hr/>						
$\frac{3.0}{2.5}$	90 \pm 5	700 \pm 17	63.0 \pm 2	3.12 \pm 0.07	2.84 \pm 0.18	8.85 \pm 0.18
	140 \pm 7	660 \pm 16	92.4 \pm 3	2.65 \pm 0.06	5.26 \pm 0.34	13.94 \pm 0.28
	220 \pm 11	620 \pm 15	136.4 \pm 5	2.44 \pm 0.06	9.44 \pm 0.61	22.42 \pm 0.45

Table 3.2 Diagnostic Data Using Double Probe

Distance between the electrode: 10 cm. Probe position: 5 cm from either electrode							
Pressure (Torr) Flow (Arb. Unit)	I mA	V Volts	I x V Watts	kT _e (eV)	n _e (10 ¹⁰ cm ⁻³)	kT _e x n _e (eV cm ⁻³)	
1	2	3	4	5	6	7	
1.0	90±5	540±13	48.6±2	3.28±0.08	3.78±0.25	12.42±0.25	
1.8	140±7	520±13	72.8±3	2.98±0.08	5.56±0.36	16.62±0.33	
	220±11	510±13	112.2±4	2.65±0.07	8.41±0.55	21.85±0.43	
1.5	90±5	625±15	56.2±2	3.41±0.09	3.71±0.24	12.63±0.25	
2.1	140±7	610±15	85.4±3	3.32±0.08	5.55±0.36	18.42±0.37	
	220±11	600±15	132.0±5	2.96±0.07	8.05±0.52	23.93±0.48	
2.0	90±5	900±22	81.0±3	4.61±0.11	1.81±0.12	8.31±0.16	
2.2-2.3	140±7	850±21	119.0±4	3.65±0.09	4.05±0.26	14.79±0.30	
	220±11	800±20	176.0±6	2.65±0.07	6.99±0.45	18.54±0.37	

....contd.

Table 3.2 (contd.)

1	2	3	4	5	6	7
$\frac{2.5}{2.4}$	90 ± 5	1050 ± 26	94.5 ± 3	4.63 ± 0.11	1.84 ± 0.12	8.52 ± 0.17
	140 ± 7	950 ± 23	133.0 ± 4	3.98 ± 0.10	3.61 ± 0.23	14.4 ± 0.29
	220 ± 11	900 ± 23	198.0 ± 7	3.06 ± 0.08	5.80 ± 0.37	17.7 ± 0.35
$\frac{3.0}{2.5}$	90 ± 5	1200 ± 30	108.0 ± 4	4.92 ± 0.12	1.59 ± 0.10	7.8 ± 0.10
	140 ± 7	1100 ± 27	154.0 ± 6	3.62 ± 0.09	4.89 ± 0.32	14.85 ± 0.30
	220 ± 11	1050 ± 26	231.8 ± 0	2.81 ± 0.07	6.22 ± 0.40	17.4 ± 0.35

Table 3.3 Diagnostic Data Using Double Probe

Distance between the electrodes: 15 cm; Probe position: 7.5 cm from either electrode							
Pressure (Torr) Flow (Arb. Unit)	I mA	V Volts	I x V watts	kT_e (eV)	n_e (10^{10} cm^{-3})	$kT_e \times n_e$ (eV cm^{-3})	
	2	3	4	5	6	7	
1.0 1.8	90 \pm 5 140 \pm 7 220 \pm 11	900 \pm 23 750 \pm 19 660 \pm 17	81.0 \pm 3 105.0 \pm 4 142.5 \pm 5	4.52 \pm 0.11 3.39 \pm 0.09 2.71 \pm 0.07	1.90 \pm 0.12 3.43 \pm 0.22 7.46 \pm 0.49	8.58 \pm 0.17 11.63 \pm 0.23 20.21 \pm 0.40	
1.5 2.1	90 \pm 5 140 \pm 7 220 \pm 11	1000 \pm 25 825 \pm 21 750 \pm 19	90.0 \pm 3 115.0 \pm 4 165.0 \pm 6	4.86 \pm 0.12 3.74 \pm 0.09 3.61 \pm 0.09	1.88 \pm 0.12 3.36 \pm 0.21 5.60 \pm 0.36	9.13 \pm 0.18 12.56 \pm 0.25 20.21 \pm 0.40	
2.0 2.2	90 \pm 5 140 \pm 7 220 \pm 11	1150 \pm 29 950 \pm 24 800 \pm 20	101.2 \pm 4 133.0 \pm 5 181.5 \pm 6	3.94 \pm 0.10 3.88 \pm 0.10 3.48 \pm 0.09	2.27 \pm 0.15 3.11 \pm 0.20 5.61 \pm 0.37	8.94 \pm 0.18 12.06 \pm 0.24 19.52 \pm 0.39	

...contd.

Table 3.3 (contd.)

1	2	3	4	5	6	7
2.5	90±5	1300±33	119.0±4	4.23±0.11	1.91±0.12	8.07±0.16
2.4	140±7	1075±27	154.0±5	3.75±0.09	3.49±0.23	13.08±0.26
	220±11	1050±26	225.0±8	3.60±0.09	6.46±0.42	23.25±0.47
3.0	110±5	1400±36	154.0±5	4.21±0.09	2.20±0.15	9.43±0.18
2.5-2.6	140±7	1325±33	185.0±7	3.78±0.10	2.78±0.18	10.50±0.21
	220±11	1200±30	275.0±10	3.57±0.09	6.30±0.41	22.49±0.45

temperature in general varied directly as the discharge voltage and inversely as both the discharge current and total power input; (ii) The electron density varied directly as the discharge current and power, and inversely as discharge voltage; (iii) The product of the electron density and the electron temperature ($n_e k T_e$) varied directly as the discharge current and power; (iv) The product of the electron density and the electron temperature ($n_e k T_e$) except at low currents, initially increased with pressure and at higher pressures either remained steady or increase by a small extent.

In the discharge tube with interelectrode spacing of 15 cm the glow was always pink in colour (Table 3.4), but was always pale yellow in the tube with 5 cm interelectrode spacing. In the case where the interelectrode spacing was 10 cm, the glow was generally pale yellow in colour except at pressures 2.0, 2.5, and 3.0 Torr and discharge current of 90 mA, when the glow had pink tinge. Qualitative relations between the plasma parameters and visual appearance of the glow could be made by comparing Tables 3.1-3.3 and Table 3.4.

3.4 Wall Temperature Data

The results of the temperature measurements, using the Chromel-Alumel thermocouple, on the outer side of the glass wall in the discharge section are presented in the Table 3.5. It can be seen that the wall temperature changed directly as power dissipated and the interelectrode distance.

Table 3.4 Visual Appearance of the Glow

Pressure Torr	I (mA)	Electrode Spacing: 5 cm		Electrode Spacing: 10 cm		Electrode Spacing: 15 cm	
		Watts		Watts		Watts	
		3	4	5	6	7	8
1.0	90	41.4	Yellow	48.6	Yellow	81.0	Pink
	140	64.4	Yellow	72.8	Yellow	105.0	Pink
	220	101.4	Yellow	112.2	Yellow	142.0	Pink white
1.5	90	49.5	Yellow	56.2	Pink	90.0	Pink
	140	72.8	Yellow	85.4	Yellow	115.0	Pink
	220	110.0	Yellow	132.0	Yellow	165.0	Pink white
2.0	90	54.0	Yellow	81.0	Pink	101.2	Pink
	150	78.4	Yellow	119.0	Yellow	133.0	Pink
	220	118.8	Yellow	176.0	Yellow	181.0	Pink white

...contd.

Table 3.4 (contd.)

1	2	3	4	5	6	7	8
2.5	90	58.5	Yellow	94.5	Pink	119.0	Pink
	140	86.8	Yellow	133.0	Yellow	154.0	Pink
	220	127.6	Yellow	198.0	Yellow	225.0	Pink white
3.0	110	63.0	Yellow	108.0	Pink	154.0	Pink
	140	92.4	Yellow	154.0	Yellow	185.0	Pink
	220	136.4	Yellow	231.0	Yellow	275.0	Pink white

Table 3.5 Wall Temperature Data

Pressure Torr Flow (Arbit. Unit)	DISTANCE BETWEEN ELECTRODES											
	5 cm				10 cm				15 cm			
	I mA	V Volts	IV Watts	Wall Temp. (°K)	I mA	V Volts	IV Watts	Wall Temp. (°K)	I mA	V Volts	IV Watts	Wall Temp. (°K)
1.0 1.8	90	460	41.4	302	90	540	48.6	303	90	900	91	328
	140	460	64.4	316	140	520	72.8	325	140	750	105	340
	220	460	101.2	338	220	510	112.2	348	220	660	142	357
2.0 2.2- 2.3	90	600	54.0	316	90	900	81.0	331	90	1150	101	331
	140	560	78.4	316	140	850	119.0	340	140	950	133	343
	220	540	118.8	335	220	800	176.0	353	220	220	181	363
3.0 2.5	90	700	63.0	316	90	1200	105.0	333	90	1400	154	345
	140	660	52.4	318	140	1100	159.0	343	140	1325	185	353
	220	620	136.4	326			231.0	353	220	1200	275	-

3.5 Total Intensity Measurements of the Afterglow

The experimental observations are presented in Table 3.6 and Figs. 3.8 - 3.10. This includes the total intensity measurements of the afterglow carried out using RCA 1P28 photomultiplier using all the three discharge tubes and the entire range of pressures and discharge currents.

It can be seen that (i) the intensity of the afterglow was maximum when interelectrode distance was 15 cm, and minimum when the interelectrode distance was 5 cm; (ii) the afterglow intensity is low in the cases where the glow colour is pale yellow. In general, the intensities, for a given interelectrode distance and at a given discharge current, increases with pressure; (iii) the intensities also increased with increasing power input, and clearly observed in the case of interelectrode distance 15 cm when the glow was consistently pink.

3.6 Effect of Variations in the Flow Rate

The results on the afterglow radiation intensity measured when the flow rate was reduced by constricting the foreline valve are presented in Fig. 3.11 and 3.12.

3.7 NO Titration Data

The results of titration of N atoms by NO are presented in Fig. 3.13. On the NO input axis, the numbers represent readings on the rotary dial of the NO flow control valve (larger number presents greater flow).

Table 3.6 Total Intensity Measurements of Afterglow (Photomultiplier Data)

Pressure Torr Flow (Arbit. Unit)	DISTANCE BETWEEN ELECTRODES														
	5 cm					10 cm					15 cm				
	I mA	V Watts	IV Watts	PMT Volts	I mA	V Watts	IV Watts	PMT Volts	I mA	V Watts	IV Watts	PMT Volts	I mA	V Watts	IV Watts
1	2	3	4	5	6	7	8	9	10	11	12	13			
1.0	90	460	41.4	0.06±0.02	90	540	48.6	0.42±0.5	90	900	91	2.0±0.5			
1.8	140	460	64.4	0.14±0.02	140	520	72.8	0.46±0.5	140	750	105	3.0±0.5			
	220	460	101.2	0.20±0.02	220	510	112.2	0.50±0.5	220	660	142	5.2±0.5			
1.5	90	550	49.5	0.20±0.02	90	625	56.2	0.50±0.5	90	1000	90	7.0±0.5			
2.1	140	520	72.8	0.30±0.02	140	610	85.4	0.56±0.1	140	825	115	6.0±0.5			
	220	500	110.0	0.50±0.02	220	600	132.0	0.64±0.1	220	750	165	10.0±1.0			
2.0	90	600	54.0	0.20±0.02	90	900	81.0	4.00±0.5	90	1150	101	10.0±1.0			
2.2-	150	560	78.4	0.30±0.02	140	850	119.0	2.50±0.5	140	950	133	13.0±1.0			
2.3	220	540	118.8	0.50±0.05	220	800	176.0	2.70±0.0	220	800	181	18.0±2.0			

...contd.

Table 3.6 (contd.)

1	2	3	4	5	6	7	8	9	10	11	12	13
<u>2.5</u> <u>2.4</u>	90	650	58.5	0.2±0.02	90	1050	94.5	4.3±0.5	90	1300	119	30.0±3.0
	140	620	86.8	0.4±0.02	140	950	113.0	2.0±0.3	140	1075	154	54.0±5.0
	220	580	127.6	0.8±0.05	220	900	198.0	2.3±0.3	220	1050	225	72.0±5.0
<hr/>												
<u>3.0</u> <u>2.5</u>	90	700	63.0	0.5±0.05	90	1200	108.0	4.4±0.5	90	1400	154	35.0±3.0
	140	660	92.4	0.6±0.05	140	1100	159.0	3.2±0.5	140	1325	185	68.0±5.0
	220	620	136.4	1.0±0.10	220	1050	231.0	3.0±0.5	220	1200	275	80.0±5.0

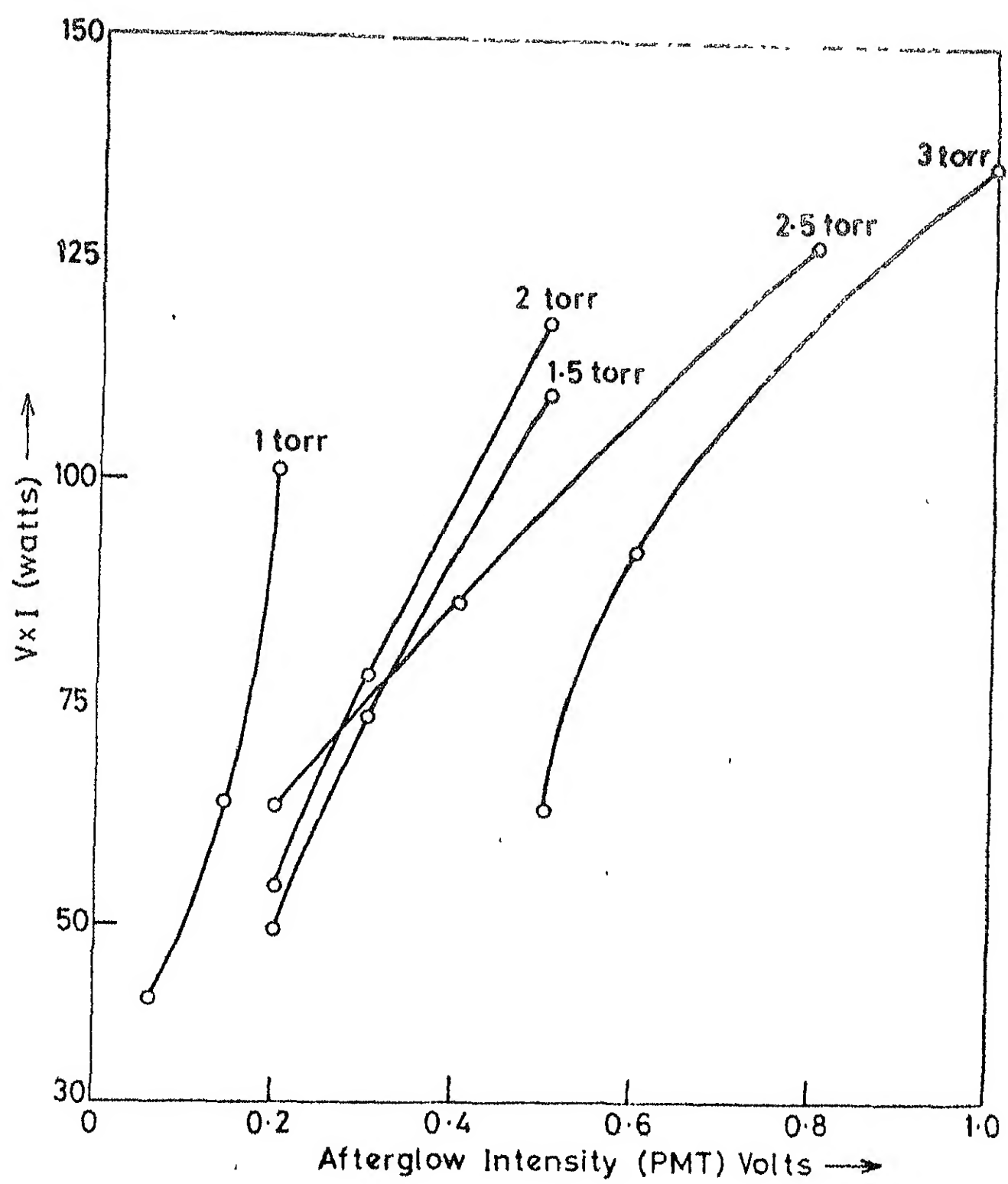


Fig. 3.8 VI vs AFTERGLOW INTENSITY (INTERELECTRODE DISTANCE 5 cm)

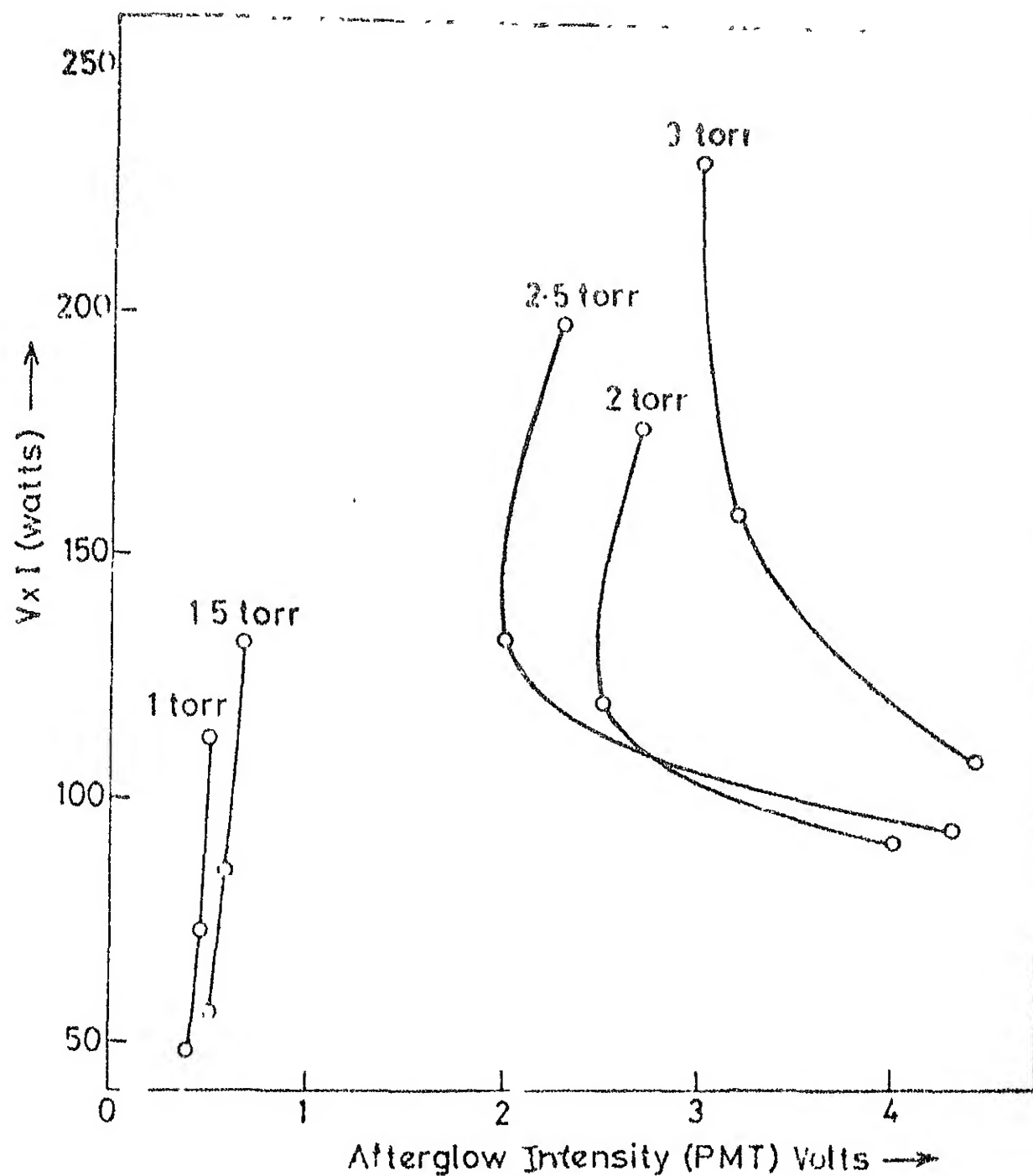


Fig. 3.9 $V I$ vs AFTERGLOW INTENSITY (INTERELECTRODE DISTANCE 10 cm)

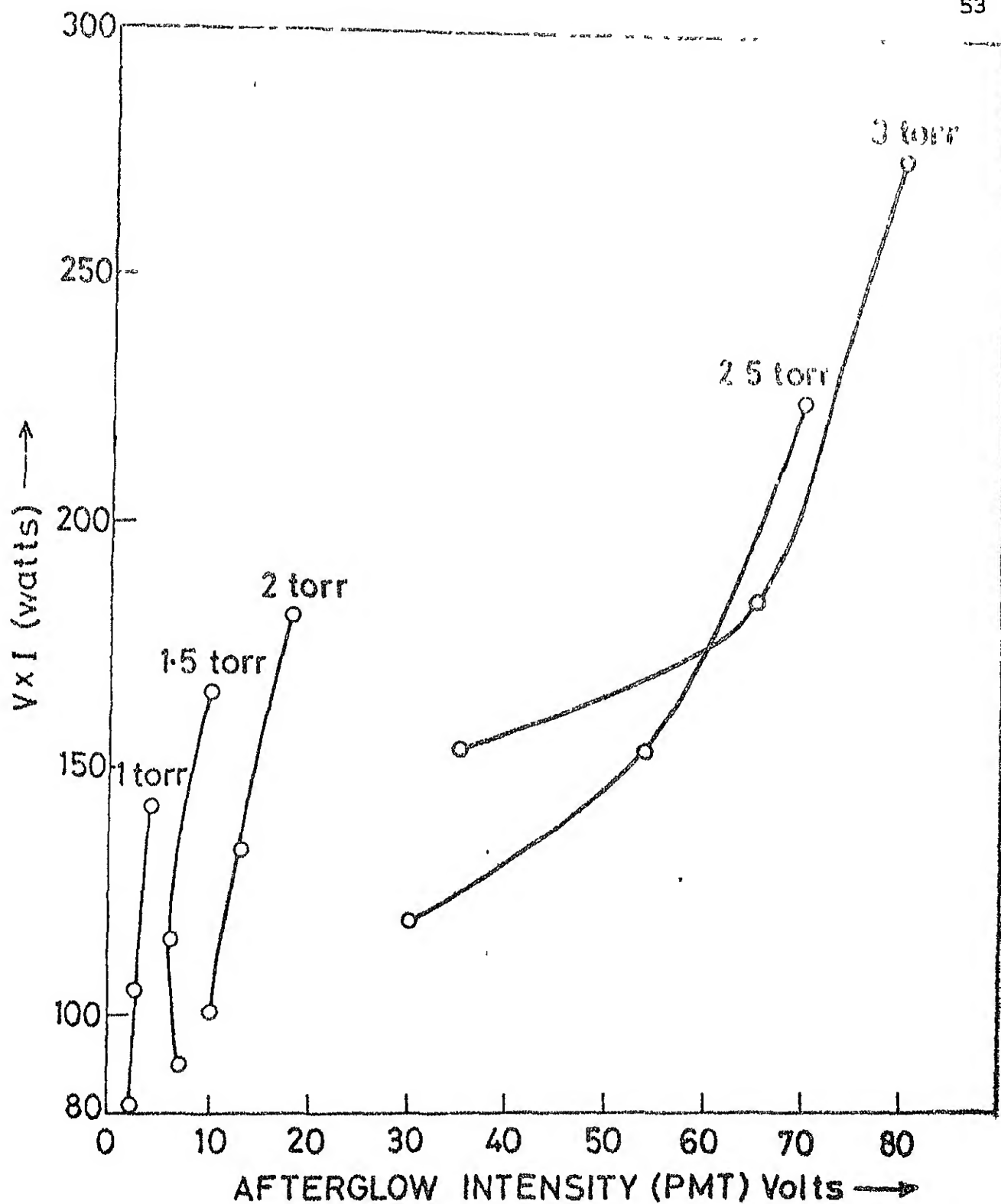


Fig. 3.10 VI vs AFTERGLOW INTENSITY (INTERELECTRODE DISTANCE 15 cm)

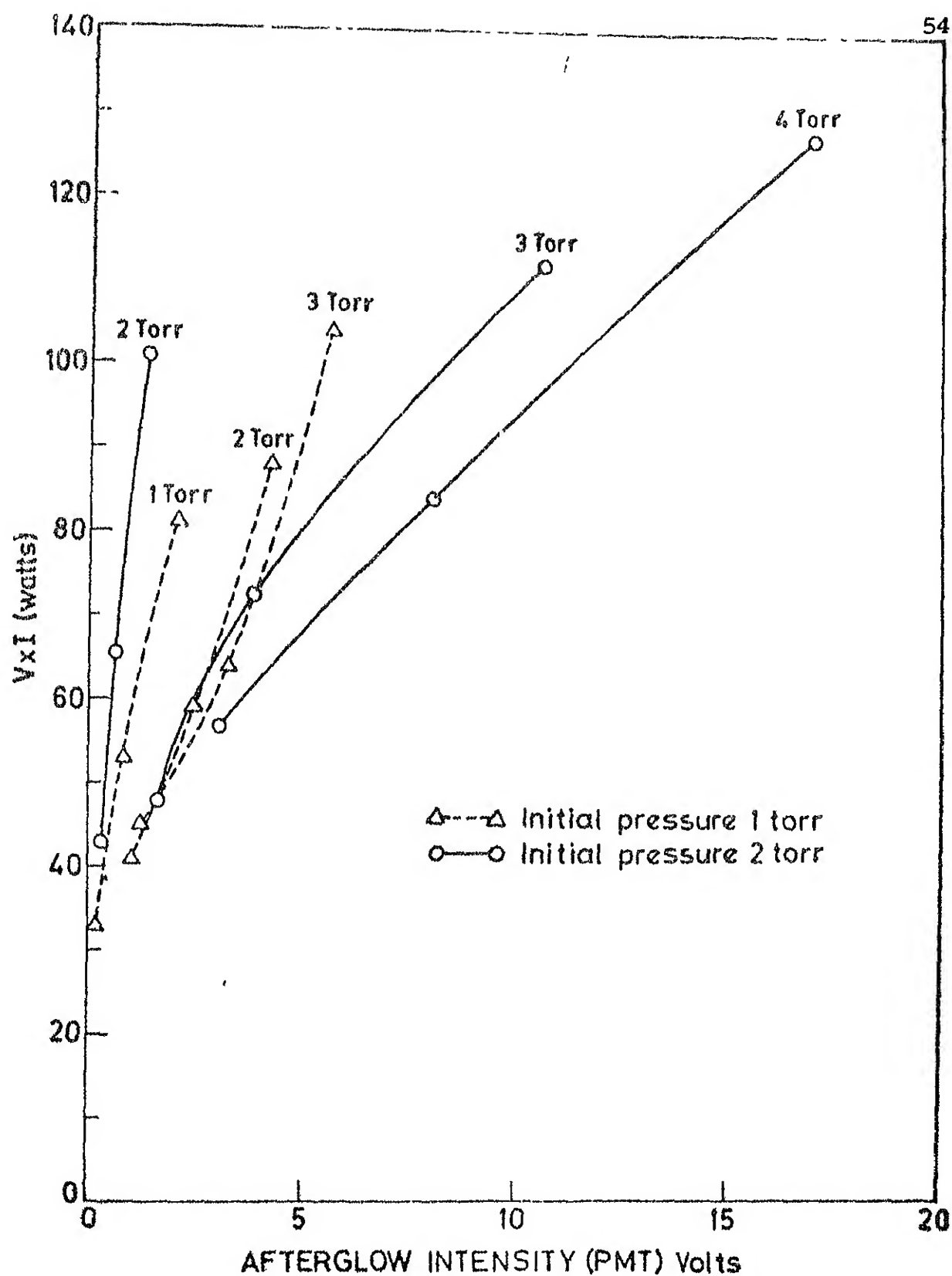


Fig. 3.11 VI vs AFTERGLOW INTENSITY MEASUREMENTS AT DIFFERENT PRESSURES REALIZED BY PARTIALLY CLOSING THE BUTTERFLY VALVE (INTERELECTRODE DISTANCE 5 cm)

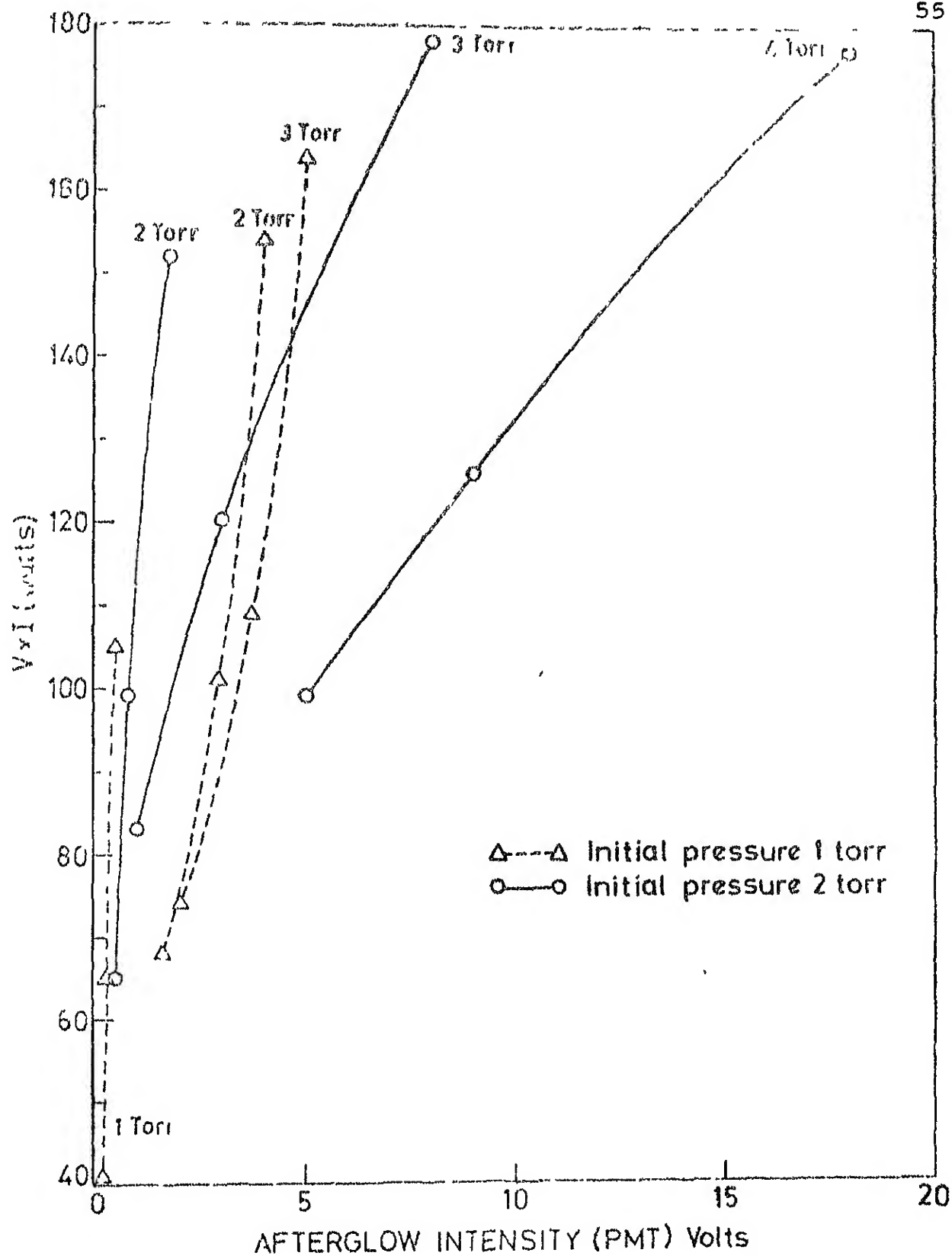


Fig. 3.12 VI vs AFTERGLOW INTENSITY MEASUREMENTS AT DIFFERENT PRESSURES OBTAINED BY PARTIALLY CLOSING THE BUTTERFLY VALVE (INTERELECTRODE DISTANCE 10 cm)

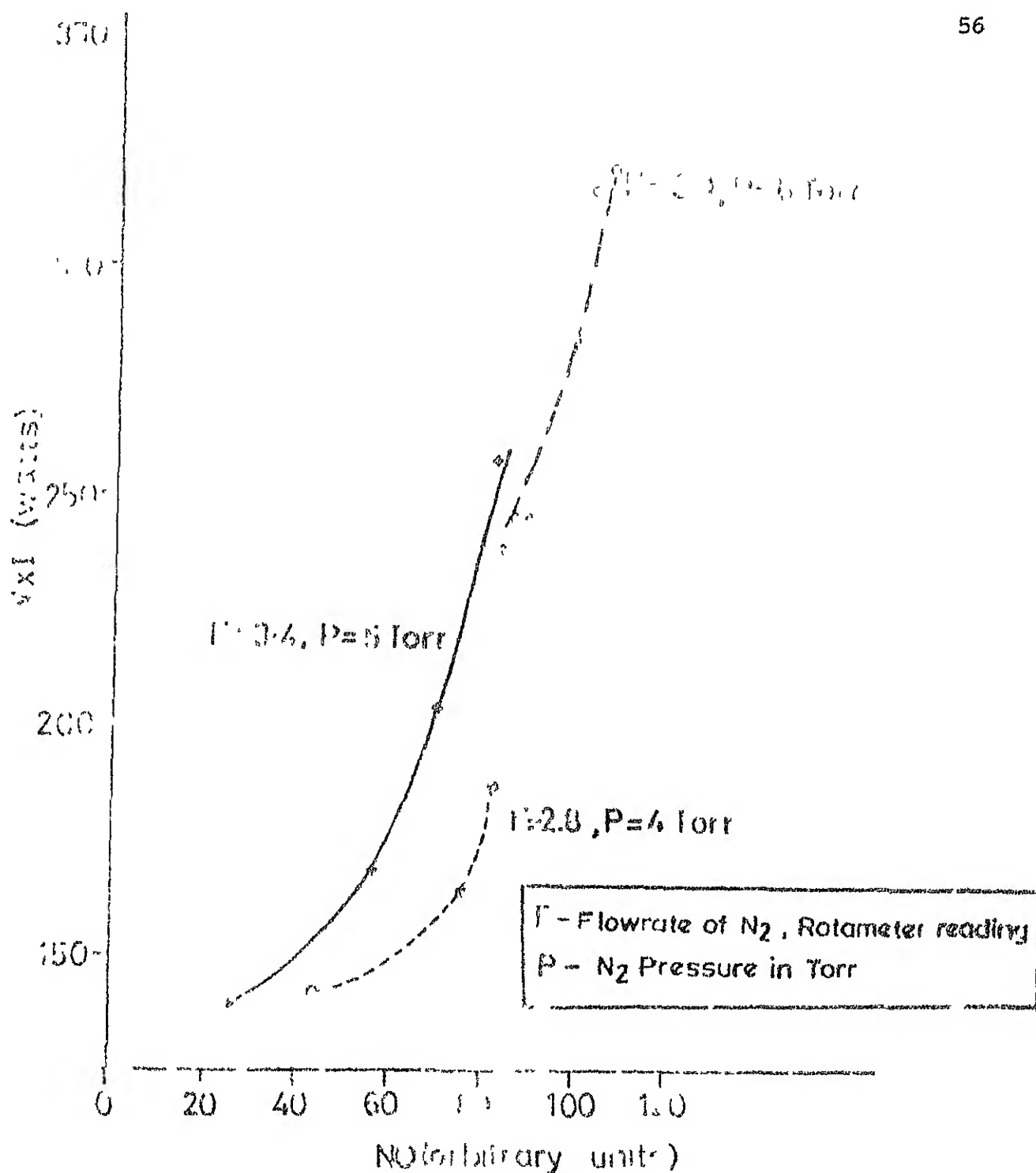


Fig. 3.13 NITRIC OXIDE FLOW NEEDED TO TITRATE THE N ATOMS TO THE END POINT (ABSCISSA SCALE REPRESENTS THE NEEDLE VALVE OPENING)

CHAPTER 4

DISCUSSION

The objective of the present chapter is to examine the experimental results, that is, the $n_e \cdot kT_e$ data, the afterglow radiation intensity data, and the NO titration data, in the perspective of atomic processes that are expected to be present in the plasma. At the pressure range of the experiments the contribution from collisions between the heavy-particles would be relatively minor to the total population of the excited states and hence to the observed phenomena, and one could expect the electron impact processes to dominate. We intend to particularly examine to what extent the N atom concentration as estimated from experimental results could be explained in terms of the electron impact dissociation and the atom recombination processes.

4.1 Present Knowledge About Electron Impact Dissociation

There have been a large number of studies of electron scattering¹⁵⁻²² as well as extreme ultraviolet absorption measurements²³⁻²⁹ on nitrogen to examine the excitation and dissociation processes. It has been shown that molecular nitrogen possesses a large number of valence and Rydberg states in the energy range 11.5 - 40.0 eV. Implications of the existence of these states have also been examined on auroral ion chemistry.³⁰⁻³² Several groups have carried out detailed measurements of extreme ultraviolet spectrum of the aurora and dayglow, and have concluded that the molecular nitrogen does not contribute significantly to the observed extreme ultraviolet flux.^{33,34} The field observations have been in complete disagreement with the results anticipated from inelastic electron scattering spectrum of N_2 and from auroral energy considerations.³⁵

Recently Zipf and McLaughlin³⁶ have done some laboratory experiments which indicate that most N_2 molecules excited to the manifold of singlet states are depopulated by predissociation and not by extreme ultraviolet photons as previously assumed. This process is the major path by which N_2 is dissociated by solar extreme ultraviolet absorption and by electron impact. Their high resolution emission and absorption data showed very clearly that the N_2 singlet bands were strongly perturbed by both homogeneous and heterogeneous interactions, that many bands were cut off at high J values, and that

individual rotational lines were often broadened. Furthermore a comparison of emission and absorption data showed that a number of optically allowed transitions were absent in the photographic emission data suggesting that predissociation competes effectively with radiation in depopulating these states. Since these observations generally involved the use of optically thick sources where entrapment effects could enhance the apparent efficiency of an otherwise weak predissociation process, the predissociation branching ratio (i.e., the fraction of excitations of the vibrational level v' of the electronic term k that predissociate) as given by

$$B_{v',k} = \frac{I_{v',k}}{A_{v',k} + I_{v',k} + AI_{v',k} + S_{v',k}}$$

where $I_{v',k}$ is the spontaneous predissociation rate, $A_{v',k}$ is the total rate for spontaneous radiative transitions, $AI_{v',k}$ is the rate for spontaneous autoionization and $S_{v',k}$ the rate at which the level is collisionally quenched, could not be quantitatively evaluated (for other relevant work, see ref.20).

Hudson and Carter³⁷ were the first to recognize that this forbidden predissociation process might be very efficient in general. The absolute measurements described in the work of Zipf and McLaughlin support this view. We shall use the cross sections obtained by these latter workers.

These authors³⁶ find that the cross sections shown here are in good agreement with the surface absorption result of Winters³⁸ and Niehaus.³⁹

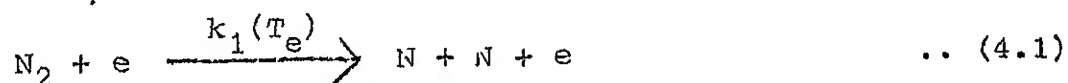
The total cross section for N_2 dissociation obtained by Zipf and McLaughlin are given in Fig. 4.1(a) and the same values are presented in Table 4.1.

The dissociation rate coefficient obtained after integration of the cross sections over Maxwellian kinetic energy distribution of electrons is shown in Fig. 4.1(b).

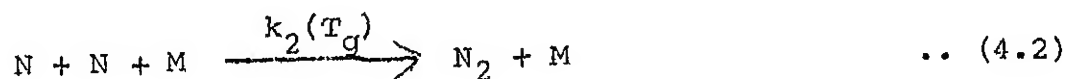
4.2 A Model of the Dissociation and Recombination Processes

A simple theoretical model for dissociation of nitrogen in glow plasmas can be constructed using a minimum number of processes, viz., electron impact dissociation of nitrogen molecules into atoms, and both volume and surface recombination of nitrogen atoms. These processes can be expressed as follows:

(i) electron impact dissociation:



(ii) three-body gas phase recombination:



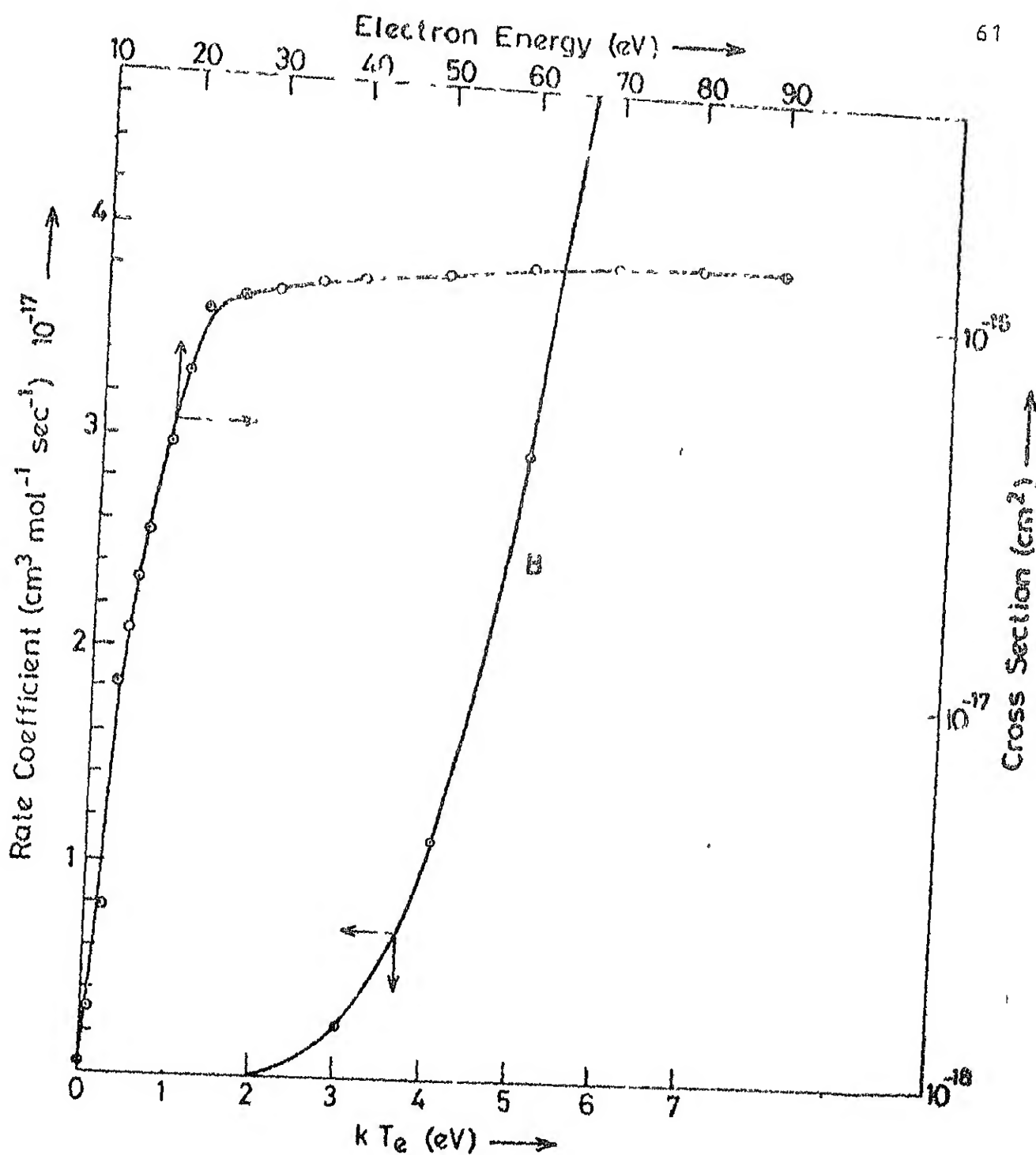


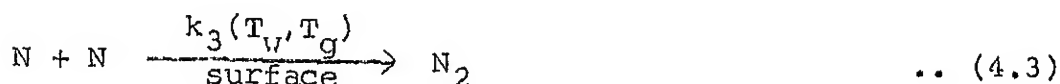
Fig. 4.1 (a) PLOT OF TOTAL DISSOCIATION CROSS SECTION vs ELECTRON ENERGY³⁶

(b) PLOT OF THE RATE COEFFICIENT vs ELECTRON TEMPERATURE (kT_e)

Table 4.1 Total Cross Section for the Dissociation of N_2
by Electron Impact³⁶

Energy	Optically thin cross section	Optically thick cross section
10.0	1.27(-18)	1.27(-18)
10.5	1.87(-18)	1.87(-18)
11.0	2.49(-18)	2.49(-18)
12.0	4.92(-18)	4.92(-18)
13.0	1.10(-17)	1.12(-17)
14.0	2.35(-17)	2.43(-17)
15.0	3.36(-17)	3.58(-17)
16.0	4.41(-17)	4.75(-17)
18.0	6.23(-17)	6.82(-17)
20.0	7.74(-17)	8.56(-17)
22.0	9.46(-17)	1.05(-16)
26.0	1.21(-16)	1.36(-16)
30.0	1.39(-16)	1.58(-16)
35.0	1.50(-16)	1.72(-16)
40.0	1.59(-16)	1.83(-16)
50.0	1.75(-16)	2.03(-16)
60.0	1.86(-16)	2.16(-16)
70.0	1.94(-16)	2.24(-16)
80.0	1.97(-16)	2.27(-16)
90.0	1.98(-16)	2.27(-16)
100.0	1.96(-16)	2.24(-16)

(iii) surface recombination:



where T_g represents the gas temperature and T_w represents the wall temperature. The rate equation expressed in terms of N atom concentration is therefore given by:

$$\begin{aligned} \frac{d[N]}{dt} = & k_1(T_e)[N_2]n_e - k_2(T_g)[N]^2[N_2] \\ & - k_3(T_w, T_g)[N]^2 \end{aligned} \quad \dots (4.4)$$

In the steady state, the concentration of N atoms, therefore, is

$$[N] = \left\{ \frac{k_1(T_e)[N_2]n_e}{k_2(T_g)[N_2] + k_3(T_w, T_g)} \right\}^{1/2} \quad \dots (4.5)$$

which at the high pressure limit becomes

$$[N] = \{k_1(T_e)n_e\}^{1/2} \quad \dots (4.6)$$

and at the low pressure limit becomes

$$[N] = \left\{ \frac{k_1(T_e)[N_2]n_e}{k_3(T_w, T_g)} \right\}^{1/2} \quad \dots (4.7)$$

4.3 The Volume and the Surface Recombination Processes

We now examine the pattern of variation the N atom concentration may be expected to follow under the conditions of the present experiments. This could be done by substituting numerical values for the terms in the denominator of Eqn. (4.5).

Some data on volume and surface recombination of nitrogen atoms are given in Table 4.2.

Golde and Thrush⁴ recommend for the process $N + N + N_2$ the following rate coefficient:

$$10^{-33.2} \exp \{ (4.2 \pm 1.3) / 2 RT \} \text{ cm}^6 \text{ molecule}^{-2} \text{ s}^{-1} \quad \dots (4.8)$$

where RT is expressed in KJ mol^{-1} . At 300°K , RT has a value of 2.49 KJ mol^{-1} , and at 500°K , it has a value of 4.16 KJ mol^{-1} . The corresponding values of the rate coefficient therefore are

$$k_2 (300^\circ\text{K}) = 3.41 \times 10^{-33} \text{ cm}^6 \text{ molecule}^{-2} \text{ s}^{-1}$$

$$\text{and } k_2 (500^\circ\text{K}) = 1.74 \times 10^{-33} \text{ cm}^6 \text{ molecule}^{-2} \text{ s}^{-1}$$

At 1 torr, one therefore has

$$k_2 (300^\circ\text{K}) [N_2]_{300^\circ\text{K}} = 1.098 \times 10^{-16} \text{ cm}^3 \text{ molecule}^{-1} \text{ s}^{-1}$$

$$\text{and } k_2 (500^\circ\text{K}) [N_2]_{500^\circ\text{K}} = 3.360 \times 10^{-17} \text{ cm}^3 \text{ molecule}^{-1} \text{ s}^{-1}.$$

Table 4.2 Nitrogen Atom Recombination Data

M	k_2		k_3	γ	Wall material and method used	Ref.
	$(10^{-32} \text{ cm}^6 \text{ molec}^{-2} \text{ s}^{-1})$	$(10^{-15} \text{ cm}^3 \text{ molec}^{-1} \text{ s}^{-1})$				
1	2	3	4	5	6	
N ₂	0.79 ± 0.1	0.13 ± 0.5		Syrupy phosphoric acid, static	40	
N ₂	1.10 ± 0.4	0.40 ± 0.1		Pyrex, static	40	
Ar	2.30 ± 0.5	0.22 ± 0.6	5.0 x 10 ⁻⁸	Pyrex, static	40	
He	2.20 ± 0.2	0.06 ± 0.01	5.0 x 10 ⁻⁸	Pyrex, static	40	
N ₂ , Ar	0.76 ± 0.06	1.44	not detected	Pyrex, flow	41	
He	1.05 ± 0.2	1.44	not detected	Pyrex, flow	41	
N ₂	0.96 ± 0.3	1.70	10 ⁻⁶	Pyrex, flow	42	
N ₂	0.75 ± 0.05	0.17	10 ⁻⁶	Metaphosphoric acid, flow	42	
N ₂ , Ar	1.05	0.002	5.0 x 10 ⁻⁷	Stainless steel, static	43	
He	0.91	-	-	Stainless steel, static	43	
N ₂	1.40 ± 0.5	not detected	2.0 x 10 ⁻⁵	Pyrex, flow	44	
N ₂	0.60 ± 0.3	2.7	7.0 x 10 ⁻⁶	Fused silica, flow	45	
			5.5 x 10 ⁻⁴			

...contd.

Table 4.2 (contd.)

1	2	3	4	5	6
N ₂	2.30 ± 0.9	2.8	5.0 x 10 ⁻⁷ 5.0 x 10 ⁻⁶	Teflon, flow	45
N ₂	2.25 ± 0.2	0.35	2.0 x 10 ⁻⁷	Fused silica, static	45
N ₂	1.57 ± 0.2		1.5 x 10 ⁻⁵	Pyrex, flow	46
Ar	0.78 ± 0.08			Pyrex, flow	46
He	0.23			Pyrex, flow	46
N ₂	0.30 ± 0.8		3.0 x 10 ⁻⁵	Pyrex, flow	47
N ₂ , Ar	3.44 ± 0.4			Pyrex, flow	48
N ₂	2.90 ± 0.5		7.5 x 10 ⁻⁵	Pyrex flow	48

In comparison, k_3 from Table 4.2 has a value of $1.7 \times 10^{-15} \text{ cm}^3 \text{ molecule}^{-1} \text{ s}^{-1}$. Therefore the disappearance of N atom due to volume recombination may be neglected in comparison to surface recombination at 1 torr; only at about 10 torr region, the former may be expected to make substantial contribution. For the present purpose we may use the low pressure limiting expression for N atoms, that is, Eqn. (4.7).

4.4 Power Dissipated in the Plasma and n_e , KT_e Variations

The power dissipated in the plasma is given by the product of the plasma current and the voltage drop across the plasma column. These data for both glows and arcs have already been presented in Figs. 3.2 - 3.5.

While the electrical characteristics of a plasma have its origin in the fundamental atomic processes that take place in the plasma, the nature of this dependence is complex. Therefore, the I-V data is not directly usable for examining the atomic and molecular processes. In diffuse plasmas, where the electron impact processes usually dominate, the quantities that can be directly correlated with atomic processes are the electron density (n_e) and the electron energy distribution (specified by KT_e if there is an equilibrium distribution). One would, therefore, first be interested in the nature of relationship between I, V values and the corresponding n_e, KT_e values, n_e and KT_e

may be expected to bear a close relationship with I and V , respectively, and from this one could expect some relationship between the products $n_e kT_e$ and IV , the latter being the power dissipated in the plasma.

In Figs. 4.2 - 4.4 we present the experimentally obtained relationships between the $n_e kT_e$ and IV products for three discharge configurations that differ in interelectrode distances. The major observation is that there is indeed a broad direct relationship between the two products. In terms of detail, the ratios of the products depend on both the interelectrode distance and pressure.

4.5 N Atom Concentration from the Model

Since at the pressure range of the present experiments the contribution of the volume recombination is negligible, we need to consider only the contribution of the surface recombination which would be constant at a given wall and gas temperature. While the wall temperature will definitely undergo a certain change depending on the extent of recombination, as a first approximation we take it to be invariant and equal to the ambient temperature; we shall later comment on the effect on the results of a change in the wall temperature. Likewise, we assume that the gas inside the plasma tube is also at the ambient temperature. With these assumptions, the N atom

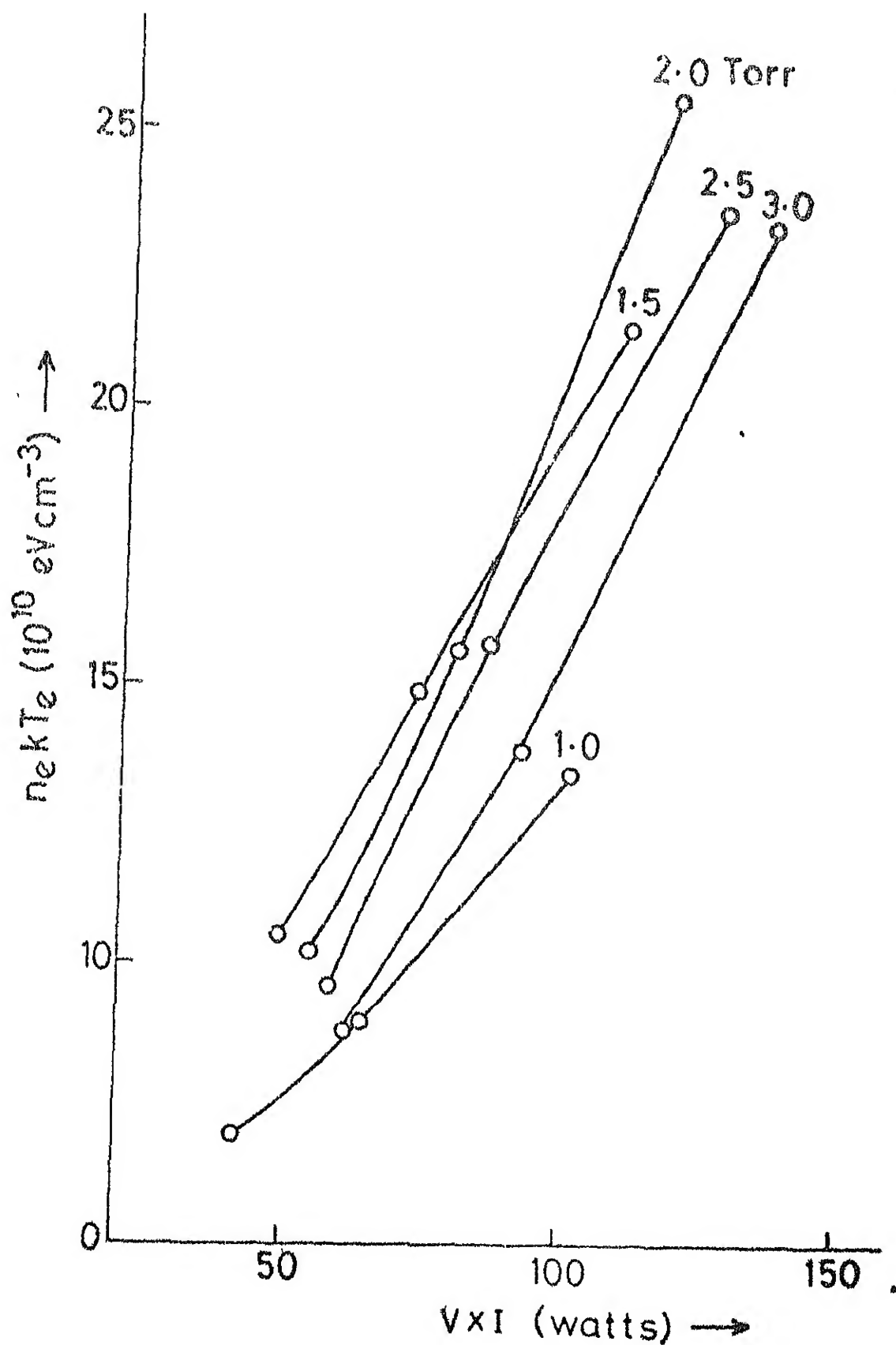


Fig. 4.2 PLOT OF THE PRODUCT OF ELECTRON TEMPERATURE AND DENSITY ($n_e k T_e$) vs $V I$ (POWER IN WATTS) (INTER-ELECTRODE DISTANCE 5 cm)

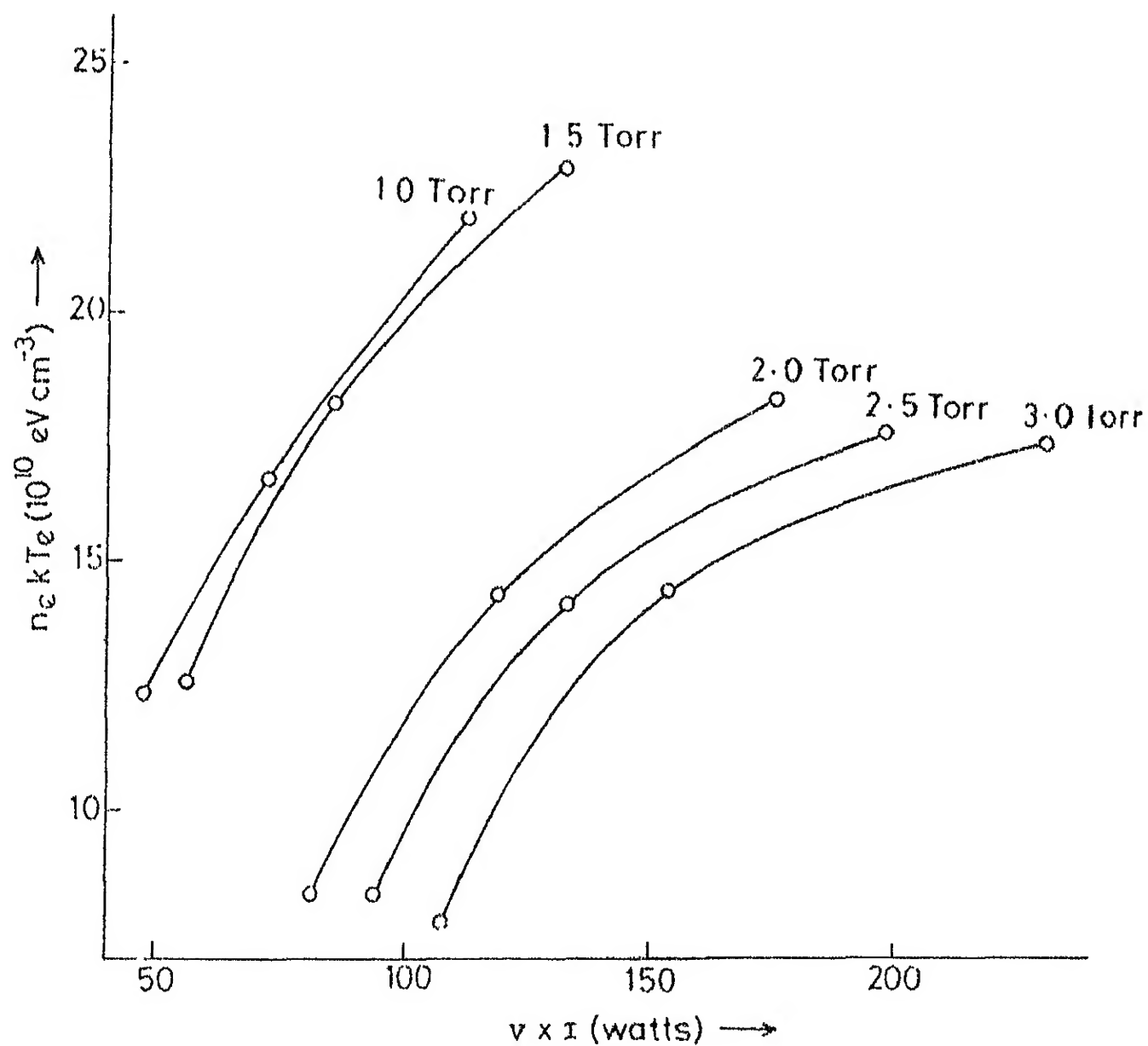


Fig. 4.3 PLOT OF THE PRODUCT OF ELECTRON TEMPERATURE AND DENSITY ($n_e k T_e$) vs $V I$ (POWER IN WATTS) (INTERPOLATED) ELECTRODE DISTANCE 10 cm)

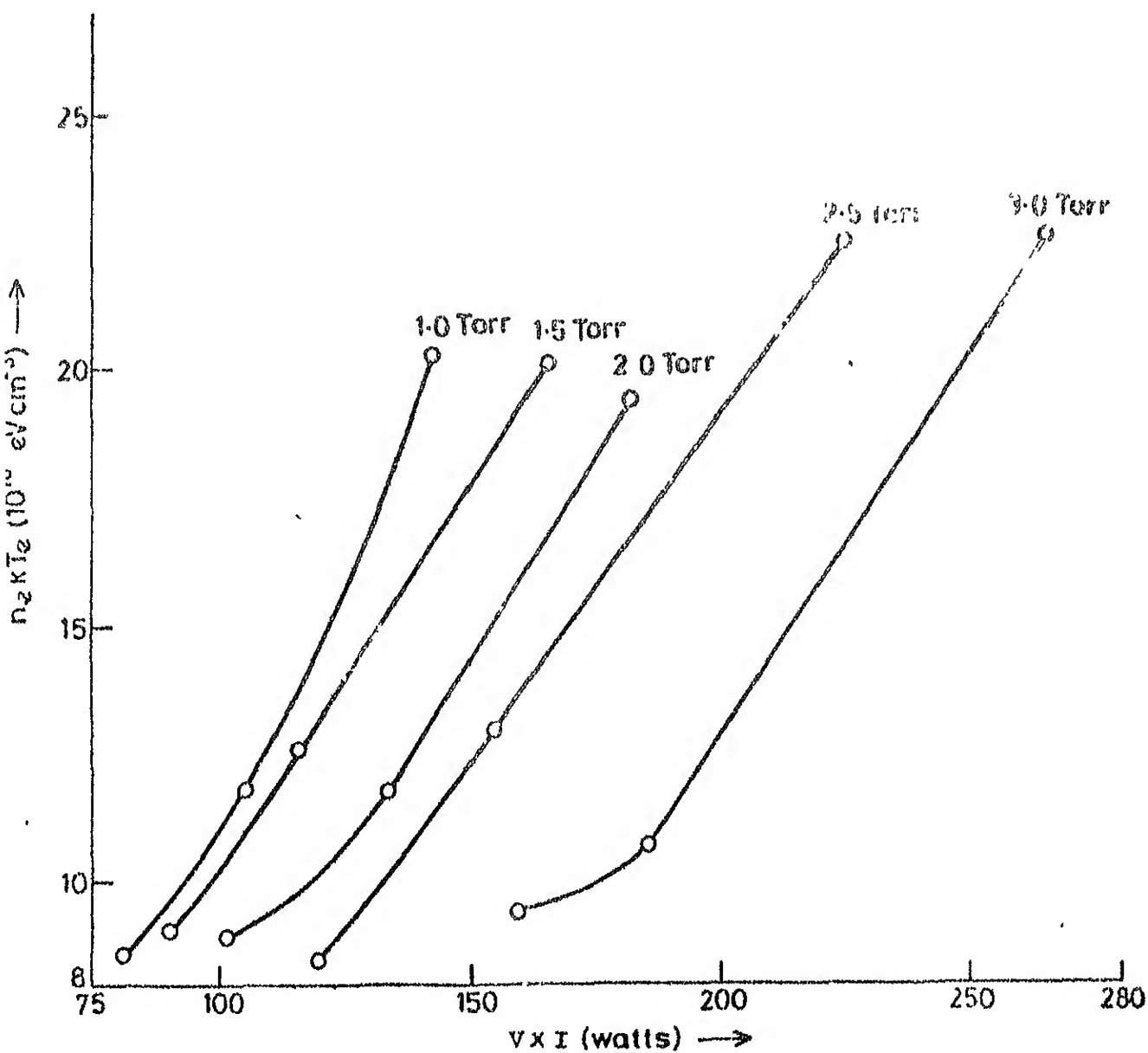


Fig. 4.4 PLOT OF THE PRODUCT OF ELECTRON TEMPERATURE AND DENSITY ($n_e k T_e$) v: VI (POWER IN WATTS) (INTERELECTRODE DISTANCE 15 cm)

concentration can be calculated directly from Eqn. (4.7) by evaluating the electron impact dissociation rate coefficient pertinent to the electron temperature of the plasma, and using relevant values of the density of N_2 molecules and that of the electrons.

n_e , kT_e data of the various plasma configurations and for a range of pressures have already been presented in Tables 3.1 - 3.3. The corresponding N atom density values, obtained by use of Eqn. (4.7), are presented in Tables 4.3 - 4.5. A plot of $k_1(T_e)$ values as a function of kT_e was already given in Fig. 4.1(b). $k_1(T_e)$ values corresponding to the kT_e values of the experiments are read off from this figure and entered into Tables 4.3 - 4.5. Evaluation of N atom density using Eqn. (4.7) and for k_3 a value of $\frac{1.7}{3.27} \times 10^{-15} \text{ cm}^3 \text{ molec}^{-1} \text{ sec}^{-1}$ then is straightforward. Plots of N atom density as a function of input power using the data from Tables 4.3 - 4.5 are shown in Figures 4.5 - 4.7.

4.6 Estimates of N Atom Density from Photomultiplier Data

A relative estimate of N atom density from experimental data can be made on the basis of photomultiplier signal data presented in Table 3.6, Figs. 3.8 - 3.10 and an assumption of a mechanism of radiation emission in the orange-yellow region, the spectral region that is seen by the photomultiplier when

Table 4.3 Nitrogen Atom Concentration From Model Using Electron Impact Dissociation and Surface Recombination

Distance between the electrodes: 5 cms; Probe position: 2.5 cms from either electrode							
I x V Watts	$n_e(10^{10})$ (cm ³)	kT_e (eV)	$k_1(T_e)$ (10 ⁻¹⁷) (cm ³ molec ⁻¹ s ⁻¹)	$n k_1(T_e)$ (10 ⁻⁷) (cm ⁶ molec ⁻¹ s ⁻¹)	$\sqrt{n} k_1(T_e)$ (10 ⁻⁴) (cm ³ molec ^{-1/2} s ^{-1/2})	(Constant x pressure) ^{1/2} $\times \sqrt{n} k_1(T_e)$ (10 ¹² cm ⁻³)	
	2	3	4	5	6	7	
<u>1.0 Torr</u>							
41.4	1.97	3.50	0.46	0.91±0.12	3.01±0.20	-	1.32±0.09
64.4	3.02	2.98	0.22	0.66±0.09	2.58±0.17		1.12±0.08
101.2	4.75	2.85	0.21	0.98±0.13	3.13±0.21		1.34±0.09
<u>1.5 Torr</u>							
49.5	3.18	3.31	0.36	1.14±0.15	3.34±0.22		1.80±0.12
72.8	4.77	3.09	0.31	1.48±0.19	3.85±0.26		2.04±0.14
110.0	8.82	2.40	0.09	0.79±0.10	2.81±0.19		1.46±0.09
<u>2.0 Torr</u>							
54.0	3.07	3.33	0.43	1.32±0.17	3.63±0.24		2.23±0.15
78.4	5.05	3.11	0.29	1.46±0.19	3.82±0.25		2.36±0.16
118.8	10.91	2.35	0.08	0.87±0.11	2.95±0.19		1.57±0.11

...contd.

Table 4.3 (contd.)

1	2	3	4	5	6	7
<u>2.5 Torr</u>						
58.5	3.05	3.16	0.31	0.98±0.12	3.13±0.21	2.11±0.14
86.8	5.69	2.81	0.20	1.14±0.15	3.37±0.22	2.30±0.16
127.6	9.22	2.58	0.10	0.92±0.12	3.04±0.20	2.09±0.14
<u>3.0 Torr</u>						
63.0	2.84	3.12	0.29	0.82±0.11	2.87±0.19	2.21±0.15
92.4	5.26	2.65	0.15	0.78±0.10	2.79±0.19	1.96±0.13
136.4	9.44	2.44	0.09	0.64±0.08	2.54±0.16	1.91±0.13

Table 4.4 Nitrogen Atom Concentration From Model Using Electron Impact Dissociation and Surface Recombination

Distance between the electrodes: 10 cms; Probe position: 5 cm from either electrode						
I x V Watts	$n_e(10^{10})$ (cm ³)	$k_1(T_e)$ (10 ⁻¹⁷) (cm ³ molec ⁻¹ s ⁻¹)	$n_e k_1(T_e)$ (10 ⁻⁷) (cm ⁶ molec ⁻¹ s ⁻¹)	$\sqrt{n_e k_1(T_e)}$ (10 ⁻⁴) (cm ³ molec ^{-1/2} s ^{-1/2})	(Constant x pressure) ^{1/2} $x \sqrt{n_e k_1(T_e)}$ (10 ¹² cm ⁻³)	
	2	3	4	5	6	7
1.0 Torr						
48.6	3.78	3.28	0.37	1.40±0.18	3.74±0.25	1.63±0.11
72.8	5.56	3.98	0.26	1.45±0.18	3.80±0.25	1.64±0.11
112.2	8.41	2.65	0.14	1.18±0.15	3.43±0.23	1.49±0.10
1.5 Torr						
56.2	3.71	3.41	0.50	1.85±0.24	4.30±0.29	2.29±0.16
85.4	5.55	3.32	0.37	2.05±0.26	4.53±0.30	2.39±0.16
132.0	8.05	2.96	0.20	1.61±0.21	4.01±0.27	2.13±0.15
2.0 Torr						
81.0	1.81	4.61	2.15	3.89±0.51	6.24±0.41	3.82±0.26
119.0	4.05	3.65	0.56	2.36±0.31	4.76±0.32	3.05±0.21
176.0	6.99	2.65	0.14	0.98±0.13	3.13±0.21	1.94±0.13

....contd.

Table 4.4 (contd.)

1	2	3	4	5	6	7
<u>2.5 Torr</u>						
94.5	1.84	4.63	1.88	3.46±0.45	5.88±0.39	4.16±0.28
133.0	3.61	3.98	0.92	3.32±0.43	5.76±0.38	4.00±0.27
198.0	5.80	3.06	0.26	1.51±0.19	3.85±0.26	2.09±0.14
<u>3.0 Torr</u>						
108.0	1.59	4.92	2.62	4.17±0.54	6.45±0.43	4.88±0.33
154.0	4.89	3.62	0.49	2.39±0.31	4.89±0.32	3.65±0.25
231.0	6.22	2.81	0.19	1.18±0.15	3.43±0.23	2.58±0.18

Table 4.5 Nitrogen Atom Concentration From Model Using Electron Impact Dissociation and Surface Recombination

Distance between the electrodes: 15 cms; Probe position: 7.5 cms from either electrode							
I x V Watts	$n_e (10^{10})$ (cm ³)	kT_e (eV)	$k_1 (T_e)$ (10 ⁻¹⁷) (cm ³ molec ⁻¹ s ⁻¹)	$n_{e1} (T_e)$ (10 ⁻⁷) (cm ⁶ molec ⁻¹ s ⁻¹)	$\sqrt{n_{e1} (T_e)}$ (10 ⁻⁴) (cm ³ molec ^{-1/2} s ^{-1/2})	(Constant x pressure) ^{1/2} $x \sqrt{n_{e1} (T_e)}$ (10 ¹² cm ⁻³)	
	2	3	4	5	6	7	
<u>1.0 Torr</u>							
81.0	1.90	4.52	1.96	3.72±0.48	6.10±0.41	2.65±0.18	
105.0	3.43	3.39	0.52	1.76±0.23	4.19±0.28	1.83±0.12	
142.5	7.45	2.71	0.18	1.34±0.17	3.66±0.24	1.58±0.11	
<u>1.5 Torr</u>							
90.0	1.88	4.86	2.40	4.56±0.59	6.75±0.45	3.59±0.24	
115.0	3.36	3.74	0.72	2.41±0.31	4.91±0.33	2.59±0.18	
165.0	5.60	3.64	0.56	3.13±0.41	5.59±0.37	2.98±0.20	
<u>2.0 Torr</u>							
101.2	2.27	3.94	1.00	2.27±0.30	4.76±0.32	2.88±0.20	
133.0	3.11	3.88	0.60	1.87±0.24	4.32±0.29	2.69±0.18	
181.5	5.61	3.48	0.52	2.92±0.38	5.40±0.36	3.32±0.23	

...contd.

Table 4.5 (contd.)

1	2	3	4	5	6	7
<u>2.5 Torr</u>						
119.0	1.91	4.23	1.56	2.97±0.39	5.46±0.36	3.78±0.
154.0	3.49	3.75	0.78	2.72±0.35	5.21±0.35	3.56±0.
225.0	6.46	3.60	0.46	3.00±0.39	5.45±0.36	3.80±0.
<u>3.0 Torr</u>						
154.0	2.20	4.21	1.40	3.08±0.40	5.55±0.37	4.18±0.
185.0	2.78	3.78	0.78	2.17±0.28	4.66±0.31	3.52±0.
275	6.30	3.57	0.60	3.78±0.49	6.14±0.41	4.60±0.

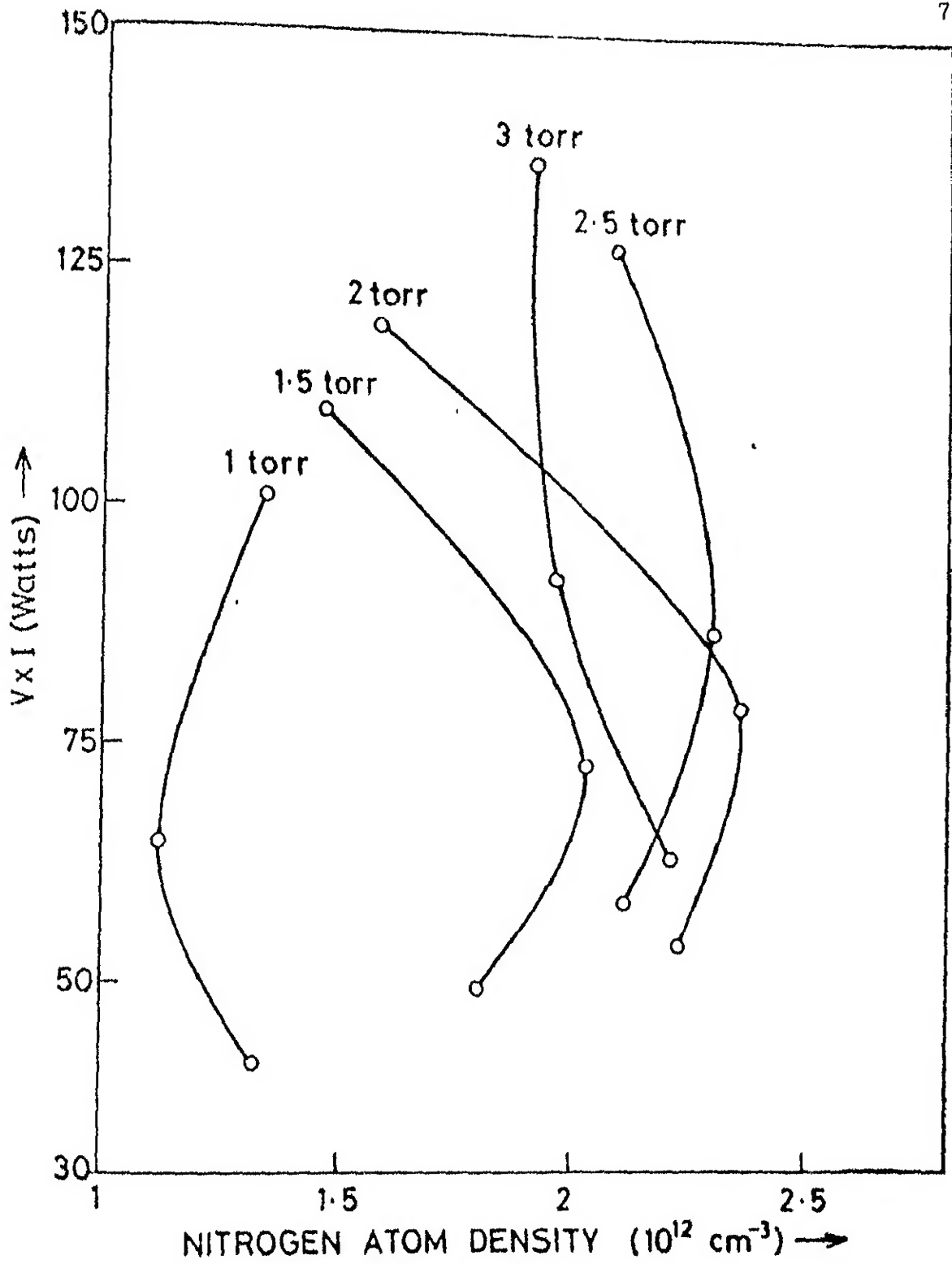


Fig. 4.5 PLOT OF $V I$ (Watts) vs NITROGEN ATOM DENSITY (cm^{-3})
 CALCULATED FROM EXPERIMENTAL VALUES OF n_e AND kT_e
 (INTERELECTRODE DISTANCE 5 cm)

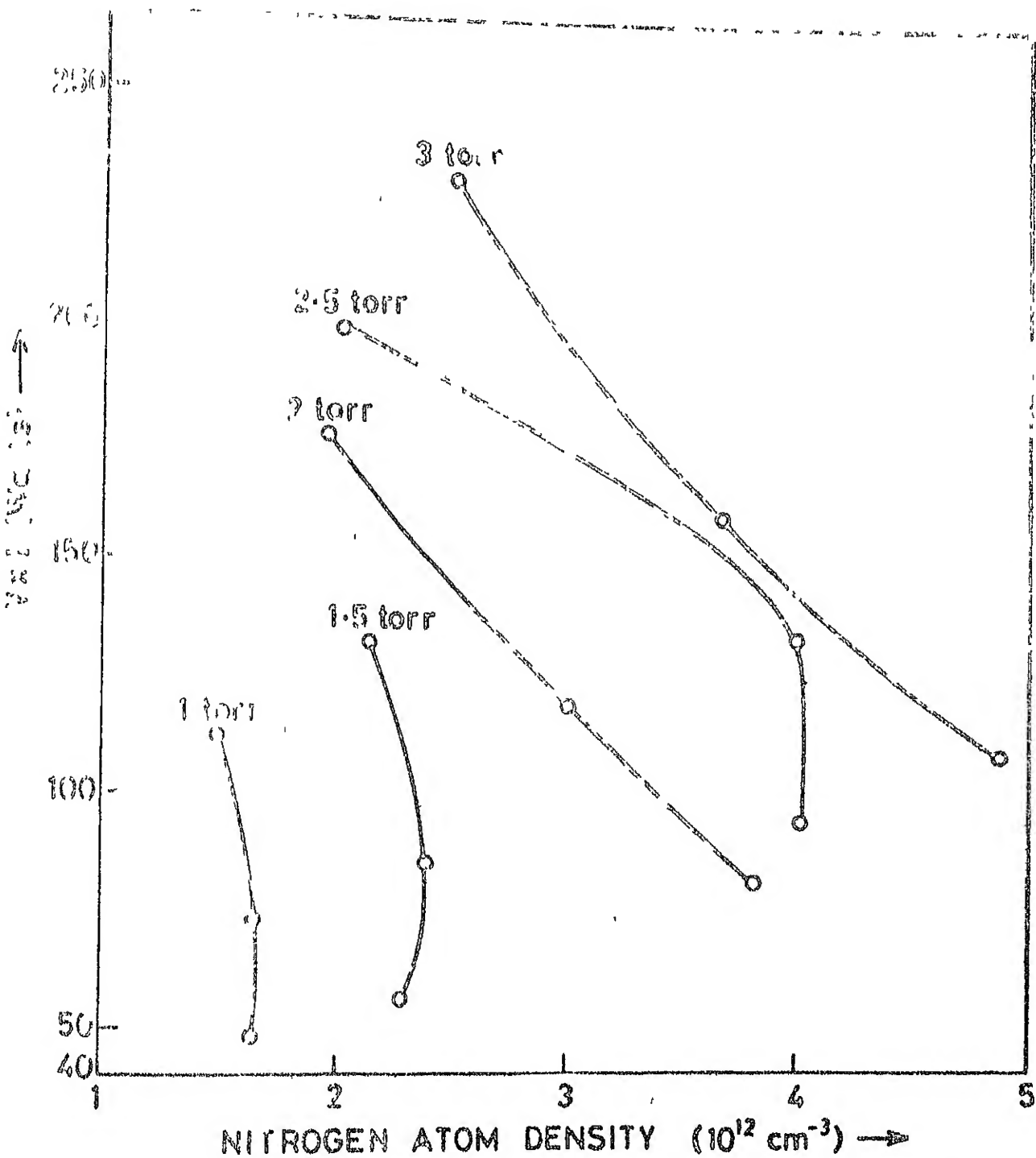


Fig. 4.6 PLOT OF VI (WATTS) vs NITROGEN ATOM DENSITY (cm^{-3})
CALCULATED FROM EXPERIMENTAL VALUES OF n_e AND KT_0
(INTERELECTRODE DISTANCE 10 cm)

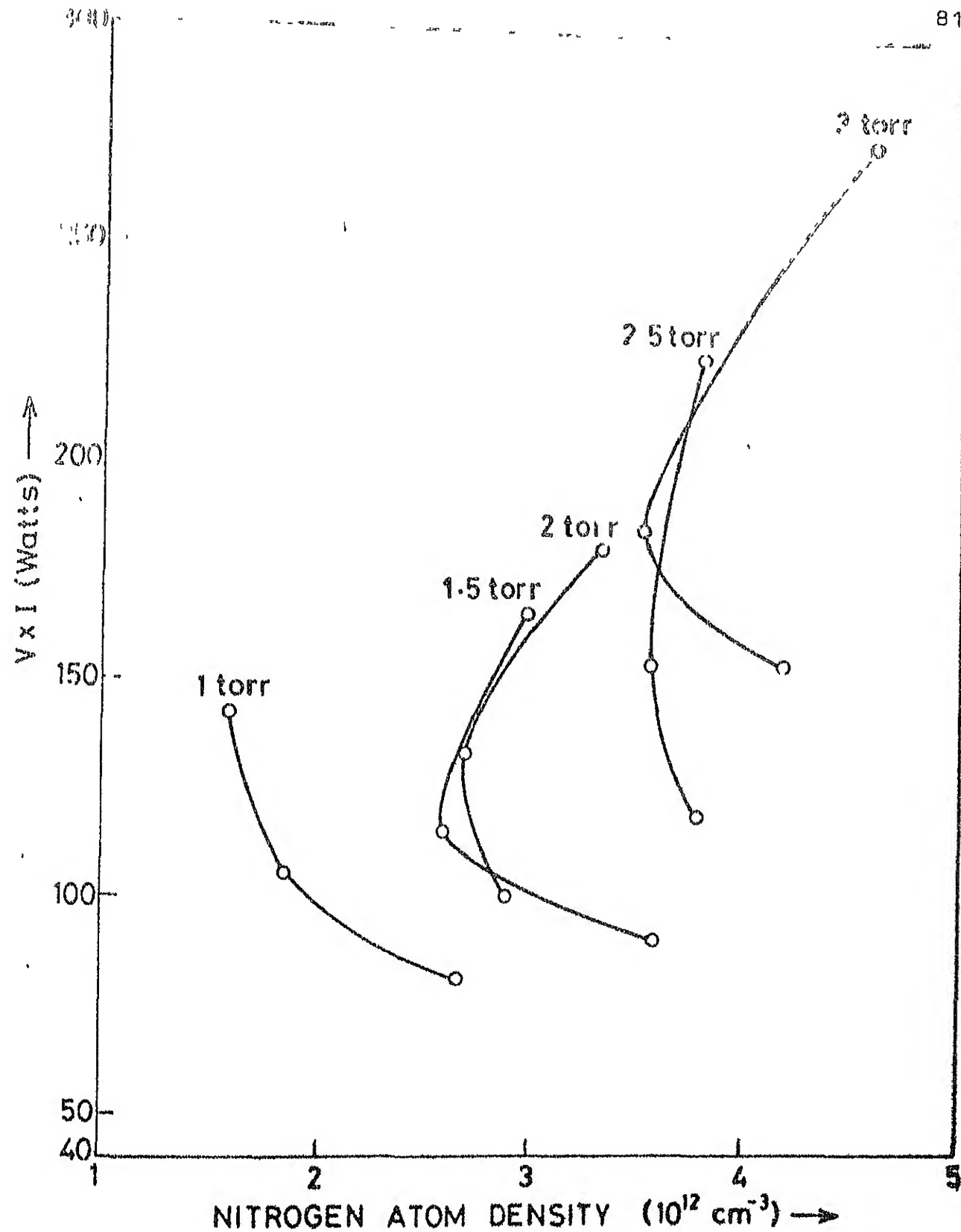
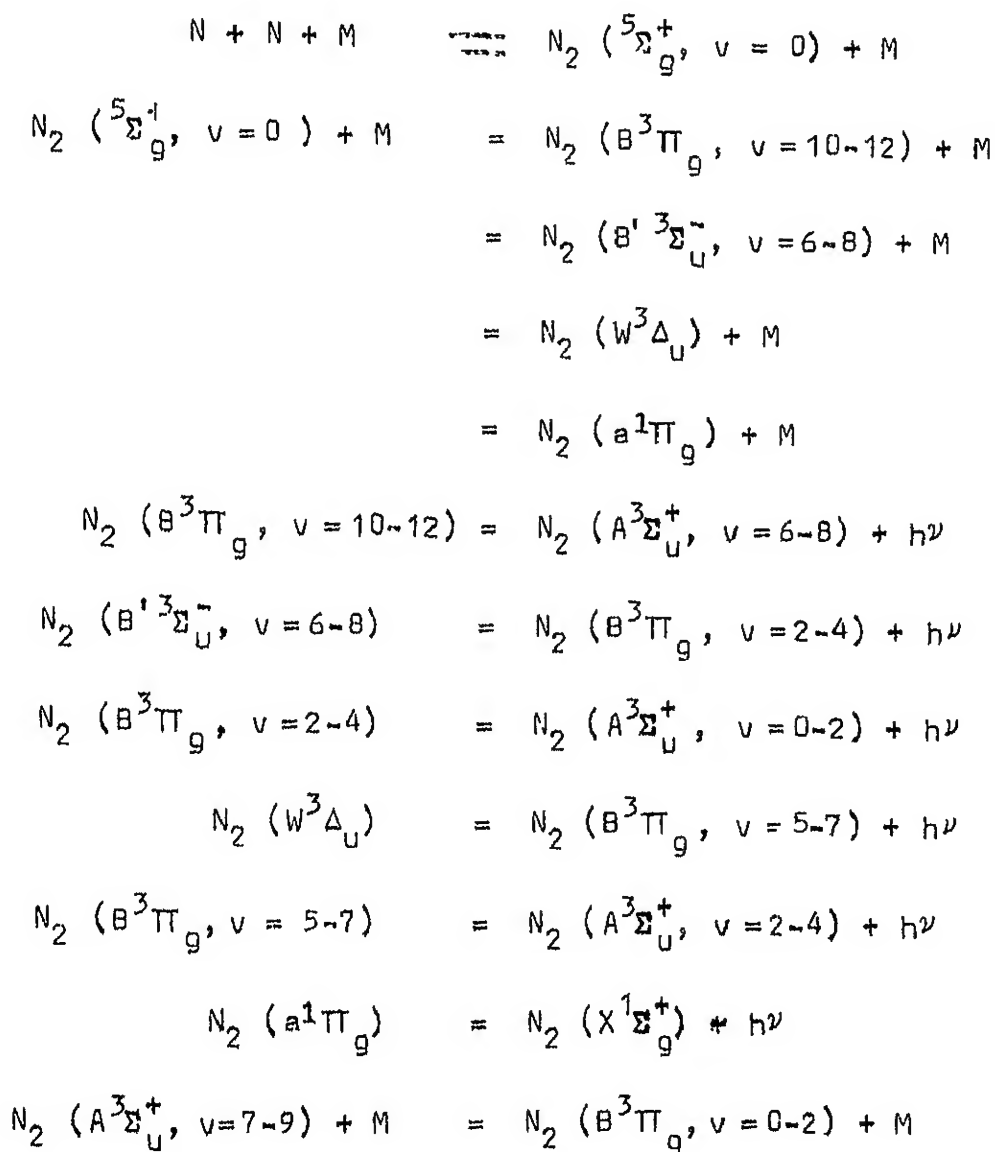


Fig. 4.7 PLOT OF $V I$ (WATTS) vs NITROGEN ATOM DENSITY (cm^{-3})
CALCULATED FROM EXPERIMENTAL VALUES OF n_e AND kT_e (INTER-ELECTRODE DISTANCE 15 cm)

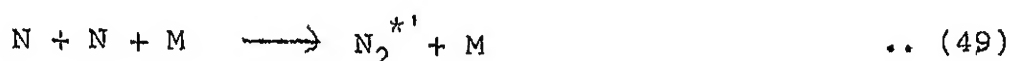
an orange filter is interposed between the afterglow and the photomultiplier tube.

The mechanism of the Lewis-Rayleigh afterglow in the gas phase is believed to consist of the following processes (Berkowitz et al.,⁴⁹ Bayes and Kistiakowsky,⁵⁰ and Anketell and Nicholls³):



The afterglow spectrum consists of first positive bands $B^3\Pi_g - A^3\Sigma_u^+$ (500 - 1100 nm), infrared afterglow $B'^3\Sigma_u^- - B^3\Pi_g$ (700-1100 nm) Lyman-Birge-Hopfield $a^1\Pi_g - X^1\Sigma_g^+$ (145 - 185 nm) and Wilkinson-Mulliken ultraviolet $a'^1\Sigma_u^- - X^1\Sigma_g^+$ (150-190 nm) systems.³

The resulting processes causing volume recombination of N atoms and emission in orange-yellow region could therefore be broadly expressed as



The rate of photon emission would be directly proportional to $[N_2^*]$, that is, it can be expressed as $A[N_2^*]$, where A is the transition probability. In the steady state $[N_2^*]$ could be expressed as

$$[N_2^*] = K' \frac{[N]^2 [M]}{A} \quad \dots (4.12)$$

or, $[N]$ can be expressed as

$$[N] = \left[\frac{A[N_2^*]}{K'[M]} \right]^{1/2} = K \left[\frac{I_p}{[M]} \right]^{1/2} \quad \dots (4.13)$$

where I_p is the photocurrent generated by the radiation intercepted by the photocathode. In this case we should expect the N atom density to be proportional to the square root of the photomultiplier current, or a voltage developed by this current. We should add here that though there exists differences in opinion about exactly what is the precursor to the emitting $B^3\Pi_g$ state, as long as it is predominantly populated by a collisional process, the expression for $[N]$ should hold. This latter data is available from Table 3.6 and are collectively plotted in Fig. 4.8. For evaluating relative N atom densities, we therefore evaluate the ratio of the square root of the photomultiplier voltage to the square root of the relevant pressure. This ratio is plotted against the input power and is shown in Fig. 4.9.

4.7 N Atom Density in the Plasma and at the Position of the Afterglow Measurements

The basis of making an estimate of N atom density using photomultiplier data is that recombination of N atoms leads to excited electronic states of N_2 , and the rate of photon emission from such excited states could be used, in a reverse application, to estimate the N atom density. It is, therefore, essential that direct electron impact excitation to the N_2 electronic states does not interfere with the afterglow measurements, and it is required that the measurements be made where such excitation is

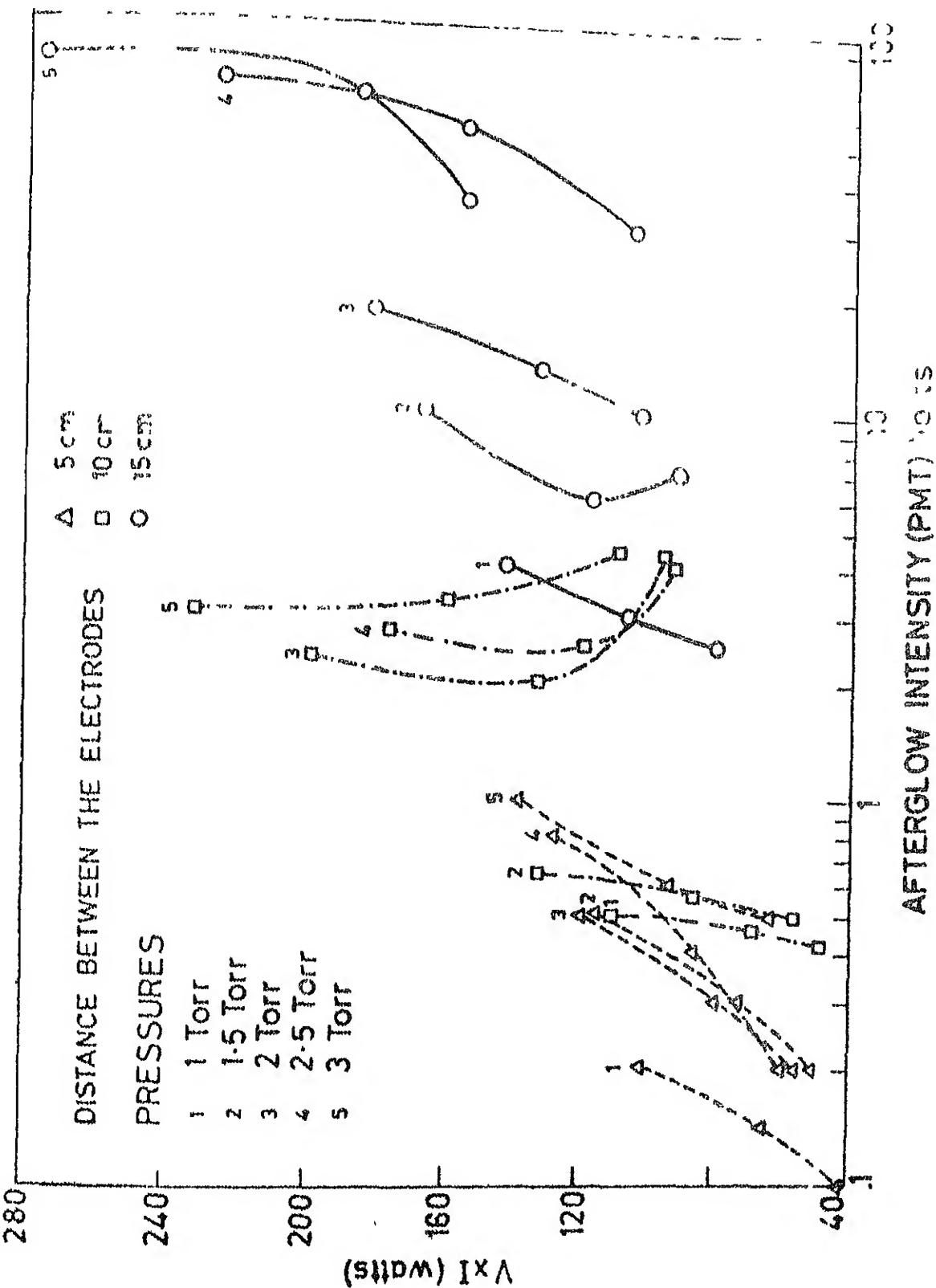
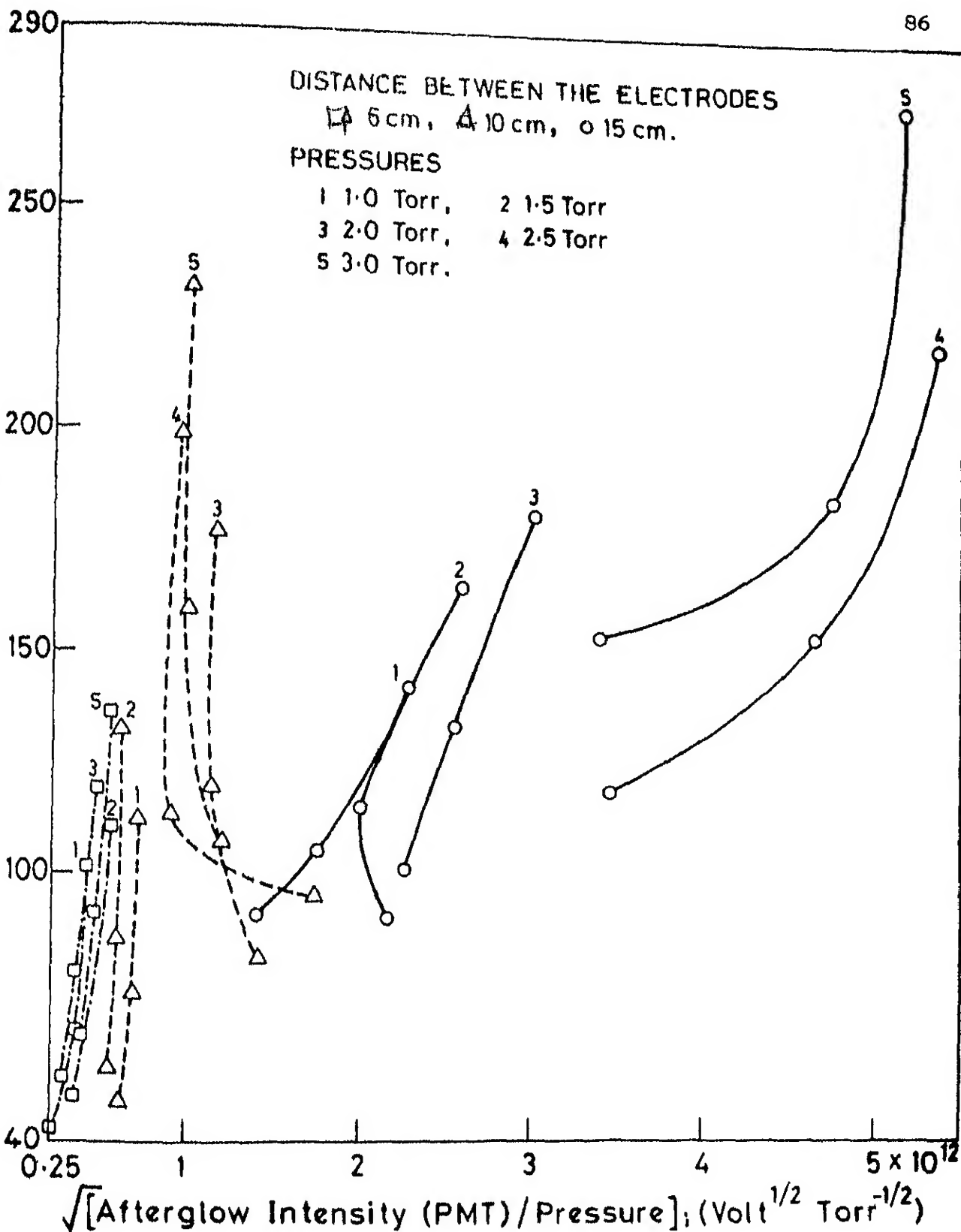
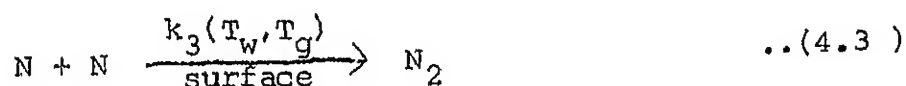


Fig. 4.6 VI (Watts) vs AFTERGLOW INTENSITY FOR ALL THE DISCHARGE TUBES
(ELECTRODE DISTANCE 5, 10, and 15 cm) AND TOP PRESSURE RANGE
1 Torr - 3 Torr



absent, as would be true at a position substantially downstream from the plasma region. For this reason, in the present experiments, photomultiplier measurements were made far downstream from the glow region. However, if a comparison of the plasma N atom density with the N atom density derived from the afterglow measurements is to be made, then it is necessary to have an estimate of the decay of N atom density from the glow region to the position of the photomultiplier measurements.

If the major process of N atom disappearance is by surface recombination



then the disappearance of N atom could be expressed as

$$-\frac{d[N]}{dt} = k_3 [N]^2 \quad \dots(4.14)$$

which on integration gives

$$[N] = \frac{[N]_0}{1 + [N]_0 k_3 t} \quad \dots(4.15)$$

where $[N]_0$ represents the density of N atoms at the initiation of the recombination process ($t=0$) and $[N]$ is the N atom density after t seconds.

The time for which the recombination process acts after the atoms leave the glow region till they reach the photomultiplier measurement point could be calculated from the linear flow rate. Taking the volume flow rate of the pump as $15.75 \text{ lit. sec}^{-1}$ (945 lit/min) the linear velocity is $15750/\pi (1.3)^2 = 27.5 \text{ m. sec}^{-1}$. The distances from the pump end of the discharge tube to the measuring point were 155 cm, 150 cm and 145 cm, respectively for the tubes with 5 cm, 10 cm and 15 cm interelectrode distance. Since $[N]$ in all the cases are of the order of 10^{12} , hence

$$t = \frac{1.5}{27.5} = 0.055 \text{ sec.}$$

For an order of magnitude estimate of the $[N]/[N]_0$ we can write, from Eqn. (4.15):

$$\begin{aligned} \frac{[N]}{[N]_0} &= \frac{1}{1 + [N]_0 k_3 t} \quad \dots (4.16) \\ &= \frac{1}{1 + 10^{12} \times 3 \times 10^{-16} \times 5.5 \times 10^{-2}} \\ &= 0.9999 \end{aligned}$$

So there is less than 0.01% disappearance of N atoms. Even if the linear velocity is one-tenth of what has been used above, (implying a residence time of 0.55 sec) difference in the N atom densities would be insignificant. Therefore, the N atom

density when the gas emerges from the plasma and at the point of photomultiplier measurements could be taken as practically the same.

4.8 Comparison of N Atom Densities from Afterglow Intensities and those from Calculations

We now compare the N atom densities calculated from the theoretical model against the relative N atom densities estimated from the experimental measurements of afterglow intensities as shown in Fig. 4.9. For this purpose we combine Figs. 4.5-4.7 into Fig. 4.10 which represents the theoretical results at 300°K . We have already commented on the limitations of using VI as a parameter to view other plasma properties that depend on atomic processes. We still use VI in Fig. 4.9 and Fig. 4.10 for convenience; however, we should keep in view the relationship of IV and $n_e kT_e$ as shown earlier.

If we ignore the details of the curvatures of the plotted lines, a few general observations can be made: (1) the relative disposition of the groups of theoretical curves for glows with interelectrode spacings 5 cm, 10 cm, and 15 cm is in agreement with that obtained experimentally from afterglow intensities, (ii) in each individual group of curves the effects of pressure on the nitrogen atom density are similar in the theoretical curves and the curves from afterglow intensities. These are

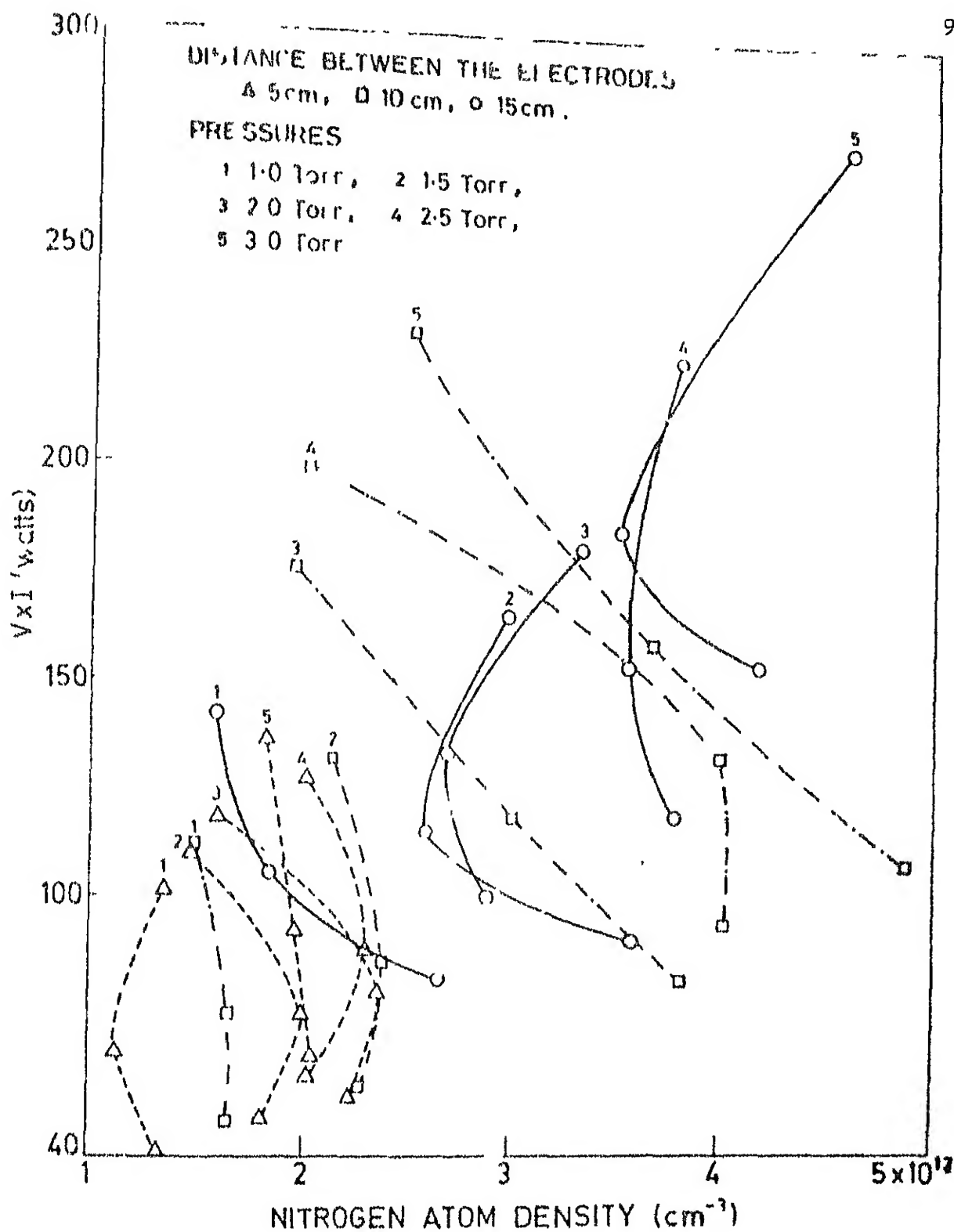


Fig. 4.10 V_I (WATTS) vs NITROGEN ATOM DENSITY (CALCULATED FROM EXPERIMENTAL VALUES OF n_e AND kT_e , OBTAINED FOR INTER-ELECTRODE DISTANCES 5, 10, AND 15 cm AND SURFACE RECOMBINATION RATE COEFFICIENT AT 300°K)

the substantial broad agreements. The ratio of maximum to minimum N atom concentration in the theoretical curves is about 5, in comparison to about 18 for the corresponding ratio from afterglow intensities.

The most striking difference between the theoretical curves and the curves from afterglow intensities is the overlap between the three sets of theoretical curves (from the three discharge tubes) while the sets from the afterglow intensities are relatively separated from each other. Clearly, if a reason could be found that would space the groups of theoretical curves somewhat apart, that would at the same time bring close the ratios between the maximum to the minimum nitrogen atom densities.

In the simple theoretical model that we considered the effect of gas temperature, wall temperature, and their effects on the recombination was not taken into account. Data exists on the temperature dependence of the surface recombination. According to Campbell and Thrush,⁴³ surface recombination has an activation energy of 620 ± 50 cal mole⁻¹ in the temperature range 196-327°K. Although we have no data on the inside wall temperature, the temperature of the outside wall increased upto about 350°K. (Table 3.5). If we consider the positive activation energy stated above, then the recombination rate would increase with temperature, and in Eqn.(4.7) since $[N_2]$ would decrease with increase of temperature, the overall effect will be a decrease

of N atom concentration. This is shown in Fig. 4.11 which is insignificantly different from Fig. 4.10. What is needed to bring the theoretical and the afterglow N atom densities close seems to be higher rate coefficients of dissociation at given kT_e values. This may mean that additional dissociation processes which have direct or indirect dependence on electron impact processes do play a considerable role.

The details of curvature of a specific plot of N atom density as power changes follows a complex pattern. While an understanding of what would improve correspondence of theoretical curvatures with those obtained from afterglow intensities are difficult, how the N atom density plots acquire a particular curvature may be understood by following the calculation of the theoretical N atom density in a specific case.

Let us consider the curve 5 for 15 cm interelectrode distance as it appears in Fig. 4.10 or Table 4.5. While the increase of power from 154 Watts to 275 Watts through 185 Watts involves a monotonic increase of electron density ($2.20 \times 10^{10} \text{ cm}^{-3}$, $2.78 \times 10^{10} \text{ cm}^{-3}$, and $6.30 \times 10^{10} \text{ cm}^{-3}$, respectively), the electron temperature kT_e drops from 4.21 eV to 3.77 eV through 3.78 eV. It is the peculiar shape of $k_1(kT_e)$ curve given in Fig. 4.1(b) that changes the pattern of the product $n_e k_1(kT_e)$, since the drop in $k_1(kT_e)$ is independent of n_e increase that took place as a result of plasma current increase

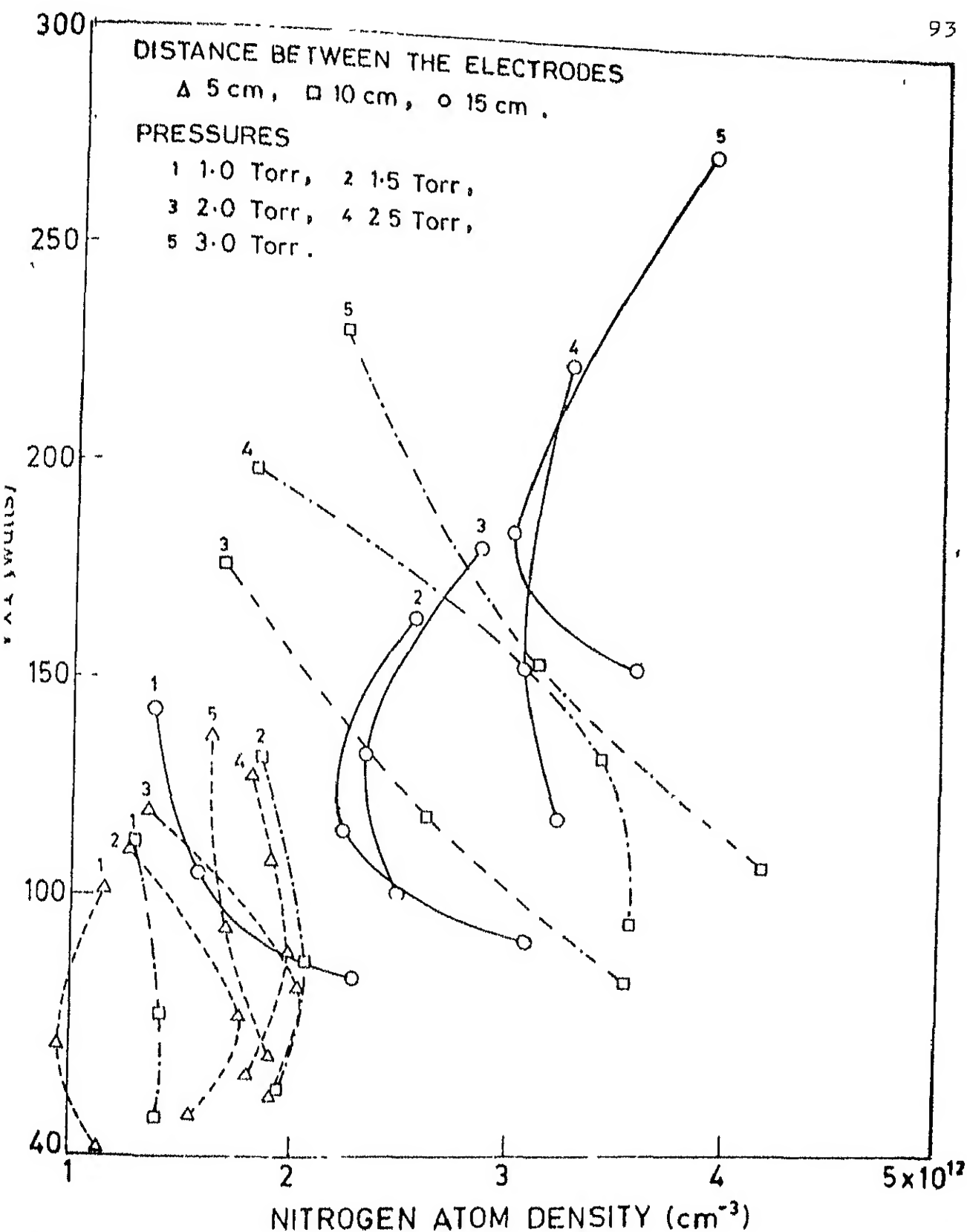


Fig. 4.11 VI(WATTS) vs NITROGEN ATOM DENSITY (CALCULATED FROM EXPERIMENTAL VALUES OF n_e AND kt_e , OBTAINED FOR INTERELECTRODE DISTANCES 5, 10, AND 15 cm AND SURFACE RECOMBINATION RATE COEFFICIENT AT 350°K)

So the shapes of the N atom density curves would be controlled by both the plasma parameters and the peculiarities of the rate coefficient curves.

4.9 Conclusions and a Critique

The work involved examination of the process of dissociation of nitrogen molecules in dc glow plasmas and an attempt to correlate the observations with the major atomic processes taking place in the plasma. n_e, kT_e were measured in the plasma, and estimates on nitrogen atom concentration were made from afterglow radiation intensities. Correlations between the theoretical predictions of nitrogen atom densities and those estimated from afterglow intensities were examined. Broad agreements in trends are observed.

A major deficiency of the work is that the nitrogen atom concentrations are not measured directly. Such a measurement would have rendered much additional strength to the conclusions that are derived from somewhat indirect data. Similarly, some simultaneous spectroscopic measurements on the glow plasma itself would have been valuable. That would have probably shown the quantitative role of a number of electronically excited molecular nitrogen states in the dissociation process.

That it was desirable to measure the nitrogen atom concentration directly was realised. However, the reasons it

could not be achieved were non-scientific, but perhaps this could be just mentioned. We had ordered a custom-built equipment - a mass spectrometric plasma sampling system for analysis of positive and negative ions as well as neutrals, and energy analysis of the ions. This imported equipment (schematic diagram in Appendix) which arrived nearly a year late, unfortunately did not perform even for once satisfactorily, either for the plasma ions or for the neutrals (the equipment was not tested by the manufacturer for actual plasma sampling). We made extensive tests for months with the system and our conclusion is that there is an inherent design problem about the alignment of the first sampling aperture, the aperture on the differentially pumped section, the ion source housing aperture, and the ion cage wherein the ionization takes place. For nearly a year we have failed to get the fault rectified by the manufacturer and there are no indications that it will be remedied in the foreseeable future. Likewise our pursuance for more than a year about a set of Matheson mass flowmeters (which would have permitted absolutely N atom concentration measurement from NO titration) have also been unsuccessful and there seems to be no hope of its arrival in the near future. However, although such direct absolute measurements would have added substantially, the afterglow intensities and nitrogen atom concentration relationships have been studied by a number of workers for one to depend on the results. As regards the spectroscopic measurements on

the plasma itself, they were not planned to be part of the present work, and this could constitute a separate investigation.

On the positive side, this is probably the first detailed attempt to correlate plasma parameters with the process of nitrogen dissociation in dc glow plasmas. A quantitative understanding of all the processes that participate in the dissociation is clearly far from complete, but the work probably constitutes a positive step,

REFERENCES

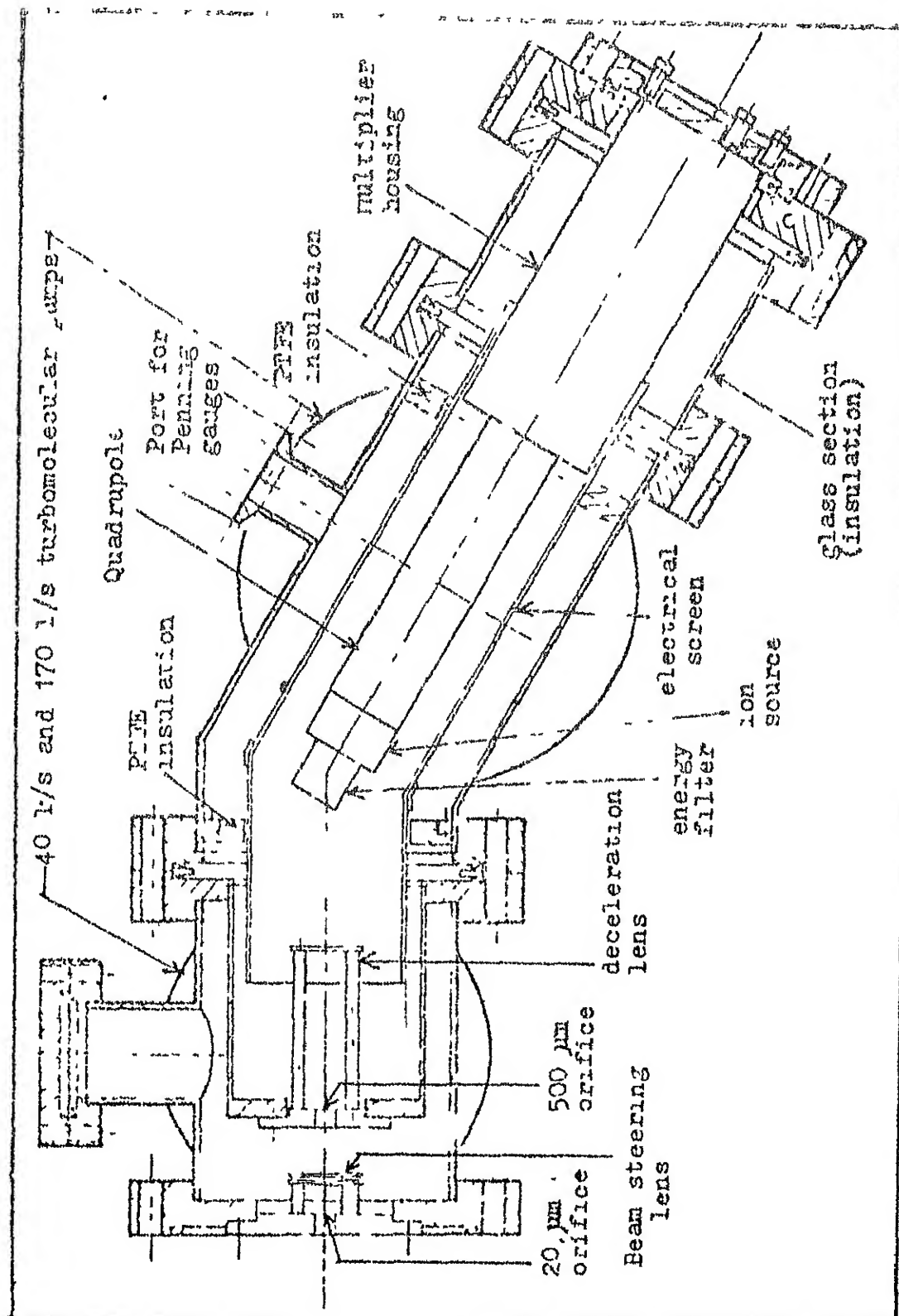
1. H.W. Drawin in "Reactions Under Plasma Conditions," Ed. M. Venugopalan, Wiley Interscience, New York, 1971, p. 55-123.
2. B. Brocklehurst and K.R. Jennings in "Progress in Reaction Kinetics," Ed. G. Porter, Pergamon, Oxford, 1967, p.1-36.
3. J. Anketell and R.W. Nicholls, Rep. Prog. Phys., 33, 269 (1973).
4. M.F. Golde and B.A. Thrush, Rep. Prog. Phys., 33, 1285 (1973).
5. M.L. Spealman and W.H. Rodebush, J. Amer. Chem. Soc., 57, 1417 (1935).
6. G.B. Kistiakowsky and G.G. Volpi, J. Chem. Phys., 27, 1141 (1957).
7. F. Kaufmann, J. Chem. Phys., 28, 352 (1958).
8. P. Harteck, R.R. Reeves and G.G. Mannella, J. Chem. Phys., 29, 608 (1958).
9. A. Westenberg and N. De Haas, J. Chem. Phys., 40, 3087 (1964).
10. H. von Weyssenhoff and M. Patapoff, J. Phys. Chem., 69, 1756 (1965).
11. M. Sutoh, Y. Morioka and M. Nakamura, J. Chem. Phys., 72, 20 (1980).
12. R.A. Young and R.L. Sharpless, J. Chem. Phys., 39, 1071 (1963).
13. E.O. Johnson and R. Malter, Phys. Rev., 80, 58 (1950).
14. D. Bohm, E.H.S. Burhop, H.S.W. Massey and R.W. Williams in "The Characteristics of Electrical Discharges in Magnetic Fields," Vol. 5, Ed. A. Guthrie and R.K. Wakerling, McGraw Hill, New York, 1949.

15. E.N. Lassattre and M.E. Krasnow, J. Chem. Phys., 40, 1248 (1964).
16. S.M. Silverman and E.N. Lassattre, J. Chem. Phys., 42, 3420 (1965).
17. J. Gieger and B. Shroeder, J. Chem. Phys., 50, 7 (1969).
18. E.N. Lassettre, Can. J. Chem., 47, 1733 (1969).
19. A.J. Williams and J.P. Doering, Planet. Space Sci., 17, 1527 (1969).
20. A.J. Williams and J.P. Doering, J. Chem. Phys., 51, 2859 (1969).
21. R.T. Brinkman and S. Trajmar, Annls. Geophys., 26, 201 (1970).
22. E.N. Lassettre in "Methods of Experimental Physics," Ed. D. Williams, Academic Press, New York, 1974.
23. R.E. Huffman, Y. Tanaka, and J.C. Larrabee, J. Chem. Phys., 39, 910 (1963).
24. S.G. Tilford and P.G. Wilkinson, J. Mol. Spect., 12, 347 (1964).
25. S.G. Tilford and P.G. Wilkinson, Astrophys. J., 141, 427 (1965).
26. G.M. Lawrence, D.L. Nicky, K. Dressler, J. Chem. Phys., 48, 1989 (1968).
27. P.K. Carroll and C.P. Collins, Can. J. Phys., 47, 563 (1969).
28. K. Dressler, Can. J. Phys., 47, 547 (1969).
29. P.K. Carroll, and K. Yoshino, J. Phys. B, 5, 1614 (1972).
30. E.C. Zipf, E.O.S., 54, 403 (1973).
31. E.C. Zipf, E.O.S., 54, 1155 (1973).
32. G.M. Lawrence and M.J. McEwan, J. Geophys. Res., 78, 8314, (1973).

33. A.B. Christensen, *Geophys. Res. Lett.*, 3, 221 (1976).
34. H. Park, P.D. Feldman and W.G. Fastie, *Geophys. Res. Lett.*, 4, 41 (1977).
35. M.H. Rees, *Planet Space Sci.*, 23, 1589 (1975).
36. E.C. Zipf and W.M.C. McLaughlin, *Planet Space Sci.*, 26, 449 (1978).
37. R.D. Hudson and V.L. Carter, *Can. J. Chem.*, 47, 1340 (1969).
38. H.F. Winters, *J. Chem. Phys.*, 44, 1472 (1966).
39. A. Niehaus, *Z. Naturf.*, A22, 690 (1967).
40. W. Brennen, and E.C. Shane, *J. Phys. Chem.*, 75, 1552 (1971).
41. M.A.A. Clyne and D.H. Stedman, *J. Phys. Chem.*, 71, 3071 (1967).
42. K.H. Becker, W. Groth and D.Kley, *Z. Naturf.*, A24, 1840 (1969).
43. I.M. Campbell and B.A. Thrush, *Proc. Roy. Soc.*, A296, 201 (1967).
44. H.H. Bromer and W. Zwirner, *Z. Naturf.*, A24, 118 (1969).
45. K.M. Evenson and D.S. Burch, *J. Chem. Phys.*, 45, 2450 (1966).
46. J.T. Herron, J.L. Franklin, P. Bradt and V.H. Dibeler, *J. Chem. Phys.*, 30, 879 (1959).
47. T. Wentink, J.O. Sullivan and K.L. Wray, *J. Chem. Phys.*, 29, 231 (1958).

48. C. Mavroyannis and C.A. Winkler, Can. J. Chem., 39, 1601 (1961).
49. J. Berkowitz, W.A. Chupka and G.B. Kistiakowsky, J. Chem. Phys., 25, 457 (1956).
50. K.D. Bayes and G.B. Kistiakowsky, J. Chem. Phys., 22, 992 (1960).

A P P E N D I X



APPARATUS FOR MASS SPECTROMETRIC SAMPLING AND ENERGY ANALYSIS OF
PLASMA IONS AND NEUTRALS

A NOTE OF CORRECTION TO THE THESIS ENTITLED : " ROLE OF
ELECTRON DENSITY AND ELECTRON TEMPERATURE IN DISSOCIATION
OF NITROGEN IN DIFFUSE GLOW PLASMAS." By G. S. Sreekanth

In the theoretical model of dissociation of nitrogen in glow plasmas discussed in the above thesis, the direct electron impact dissociation rate coefficient k_1 was evaluated by integrating the relevant cross section from the work of Zipf and McLaughlin³⁶. I have recently detected an error in the numerical evaluation of this rate coefficient. The correct rate coefficients are of the order of $10^{-9} \text{ cm}^3 \text{ sec}^{-1}$. As a result the theoretical density of N atoms $[N]$ calculated for the experimental n_e, kT_e conditions would now come out as $\sim 10^{16} \text{ cm}^{-3}$, implying a large percentage of dissociation. In view of this we reconsider the model, with some additional rate process along the following lines.

The steady state equations involving the rates of $[N_2^+]$ and $[N]$ changes are given by

$$k_{ei} [N_2] n_e - k_{dr} n_e [N_2^+] - k_{wd} [N_2^+] - k_{ct} [N] [N_2^+] = 0 \quad (1)$$

and

$$2k_1 [N_2] n_e + 2k_{dr} [N_2^+] n_e - 2k_3 [N]^2 - 2k_2 [N]^2 [N_2] - k_{ct} [N_2^+] [N] = 0 \quad (2)$$

where the rate coefficient k_{ei} stands for electron impact ionization, k_{dr} represents the dissociative recombination of N_2^+ ions with electrons to yield N atoms, k_{wd} the first order diffusion rate coefficient of N_2^+ ions, k_{ct} the rate coefficient for the charge transfer reaction between N_2^+ ion and N atoms, k_1 represents the direct electron impact dissociation of N_2 into N atoms, and k_3 and k_2 are respectively the rate coefficients for surface and

volume recombination of N atoms.

k_{ei} is evaluated using the cross section from Märk ⁵¹. k_{dr} is taken from Cunningham and Hobson ⁵². The first order diffusion rate coefficient k_{wd} is obtained by assuming $k_{wd} = 5.78 D_a / r_0^2$ (see. for example, ref.53) with $D_a P \simeq 200$ $\text{cm}^2 \text{ torr s}^{-1}$ (ref. 54) (D_a : ambipolar diffusion coefficient, r_0 : tube radius). k_{ct} is taken as $10^{-9} \text{ cm}^3 \text{ s}^{-1}$ (ref.53). The electron impact dissociation k_1 is evaluated using the total cross section from Zipf and McLaughlin ³⁶. Both the electron impact ionization and dissociation rate coefficients are evaluated by integration of the relevant cross sections over Maxwellian electron energy distributions in the kT_e range of the present experiments.

Among the terms containing $[N_2^+]$ in eq. (1), both $k_{dr}n_e$ and k_{wd} are of the order of 10^3 s^{-1} and could be neglected in comparison with $k_{ct}[N]$ even if the extent of dissociation is as low as 0.1 per cent, i.e., $[N] = 10^{13} \text{ cm}^{-3}$. Hence the left side of eq. (1) reduces to only the first and the fourth term.

We have already shown that the volume recombination term is negligible in comparison to the term involving surface recombination. Further, k_{dr} being of the order of $10^{-7} \text{ cm}^3 \text{ s}^{-1}$, n_e of the order of 10^{10} cm^{-3} (and hence $[N_2^+]$ not greater than 10^{10} cm^{-3}), k_1 of the order of $10^{-9} \text{ cm}^3 \text{ s}^{-1}$, $[N_2]$ of the order of 10^{16} cm^{-3} , the second term of eq. (2) is about 3-4 orders of magnitude smaller in comparison to the first term; hence the former may be neglected for the conditions of the present experiment.

Using the rate coefficients as stated above, substituting an expression for $[N_2^+]$ from eq. (1) into eq. (2) and solving for $[N]$, $[N]$ for the entire range of experimental conditions could be obtained. Earlier, the $[N]$ was presented in Fig. 4.10. With the present rates, the pattern remains similar, however with a change of scale from $1-5 \times 10^{12}$ to $1-6 \times 10^{16} \text{ cm}^{-3}$.

As regard the $[N]$ from photomultiplier signal intensity, the $[N]$ in the steady state could be expressed as

$$[N] = \left\{ \frac{A[N_2^*] + Q[N_2^*][N_2]}{k_2 [N_2]} \right\}^{\frac{1}{2}} = \left\{ \frac{CI_p}{k_2 [N_2]} + \frac{Q[N_2^*]}{k_2} \right\}^{\frac{1}{2}}$$

where Q is the quenching coefficient of the excited state and C a correction factor to quantitatively include all the photons emitted cm^{-3} of the afterglow system. In the absence of the quenching term, $[N]$ may be expected to be proportional to the ratio of the square root of the photocurrent and the square root of $[N_2]$. This ratio was plotted against the IV product and was shown in Fig. 4.9.

Although the quenching coefficients are known and there are reports in the literature^{55,56} wherein they have been used in estimating population densities of excited nitrogen molecular states in the pressure range 1-10 torr, we are unable to add the contribution of the quenching term to the emission term since the latter is not an absolute intensity measurement. However, if the first term in eq. (3) is taken as a partial contribution to the $[N]$, then because of the second term it may be expected (since $[N_2^*]$ would be proportional to the square of $[N]$) that inclusion of the quenching correction in Fig. 4.9 would have relatively more effect

on the high $[N]$ points. As a result the span of $[N]$ would increase, and for the same reason there is likely to be overlaps in $[N]$ obtained from the three different discharge tubes.

If we compare the (new) calculated values of $[N]$ from fig. 4.10 with $[N]$ variations as presented in Fig. 4.9 ignoring the details of the curvature of the plotted lines (the curvatures arise primarily due to the peculiarities of the $k_1 - kT_e$ curve) a few general observations can be made : (i) the relative disposition of the groups of theoretical curves for glows with interelectrode spacings of 5 cm, 10 cm, and 15 cm is in agreement with that obtained experimentally from afterglow intensities; (ii) in each individual group of curves the effects of pressure on the nitrogen atom density in the theoretical curves are similar to those on the corresponding curves obtained from afterglow intensities. These are the substantial broad agreements. The ratio of maximum to minimum $[N]$ in the theoretical curves is about 3.6, in comparison to about 18 for the corresponding ratio from afterglow intensities. Another striking difference between the theoretical curves and the curves from afterglow intensities is the substantial overlap between the three sets of theoretical curves (from the three tubes) while corresponding sets from the afterglow intensities are considerably separated from each other.

The most disturbing result from the calculations is the very high percentage of dissociation of N_2 molecules, contrary to the generally held view that in nitrogen glows the dissociation is of the order of a few per cent. We have no experimental quantitative data on the absolute density of nitrogen atoms in the present work against which our calculated results could be compared.

We can only examine the various aspects of the atomic processes that have been considered in the calculations that result in the apparent high value of $[N]$.

A high value of $[N]$ can result due to excessive importance of the source terms and inadequate weightage given to the loss processes. The overwhelming source term is the direct electron impact dissociation. If the total cross section of Zipf and McLaughlin³⁶ is taken, the rate coefficients are of the order of $10^{-9} \text{ cm}^3 \text{ s}^{-1}$ (integration of the cross section carried out between 10-100 eV; contribution from the region beyond 100 eV is negligible). There is little difference between optically thick and optically thin rate coefficients in this range (at $kT_e = 4 \text{ eV}$, k_1 (optically thin) $= 1.40 \times 10^{-9} \text{ cm}^3 \text{ s}^{-1}$, k_1 (optically thick) $= 1.55 \times 10^{-9} \text{ cm}^3 \text{ s}^{-1}$). These cross sections imply a rate of N atom production $\sim 10^{17} \text{ cm}^3 \text{ s}^{-1}$ in the glow, and it must at least be so in the axial region where the n_e, kT_e measurements were carried out. Addition of any other hitherto unsuspected major source term in eq. (2) would only increase $[N]$ further.

Among the loss processes, the surface recombination and the charge transfer process are comparable in significance; their relative weightage depends on the nitrogen atom density; a high surface recombination rate or additional N atom reactions could lower $[N]$. Among additional N atom reactions the following sequence suggested by Young⁵⁷ should be considered: $N_4^+ + N \rightarrow N_3^+ + N_2$; $N_3^+ + N \rightarrow N_2^+ + N$, where N_4^+ is generated by a reaction of N_2^+ with N_2 molecules.

Quantitatively, however, the N atom loss process in reactions with N_3^+ and N_4^+ would proceed parallel to the reaction of N atom with N_2^+ , which is the major reactive loss process besides the surface recombination. If we take $10^{-9} \text{ cm}^3 \text{ s}^{-1}$ for rate coefficient of all these reactions, the N atom loss rate would then depend on the steady state concentration of the ionic reactant. Since in mass spectrometric studies ^{of low pressure} / pure nitrogen glow discharge $[N_3^+]$ and $[N_4^+]$ are substantially lower than that of N_2^+ (see, for example, ref 58), so although the reactions of N with N_3^+ and N_4^+ would contribute to the N loss process, their contribution may be expected not to be overwhelming.

Another possibility due to which a lower $[N]$ may be expected is when the effective kT_e in the glow is substantially lower than that measured in the axial region. This would result in the direct electron impact dissociation producing much less N atoms. We find that at kT_e of 1.5 eV, k is $7.29 \times 10^{-12} \text{ cm}^3 \text{ s}^{-1}$, and it has a value of $1.38 \times 10^{-13} \text{ s}^{-1}$ at kT_e of 1.0 eV. In terms of the cross sectional area of the tube, the halfway value is realized at about $0.75r_0$. From the radial electron temperature profile of arcs, at $0.75r_0$, kT_e drops to about half of that on the axis. If the glow, behaviour is qualitatively similar then this would tend to explain the lower $[N]$ since while the charged particle concentration also drops radially, the dissociation rate coefficient drops much faster.

References

- 51 T.D. Märk, J. Chem. Phys. 63, 3731, 1975.
- 52 A.J. Cunningham and R.M. Hobson, J. Phys. B, 5, 2328, 1972 .
- 53 F. Kaufman, Advan. Chem. Ser. 80, 29, 1969.
- 54 A.C. Faire and K.S.W. Champion, Phys. Rev. 113, 1, 1959.
- 55 D.C. Cartwright, J. Geophys. Res. 83, 517, 1978.
- 56. A. Ali and P.K. Ghosh, J. Quant. Spectrosc. Radiat. Transfer 29, 353, 1983.
- 57 R.A. Young, C.R. Gatz, and R.L. Sharpless J. Phys. Chem. 69, 1763, 1965.
- 58 M.M. Shahin, Advan. Chem. Ser. 58, 315, 1966.

APPENDIX

Following additional references were cited by the examiners of the thesis:

- a) M. Capitelli and E. Molinari, in "Topics in Current Chemistry", Vol. 90, p.59, 1980.
- b) M. Capitelli, M. Dilonardo, O. Gorse, Chem. Phys. 56, 29 (1981).
- c) M. Capitelli, O. Gorse, and G. D. Billing, Chem. Phys., 52, 299 (1980).
- d) G. Cernogora, L. Hochard, M. Touzeau, A. Ricard, and C. Ferreira, Int. Symp. Plasma Chem. 5, 1981.
- e) H. Brunet and J. Rocca Serra, Int. Symp. Plasma Chem. 7, 1985.
- f) F. Oramarossa, Int. Symp. Plasma Chem. 4, 1979.
- g) L. S. Polak, High Temperature, 15, 13 (1977).

Response to the comments of the First Report:
(Serial numbers refer to the examiners' queries)

On use/neglect of residence time measurements and correlations with N atom formation:

Quantitative measurements of the absolute residence times could not be made due to lack of calibrated flowmeters. However, the effect of residence time on N atom concentration, when the volume flow rate is changed, has been presented in Figs. 3.11 and 3.12. It clearly shows that in the range of experimental conditions, there is a direct dependence of the N atom concentration on the residence time. Since the extent of atom recombination is insignificantly affected (as shown in the thesis), the results may be taken to indicate electron impact dissociation of a larger number of molecules when the sojourn time is high.

On the relative role of vibrational energy exchange and direct electron impact dissociation:

According to refs. (a) and (c), the vibrational exchange contributions are important for $E/N < 6 \times 10^{-16}$ volt-cm²; at higher E/N values they are relatively unimportant. The present experimental studies are in the E/N range of $1-3 \times 10^{-15}$ volt-cm² (evaluated using Tables 3.1-3.2) where the vibrational excitation contributions are expected to be relatively minor and could be

3. representation of Arc data although no analysis has been made using them:

The thesis presents studies on the glow region. The phenomenological I-V data of the arc were presented just for the purpose of a comparison with glow data as some preliminary experiments with arcs were carried out. No conclusions on the arc processes are claimed.

4. On keeping the wall temperature constant by a water jacket and estimating the wall temperature:

The primary reason we did not use a water jacket is that measurements are much more convenient without it. We made temperature measurement of the outer wall of the tube with a thermocouple and assumed it to be close to the inner wall temperature. The justification is that in convective cooling in stationary ambient air, the heat loss is small, and so is the temperature differential across the wall, which ensures proximity of the inner and the outer wall temperatures. (A rough calculation shows that for an outside wall temperature of 375°K , an inside wall temperature of about 390°K may be expected.)

5. On the assumption of Maxwellian distribution of electron energy and effect on results:

The linearity in the double probe semilog plot of I-V data shows that the distribution is not far from Maxwellian. However we may add that with the direct electron impact dissociation cross section used in the present work and a consideration of Maxwellian and Druyvesteyn distribution of same average energy (as shown for example on p. 549, "Collision Phenomena in Ionized Gases" by E. W. McDaniel, Wiley, 1964) show that, at $kT_e \approx 2$ eV the Druyvesteyn distribution yields a somewhat higher k_1 , while at $kT_e \approx 5$ eV the Maxwellian distribution yields a somewhat higher value.

* For No. 6, see p. 3.

On minor corrections:

1. On Eq. (4.6) being incorrect, as $k_2(T_g)$ is missing in the denominator:

This is a typographical error. $k_2(T_g)$ should be in the denominator of Eq. (4.6). This error has now been corrected.

2. On flow estimation from theoretical pump speed values:

The idea of using linear flow rate was to arrive at an order of magnitude value of the time involved for the gas to flow from the active plasma region to the photomultiplier measuring point. We showed that even an order of magnitude error would not make any significant difference in the nitrogen atom concentration at the photomultiplier measuring point. So the result we arrived at was very conservative (and takes into account possible errors due to any flow rate decreases arising out of low line conductances).

On Additional Comments of the First Report:

1. On the " 10^{-17} cc/mole-sec value of the rate constant (k_{ed}) which would mean an extremely low value of 10^{-40} cc/molecule-sec.":

Throughout the thesis, rate constants have been reported as cc molecule $^{-1}$ sec $^{-1}$. Only in Fig. 4.1(b), on the ordinate, cc molecule $^{-1}$ sec $^{-1}$ was inadvertently abbreviated as cc mol $^{-1}$ sec $^{-1}$. (mol $^{-1}$ and not mole $^{-1}$.) So the 10^{-17} value is actually for cc molecule $^{-1}$ sec $^{-1}$; therefore the question of 10^{-40} cc molecule $^{-1}$ sec $^{-1}$ value does not arise.

2. On use of low rate constants to match with the lower values of N atom production:

N atom concentration, according to the model used, is proportional to $k_{ed}^{1/2}$. Therefore, in order to reduce N atom concentration by a factor of 50, k_{ed} must decrease by a factor of 2500. However, this is only when radial homogeneity of n_e and kT_e is assumed, which, of course, is not quite valid. A more likely reason is probably existence of regions where N atom production rate is much smaller bringing the overall rate down.

*6. On N atom concentration from NO titration measurements:

We had a number of difficulties in NO flow rate measurements. The NO flow measurements for relative N atom concentration were carried out before we could procure the pressure transducer for plasma gas inlet pressure. But right after these experiments we had corrosion

problems with the main NO regulator; as a result, we could not make an absolute calibration of NO flow. We refrained from using capillary and other manometric methods because of errors that might enter due to manometric fluids.

Response to the comments of the Second Report:

2. On the work reported in ref. (d):

Cernogora et al in their studies on the positive column of nitrogen glow discharges using a system of slightly different geometry than our's, reported that an increase of either pressure or discharge current results in an increase of electron density. It was also noticed that E/N decreases with increasing pressure. Our observations are similar to these.

3. On additional information about the mass spectrometric apparatus that was planned to be used in the investigation:

This imported⁴ equipment was supposed to be designed according to our specifications and was to mass analyze both plasma neutrals and ions. We had asked for a built-in energy analyzer for the ions which would be followed by the mass analyzer. For analysis of neutrals, the plasma ions would be diverted from the ion source that would ionize the neutrals, and the mass spectrum would then pertain to the neutral composition. The system was to consist of two stages of differential pumping to enable sampling of the plasma going up to 1 bar pressure.

The equipment that the manufacturer supplied has not stood up to any of the specifications. What they provided is a parallel plate energy analyzer right after the entrance to the second differentially pumped chamber which is followed by an ion source. As a consequence, the ion source entrance aperture is out of line-of-sight of the entrance aperture through which the plasma particles enter the first differentially pumped chamber; so the neutrals cannot make it to the ion source directly without undergoing some wall collisions, therefore potentially altering information on the neutral composition.

at installation that it would be delivered by May 1984. After several extensions, the equipment was finally delivered in November 1984. In January 1985 a manufacturer's technical representative came for installation but could not demonstrate ion (or neutral) mass spectrum from the plasma. The manufacturer made no effort to come and repair the instrument during practically the rest of 1985. In December 1985 another technical person representing the manufacturer visited to examine the equipment and agreed to install an ion source in the first chamber to permit ionization of the plasma neutrals. In April 1986 an ion source was installed in the first chamber, but it was then found that one of the two turbomolecular pumps is not operational. The instrument is still not working.

4. On measurements of absolute values of volume flow rate:

The rotameter was originally available (borrowed) with a stainless steel float. As this float was found unsuitable for the present work, we fabricated an aluminium float and employed it as a flow index. However, a calibration could not be done due to the non-availability of a standard flow meter. An ab initio calibration was not possible because the "flow parameter" which is a function of (1) the ratio of the diameters of the float and the tube, and (2) densities of the float and fluid, was not available.

5. On Reynolds number of the flow used:

Calculating for an internal tube diameter of 2.5 cm, a maximum linear flow rate of $3 \times 10^3 \text{ cm sec}^{-1}$, a density of about $9 \times 10^{-7} \text{ g cm}^{-3}$, viscosity of the order of 2.5×10^{-2} poise, one obtains $Re \approx 25$. This is very much in the laminar flow region.

Response to the comments of the Third Report:

1. On the role of N_2^+ :

This has been clarified in Appendix 1. Briefly, the N_2^+ influences the N atom concentration through the charge transfer process involving N atoms. There is, of course, an additional possibility of N being depleted through reactions with N_3^+ and N_4^+ , species which are formed by reaction with N_2^+ . However, these are of minor significance.

A 99203

CHM-1985-D-SRE-ROL